LIBRARY COLLEGE

JOURNAL OF APPLIED PHYSICS

JUNE
1939
Vol. 10 No. 6

Successive Snapshots of a Flame in a Closed Tube

B. LEWIS
AND
G. VON ELBE

JOURNAL OF APPLIED
PHYSICS

JUNE, 1939 Vol. 10, No. 6

In This Issue

Page

That Publication Problem, Again! 343

Physics of Flames and Explosions of Gases
BERNARD LEWIS AND GUENTHER VON ELBE 344

Recreating Geological History with Models
MILTON B. DOBRIN 360

Resumés of Recent Research 372

New Million-Volt X-Ray Outfit
E. E. CHARLTON, W. F. WESTENDORP, L. E. DEMPSTER AND GEORGE HOTALING 374

Contributed Original Research

Dielectric Resonators R. D. RICHTMYER 391

Studies in Lubrication. V M. MUSKAT AND F. MORGAN 398

Phosphorescence of Zinc Silicate Phosphors
GORTON R. FONDA 408

Reignition of Short Arcs at High Pressures
J. D. COBINE, R. B. POWER AND L. P. WINSOR 420

In Every Issue

Here and There 386

Contributors to this Issue 388

Letter to the Editor 389

New Books 390

Innovations in Instruments x

Index to Advertisers xiv

BOARD OF EDITORS

ELMER HUTCHISSON, *Editor*

Associate Editors

J. BITTER
W. E. FORSYTHE
L. A. JONES
W. F. MEGGERS
B. E. WARREN
J. B. WHITEHEAD
V. K. ZWORYKIN

Publication of the
American Institute of Physics

ADMINISTRATIVE STAFF

HENRY A. BARTON, *Director*

MADELINE M. MITCHELL, *Publications Manager*

F. K. RICHTMYER *Chairman, Advertising Committee*

GOVERNING BOARD

JOHN T. TATE, *Chairman*
KARL T. COMPTON
E. C. CRITTENDEN
WHEELER P. DAVEY
FLOYD A. FIRESTONE
HARVEY FLETCHER
ARTHUR C. HARDY
PAUL E. KLOPSTEG
MELVIN MOONEY
FREDERIC PALMER, JR.
R. L. PEEK, JR.
GEORGE B. PEGRAM
W. B. RAYTON
F. K. RICHTMYER
WALLACE WATERFALL

THE JOURNAL OF APPLIED PHYSICS, published monthly at Prince and Lemon Sts., Lancaster, Pa., is devoted to physics in its role as the science basic to other natural sciences and to the arts and industries. Previous to 1937 this publication was known as PHYSICS. It aims to be of service not only in physical laboratories, but also in the laboratories of industrial, chemical, geological, geophysical, meteorological, radio, and similar concerns. THE JOURNAL OF APPLIED PHYSICS publishes editorials, news of physicists and reviews, as well as technical papers of applied physics.

SUBSCRIPTION PRICE

	U. S., POSS. AND CANADA	FOREIGN
To members of scientific societies	$5.00	$5.70
To all others	7.00	7.70

Manuscripts should be submitted to Elmer Hutchisson, Editor, University of Pittsburgh, Pittsburgh, Pennsylvania.

Changes of address, proofs, and complaints of failure to receive the JOURNAL OF APPLIED PHYSICS should be addressed to the Publications Manager. New copies can be sent free only if notice of nondelivery is received within three months of date of issue.

Subscriptions and orders for back numbers should be addressed to Prince and Lemon Streets, Lancaster, Pa. or to the American Institute of Physics, 175 Fifth Avenue, New York, N. Y.

Advertising rates supplied on request. Orders, advertising copy and cuts should be sent to the American Institute of Physics.

Entered as second class matter at the Post Office at Lancaster, Pennsylvania, under the Act of March 3, 1897. Accepted for mailing at the special rate of postage provided for in the Act of February 28, 1925, authorized May 2, 1932.

Copyright 1939, by the American Institute of Physics.

Two of the twenty-seven types of potentiometers made by L&N. At left, a Wenner, with an accuracy unique among wide range potentiometers, is measuring temperatures near absolute zero. At right, a Portable Indicator is measuring pH of an electroplating solution. L&N also makes automatically balancing potentiometers to indicate, record and control.

A POTENTIOMETER FOR EVERY PURPOSE

L&N Potentiometers are available to meet practically any specifications for accuracy, reliability, speed and convenience.

Making potentiometers of exceptionally high accuracy has led to instrument refinements and better calibration methods which also apply to instruments for routine testing. On the other hand, making equipment for routine tests has brought about design improvements by which research instruments are made to operate for years with complete reliability. Developments which arise from the manufacture of each type are thus available for incorporation into all types.

If, among the twenty-seven standard L&N potentiometers, none meets your need, we'll make one to your specifications. Write, describing the characteristics you want, and we shall be glad to recommend the most suitable instrument.

LEEDS & NORTHRUP COMPANY, 4978 STENTON AVE., PHILA., PA.

LEEDS & NORTHRUP

MEASURING INSTRUMENTS · TELEMETERS · AUTOMATIC CONTROLS · HEAT-TREATING FURNACES

Jrl Ad EH(2)

PRECISION INSTRUMENTS FOR MEASUREMENT AND CONTROL

GM

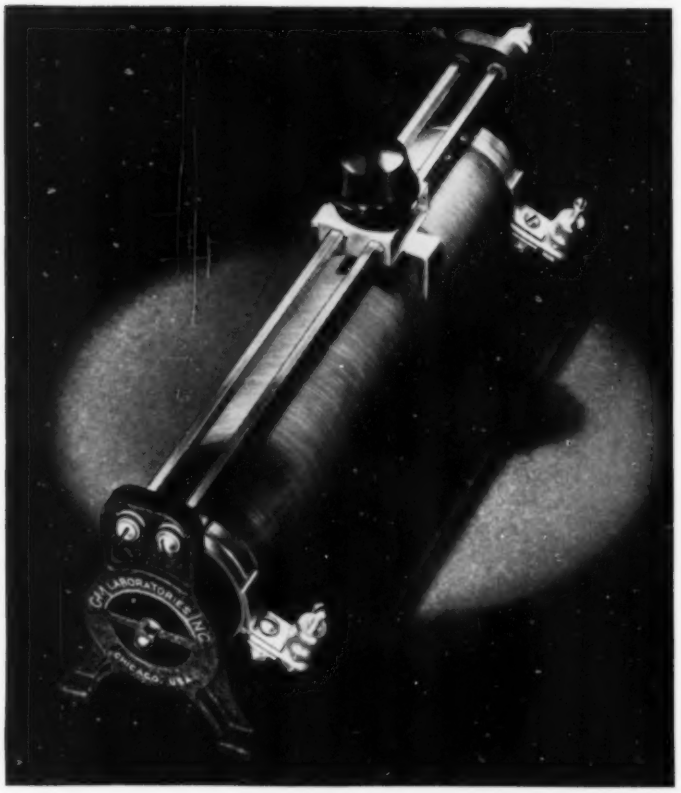

Slide Wire Rheostats

Your slide-wire rheostat gets rough treatment. It is not pampered. That is why this G-M instrument has rugged strength as well as smooth action built into it.

Of special benefit to the laboratory technician is the Dual-Control slider mechanism. This provides a two-movement adjustment. You can slide the contact carriage; or adjust it by a geared vernier action. A slight pressure on the control knob depresses and disengages the gear.

On most models, nested brushes with multiple spring contacts are used, providing contact surfaces of large area. On rheostats wound with fine wire, a single contact shoe with an auxiliary pressure spring is used to avoid unnecessary wear to the wire.

To insure maximum service under most severe use, exacting care is taken in every manufacturing step. There is extra dielectric strength in the porcelain enameled steel tubing, which is covered by a special insulating material. The rack and gear assembly has been life-tested. The end brackets are die cast, not sand cast or stamped. Finally, the alloy resistance wire is selected to rigid specifications.

G-M rheostats are manufactured in 12 and 20-inch sizes. There are 32 ratings, ranging from 0.6 to 48,000 ohms. The measured total resistance of each rheostat is stamped on the frame. Write for the G-M catalog giving specifications and prices on slide wire rheostats, and the complete line of G-M precision instruments.

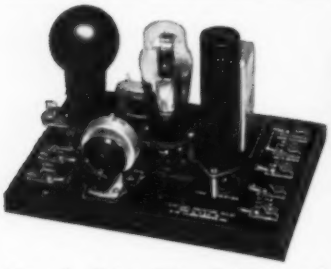

Phototube Relay. This G-M special demonstration unit comprises a phototube, thermionic amplifier, resistor, potentiometer, condenser, and electromagnetic amplifier relay. It is suitable for demonstrations and experimental or research work. Write for descriptive Bulletin CS-593A.

Moscow, Idaho. At the University of Idaho, the Physics Department uses a G-M suspended coil D'Arsonval galvanometer and a G-M power supply unit. Other G-M instruments available for laboratory work are: galvanometer relays, portable galvanometers, electric thermometers, and phototubes.

G-M LABORATORIES INC.

DEPT. B. 1731 BELMONT — CHICAGO, U. S. A.

FOUR OUTSTANDING NEW BOOKS

MATTER, MOTION AND ELECTRICITY. A Modern Approach to General Physics

By HENRY D. SMYTH, Princeton University, and CHARLES W. UFFORD, Allegheny College. In press—ready in August

In this distinctive new book the authors' purpose has been twofold: (1) to review fundamental principles and definitions sufficiently to insure a solid base on which to build; and (2) to present the subject from a fresh approach that avoids a repetition of the conventional beginners' course.

INTERNAL CONSTITUTION OF THE EARTH

Edited by B. GUTENBERG, California Institute of Technology. 401 pages, 6x9. $5.00

This important new book is Volume VII of Physics of the Earth, a series of monographs prepared under the direction of the various committees of the National Research Council. Preceding volumes have been published by the Council. The present book gives a review of the features of the interior of the earth written by a group of distinguished geologists and geophysicists.

THE PHOTOGRAPHIC PROCESS

By JULIAN E. MACK and MILES J. MARTIN, University of Wisconsin. In press—ready in June

Here is a unified modern treatment of the subject, presented simply enough for the general student, yet with sufficient scope and scientific rigor to justify its use in a college course in photography.

ELECTRICITY AND MAGNETISM. An Introduction to the Mathematical Theory

By J. B. WHITEHEAD, Johns Hopkins University. *Electrical Engineering Texts.* In press—ready in August

This book represents a compact development of the physical theories of electricity and magnetism beginning with the simplest manifestations of mechanical force by electrostatic and magnetic phenomena.

Send for copies on approval

McGRAW-HILL BOOK COMPANY, Inc.

330 West 42nd Street **New York, N. Y.**

RESEARCH POLARIMETER

(LIPPICH, TRIPLE FIELD)

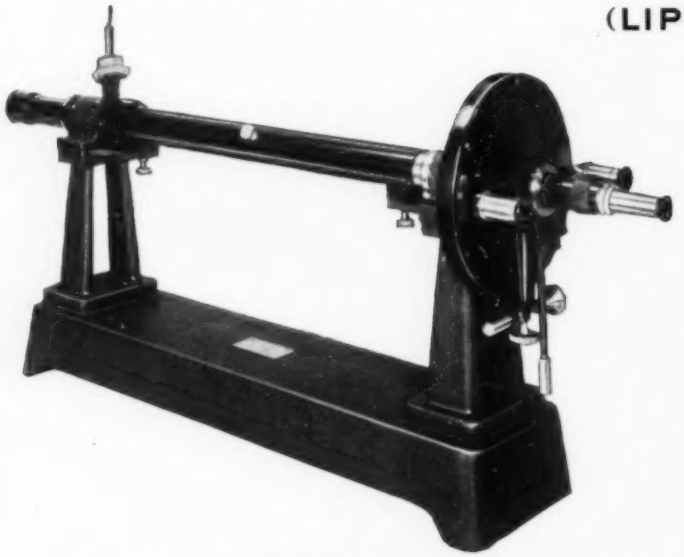

Designed optically and mechanically for analytical work of high order, this polarimeter accommodates tubes up to 400mm long. The large circle reads to .01°; lamps and magnifiers are built in. Accuracy and ease of setting are provided by the triple field feature. The dividing line disappears completely at the match point and the half-shadow angle is adjustable to 0.1° over a range of 20°.

Full details available on request

THE GAERTNER SCIENTIFIC CORP.

1212 WRIGHTWOOD AVENUE • CHICAGO • U. S. A.

Standard or Experimental

RESISTORS

ALL TYPES · ALL SHAPES · ALL SIZES

Common resistor types made to uniformly high standards of quality . . . or special resistors for unusual applications . . . whatever the units you need IRC can supply them. The following bulletins detailing various IRC resistance types are available upon request:

☐ BULLETIN No. 1—Volume Controls and Potentiometers. 6 std. sizes, any needed combinations.

☐ BULLETIN No. 2—Metallized Type Resistors. Insulated ½, 1 and 2 Watts; High Frequency; High Range; High Frequency Power and High Voltage Power Resistors.

☐ BULLETIN No. 3—Insulated Wire Wound Resistors. Type BW from ½ to 1 and 2 Watts. Type MW 5 to 20 Watts,

☐ BULLETIN No. 4—Power Wire Wound Resistors. Types from 10 to 200 Watts, fixed and adjustable types, all mountings. Precision units, 14 types, 1/10 of 1% accuracy.

☐ BULLETIN No. 5—Attenuators.

☐ BULLETIN No. 6—Power Rheostats.

INTERNATIONAL RESISTANCE CO.

419 N. Broad St., Philadelphia, Pa.

IRC

GE PORTABLE UVIARC
for ultra-violet radiation

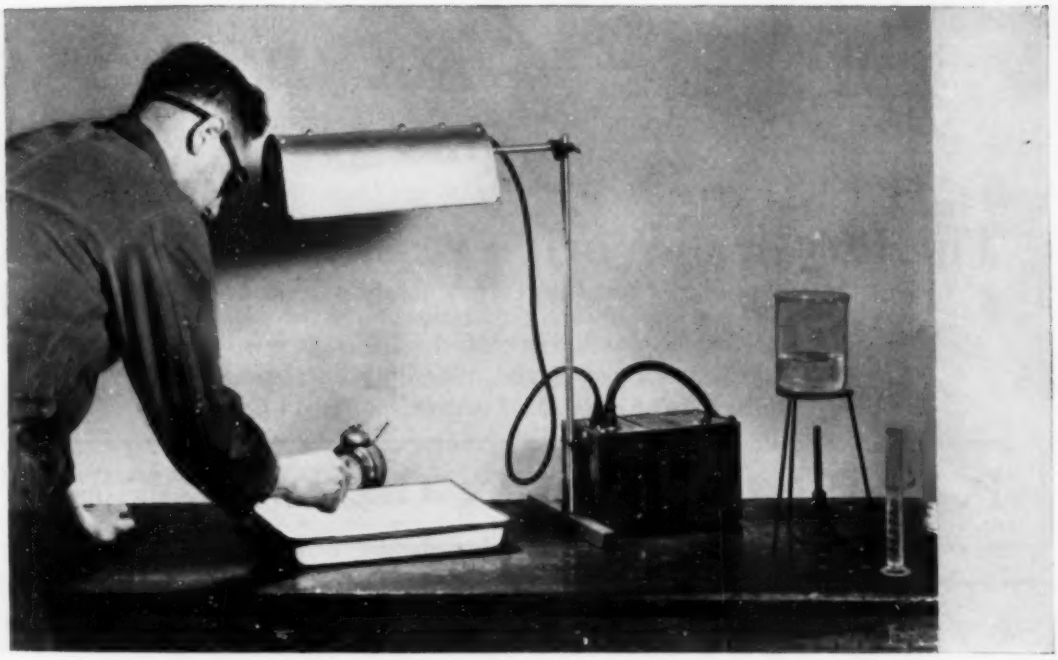

1. *Complete* – Laboratory outfit includes a.c. Uviarc tube, reflector, stand and transformer.

2. *Efficient* – Ultra-violet radiation per watt of electrical input exceeds that of other types of ultra-violet sources.

3. *Dependable* – Radiation output during a relatively long operating period can be held constant to better than ± 2 per cent by maintaining constant tube wattage.

4. *Durable* – Rated operating life is 2,000 hours, with an unusually slow rate of depreciation.

5. *Convenient* – Uviarc outfit is portable and self-starting; it can be used in any operating position at full efficiency.

• • •

Applications: The G. E. portable Uviarc outfit is ideally adapted to use in laboratory experiments in bacteriology, biochemistry, fluorescence, halogenation, hydrogenation, pharmacology, photochemistry, phototherapy, polymerization and spectroscopy. Write for a copy of descriptive bulletin. General Electric Vapor Lamp Company, 835 Adams Street, Hoboken, N. J.

GENERAL ELECTRIC VAPOR LAMP COMPANY

960Q

Two Lucid Texts for Physical Science

Survey of Physical Science for College Students—McCorkle

This text provides a three-hour course for one year. Material is presented simply and accurately and laboratory experiments suitable for classroom demonstration or individual work are given at end of each chapter.

273 Illus. Appendices. Review Questions. 471 Pages.
Washable Fabric $2.75
By Paul McCorkle, Ph.D., State Teachers College, West Chester, Pa.

The Physical World—Heil

This book is primarily for college students who desire some knowledge of physical science but do not intend to major in science. Rich in facts, it combines physics, chemistry and astronomy in a one year's course.

426 Illus. 566 Pages. Washable Fabric $2.75
By L. M. Heil, Ph.D., Formerly of Ohio University

P. Blakiston's Son & Co., Inc., 1012 WALNUT STREET PHILADELPHIA, PA.

DUO-SEAL TWO STAGE VACUUM PUMP

This Vacuum Pump, although smaller than the 1405 which has made such phenomenal service and endurance records, has the same internal vane movements and other important mechanical features.

No. 1400B

FIVE SPECIAL FEATURES

1. The proper pump speed is approximately 475 R.P.M., which produces a free air capacity of nineteen liters per minute.
2. Each pump is tested on our certified McLeod gauges to less than 0.1 micron (.0001 mm Hg) and many register less than .07 micron.
3. The mechanical action is unusually quiet for a vacuum pump.
4. The exhaust chamber is arranged for the collection of gases where this is desired.
5. The oil level is visible and the oil can be conveniently drained. Positive oil seal—no oil can back up.

No. 1400B—DUO-SEAL VACUUM PUMP, Two Stage, Motor driven. Mounted on a cast iron base with 1/6 H.P. 110 volt A.C. motor and V belt with belt tightening device..Each, $85.00

No. 1400—DUO-SEAL VACUUM PUMP, Two Stage, with pulley but without belt, motor or base.....Each, $60.00

WELCH

Catalog lists over 10,000 items for Science Laboratories.

WRITE FOR IT

Includes many new and interesting pieces.

W. M. WELCH SCIENTIFIC COMPANY
Established 1880
1515 Sedgwick Street Chicago, Illinois, U. S. A.

NEW WILEY BOOKS

Spring — Summer 1939

Wavelength Tables

Measured and Compiled under the Direction of

George R. Harrison, *Professor of Physics*
Massachusetts Institute of Technology

A systematic survey of spectrum lines giving intensities in arc, spark, or discharge tube of more than 100,000 spectrum lines most strongly emitted between 10,000 and 2,000 A by the atomic elements under normal conditions of excitation. In addition to the pages of data on the lines, the book has short tables containing lists of sensitive lines of the elements, and descriptive material interpreting the tables and telling how the measurements were made.

To be Ready for Fall Use

Spectroscopy and Its Applications

Proceedings of the Sixth Summer Conference (1938)

Edited by **George R. Harrison**

This volume contains, in somewhat abbreviated form, the thirty-one papers which were presented during the three days of the 1938 conference on spectroscopy. Although space limitations decreed that not much more than half of the orally presented material be included, the condensations have been carried out by the respective authors, and little essential material has been omitted.

Published in April; 172 pages; 7½ by 10; 91 figures; $3.00

Photography by Infrared

By **Walter Clark,** *Kodak Research Laboratories*

This is an important monograph, as complete as the resources of today permit, containing the fullest account of the history of infrared that has yet appeared. It deals equally with the general practice of infrared photography, the materials available, and the application of its methods to practically every field wherein it has been used.

Published in May; 397 pages; 103 illustrations; 6⅛ by 9½; $5.00

Household Physics

By **Walter G. Whitman,** *Head of the Department of Physical Science*
State Teachers College, Salem, Massachusetts

The third edition of "Household Physics" constitutes a thorough revision and rewriting, and the content is now completely up to date. The book has had to be somewhat enlarged, due to the recent data which have been incorporated. The content follows along practical lines and includes much new equipment available today for the home. Three entirely new chapters are presented, dealing with "Protection against Fire," "Visual Aids," and "Photography."

Ready in August; Approximately 490 pages; 6 by 9; probable price $3.00

JOHN WILEY & SONS, INC.

440 FOURTH AVE. NEW YORK, N. Y.

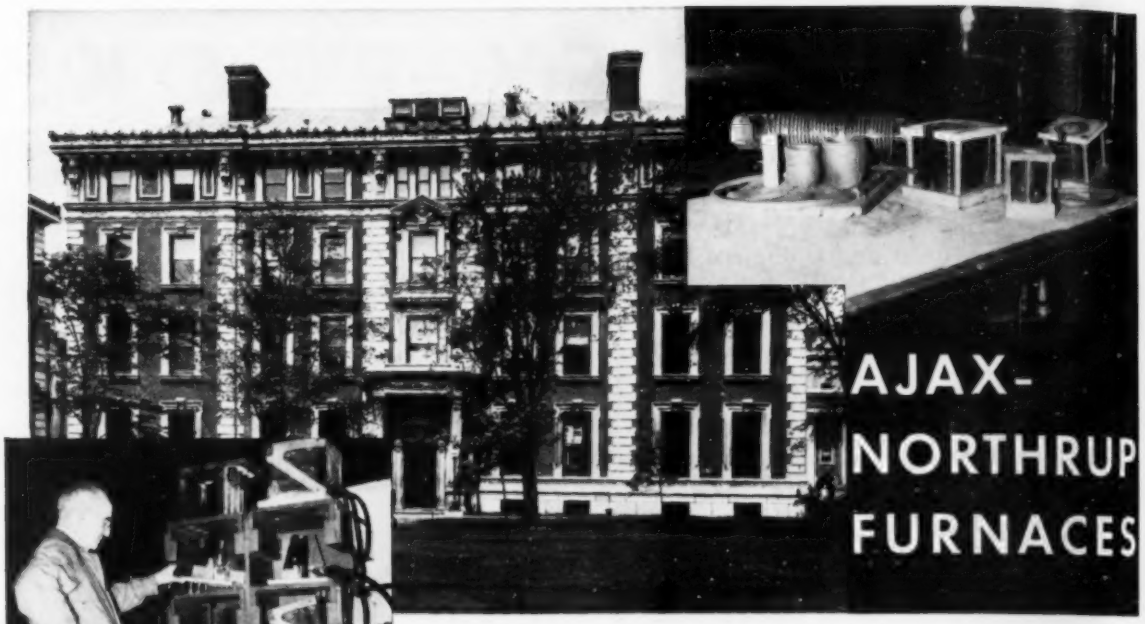

AT COLUMBIA UNIVERSITY

The Mines Building at Columbia and some of the melting units used in connection with Ajax-Northrup Furnaces.

The Departments of Mining Engineering and Metallurgy have used Ajax-Northrup Furnaces since 1928.

The extent of use is illustrated by the pyramid of Ajax-Northrup coils (at the left) of various types and sizes covering every conceivable requirement for thesis and sampling work.

In the laboratory for applied electrochemistry smaller Ajax-Northrup Furnaces are used. A detail view of the accessory equipment is shown at the top right.

AJAX-NORTHRUP MELTING FURNACE CAPACITIES: ONE OUNCE TO EIGHT TONS

AJAX

AJAX ELECTROTHERMIC CORPORATION
•
AJAX PARK
TRENTON, N. J.

AJ-14-C

HARVARD COLLEGE
JUN 6 1939
LIBRARY

Journal of Applied

Physics

Volume 10 June, 1939 Number 6

That Publication Problem, Again!

THE program of the Washington meeting of the American Physical Society listed the extraordinary number of 182 papers on recent research developments in all branches of physics. General trends in research may be judged by noting how these papers are distributed in subject matter. We find 45 papers on nuclear physics, 29 on physics of metals, 29 on spectroscopy, 19 on electrical discharges, 12 on x-ray diffraction, at least 7 on Geiger-Müller counters, a few on the nature of cosmic rays, a few on quantum mechanical calculations and the remaining 30 in general classical physics. The great interest in this new research and in the other phases of the meeting is attested by the fact that the registration was well over 600 by the second day of the meeting.

This increase in research activity has not confined itself to the field of the so-called "pure" physics. The Editor of the *Journal of Applied Physics* is becoming increasingly distressed by the large number of good research papers in applied physics which are submitted for publication but which he is unable to publish. A good scientific journal prides itself on its ability to publish a paper within a short time after receiving the manuscript. However, with a given income from subscriptions there is only a finite number of pages which can be published in a year. Unlike some other institutions a journal must operate on a balanced budget. Because good and acceptable papers are being received at a much greater rate than the budget allows them to be published, there is grave danger that an unacceptable delay in publication time will result. Realizing this danger a special appropriation has been made to allow temporary relief by publishing an extra 16 pages per issue starting with the present issue and continuing for six months. This procedure cannot be continued. If the journal is to publish the worth-while research papers in applied physics and be reasonably up-to-date we must have more subscribers. Since the journal is entirely a non-profit making venture, the larger the circulation, the larger and better journal each subscriber will receive. We need your help. If every subscriber could obtain one other subscription our publication crisis would be over.

THE EDITOR.

For July Television Issue

Associate Editor—V. K. ZWORYKIN

Probable Influence of Television on Society, by DAVID SARNOFF

High Definition Television, by PIERRE MERTZ

Survey of Television Pickup Devices, by KNOX MCILWAIN

Television Receiving and Reproducing Systems, by E. W. ENGSTROM

Problems of Television Transmission, by PETER C. GOLDMARK

Electron Optics, by E. G. RAMBERG *and* G. A. MORTON

Luminescent Materials, by H. W. LEVERENZ *and* F. E. SEITZ

Also contributed original research.

Physics of Flames and Explosions of Gases*

By Bernard Lewis† and Guenther von Elbe‡

COMBUSTION processes present a variety of problems that require the application of numerous branches of theoretical and experimental physics. In the study of the self-ignition of combustible mixtures there arise gas kinetic problems of reaction rates and heat exchange. Studies of local ignition, as by a spark, and of the reaction zone in stationary and moving flames involve, in addition, kinetic problems of transport of heat and material particles. The absence of complicated disturbances in spherical flames and stationary flames of the Bunsen type make these particularly suitable for fundamental studies of the progress of the reaction zone or flame front into the unburned gas. The considerable technical importance of stationary flames directs attention, among other things, to problems of burner design, flame shape, stability and rigidity of the flame. Gas motion introduces additional problems in flame propagation which are of the greatest practical importance but are often too complex for theoretical analysis; in this field photographic methods, particularly *schlieren* photography, have given valuable information. In the case of flames traveling in tubes with extreme velocity, known as detonations, a hydrodynamic analysis of the shock wave has succeeded in describing the essential features of the phenomenon without recourse to the chemical kinetics of the process. The flame formed between a stream of fuel gas and the atmosphere can, in the absence of turbulence, be rather well described by diffusion equations expressing the rates of intermixing of the two gases. Finally, thermodynamics in conjunction with band spectroscopic data of energy contents and dissociation equilibria of gases allows the ideal state of the burned gas to be calculated and standards for the internal-combustion engine to be determined; it has led to the discovery of deviations from equilibrium conditions in the burned gas. Important experimental methods for determining the state of the burned gas are measurements of explosion pressures, flame volumes and flame radiation. In the latter, measurements are made of the radiation from the flame gases themselves or, as in the line-reversal method, from admixed metal atoms emitting in the visible part of the spectrum.

1. Self-Ignition

The self-ignition of an explosive mixture enclosed in a vessel is found to depend on a number of variables, namely, temperature, pressure, mixture composition, and in most cases also upon gas motion and vessel factors, such as size and the condition of the inner surface of the vessel. In some cases ignition can be produced by irradiation. Almost always a measurable time elapses before ignition occurs. This time, known as the induction period, may range from a fraction of a second to several hours. The phenomenon of ignition is understood to be the transition from a slow to a very fast and approximately adiabatic chemical reaction. Two known processes bring this about. One is self-acceleration of the reaction by the heat developed until the rate of heat liberation exceeds the rate of heat loss to the surroundings, the so-called *thermal explosion;* the other is the formation of chemically active particles, such as atoms and radicals, at a rate that exceeds the rate of their destruction, the so-called *branched-chain explosion.*

A sharp division between these two types of explosions cannot be made, since both processes may occur simultaneously. However, a purely thermal explosion arises when the chemical reaction is of a simple order, like a unimolecular reaction for which there is evidence in the decomposition of azomethane[1] and ethyl azide.[2]

---

* Published by permission of the Director, Bureau of Mines, U. S. Department of the Interior, and the Director, Coal Research Laboratory, Carnegie Institute of Technology (not subject to copyright).

† Physical Chemist, Explosives Division, Central Experiment Station, Bureau of Mines, Pittsburgh, Pennsylvania.

‡ Coal Research Laboratory, Carnegie Institute of Technology, Pittsburgh, Pennsylvania

The quantitative treatment[3] of the temperature-time relations in the reaction vessel is based on the equation for the rate of heat, q, accumulating in the vessel, *viz.*

$$\frac{dq}{dt}=QVmAe^{-E/RT}-aK(T-T_0), \qquad (1)$$

where Q is the heat of reaction per mole of gas decomposed, V the volume of the reaction vessel, m the number of moles of reacting gas per unit volume, E the energy of activation, R the gas constant, a the wall area, T and T_0 the temperatures of the gas and the reaction vessel, respectively, and K and A constants. $Ae^{-E/RT}=k$, the reaction-rate coefficient. From the equation $-dm/dt=km$, and assuming k to be constant during the induction period where the temperature rise is small, $m=m_0e^{-kt}$, where m_0 is the initial molar concentration. The first term on the right side of Eq. (1) is the rate of heat production and the second term the rate of heat loss. On dividing the equation by the total heat capacity of the gas in the vessel, it becomes an equation connecting temperature with time. Its solution by numerical method leads to the result that above a certain sharply defined initial pressure, i.e., m_0, a sudden temperature rise corresponding to an explosion occurs after an initial stage of slow temperature rise which may be regarded as the induction period. The foregoing illustrates the complexity of the quantitative treatment, even for the simplest case of a unimolecular reaction. In the more common case of a complex reaction mechanism involving a sequence of many elementary reactions, the treatment becomes quite hopeless. One may nevertheless appreciate the main features of the thermal theory by the general formulation of the explosion condition; that is, at the boundary between nonexplosive and explosive reaction the rates of heat liberation and dissipation are equal, *viz.*

$$\frac{dq}{dt}=QVr-aK(T-T_0)=0. \qquad (2)$$

r is the number of moles of gas reacting per unit time and volume, and, in most instances, is a complicated and incompletely known function of all the variables enumerated above. It is generally, however, a function of pressure in the sense that it increases with the latter, and of temperature of the form $e^{-E/RT}$. If Eq. (2) has a real root in T, the system will come to equilibrium at this temperature, and the reaction will proceed normally; but if for fixed values of the other constants, the pressure or T_0 is increased sufficiently, the equation will have no real root, dq/dt will be always positive, the temperature will increase and the process of self-acceleration of the reaction, i.e., explosion, will set in. This shows that the ignition temperature T_0 is lowered by increasing pressure and also by increasing vessel diameter which increases V more than a. A plot of ignition temperature *vs.* pressure may generally be expected to follow approximately an equation of the form $\log P=A/T_0+B$, where A and B are constants, the latter depending, among other things, upon vessel factors. The latter equation agrees with many experimental observations, but since the case of branched-chain explosion where the active species are destroyed at the wall of the vessel yields a similar equation, this general form does not serve as a criterion to distinguish between the thermal and branched-chain explosion.

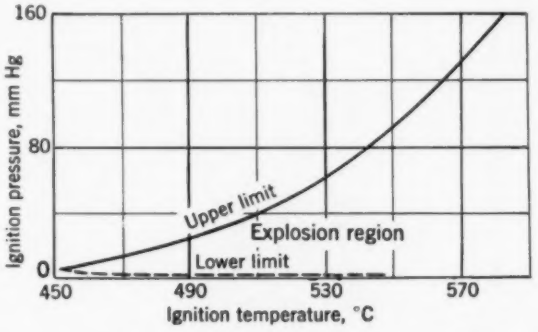

FIG. 1. Low pressure explosion region of a stoichiometric mixture of hydrogen and oxygen.

Many explosive mixtures exhibit an ignition phenomenon to which the thermal theory cannot apply. An illustration is given in Fig. 1 for a stoichiometric mixture of hydrogen and oxygen. Here part of the ignition region is shown in a pressure-temperature diagram. If the mixture is admitted, say, to a quartz vessel at 530°C and above about 60 mm Hg pressure, a slow reaction is observed. The reaction rate decreases on reducing the pressure, but on reaching about 60

mm explosion occurs. The mixture remains explosive down to very low pressures of the order of a few mm. The upper branch of the peninsula-shaped curve is called the upper explosion limit. The position of the latter is practically independent of vessel factors. It is evidently impossible to fit these combined facts into a thermal theory, whereas the branched-chain theory lends itself readily to interpretation of the phenomenon. Suppose an atom, H, is formed in the mixture by thermal dissociation. Then the following chain of reactions has a chance to occur.

$$\begin{aligned} H+O_2&=OH+O,\\ O+H_2&=OH+H,\\ OH+H_2&=H_2O+H. \end{aligned}$$

In the second step an H is regenerated, and in the third step an additional H is formed. The chain has thus branched since both H atoms may repeat the same cycle. The concentration of H atoms thus increases at a rate $d(\mathrm{H})/dt = \alpha(\mathrm{H})$. If the reaction is to remain nonexplosive a chain-breaking reaction must operate by which

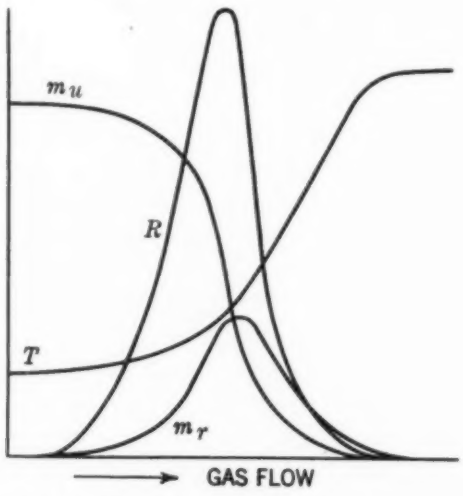

FIG. 2. Structure of flame front. Curves: m_u = concentration of reactants; m_r = concentration of atoms and radicals; T = temperature; R = reaction rate.

the H atoms are removed at the rate $-d(\mathrm{H})/dt = \beta(\mathrm{H})$, so that $\beta > \alpha$. If it is now assumed that α is independent of, and β proportional to, the pressure, then on lowering the latter, some critical pressure is reached at which $\alpha = \beta$ and below which $\alpha > \beta$ and explosion always occurs. The analysis of the reaction mechanism is based

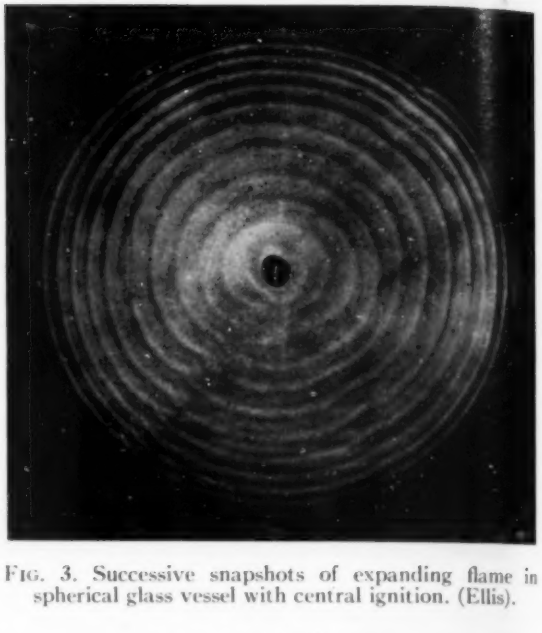

FIG. 3. Successive snapshots of expanding flame in spherical glass vessel with central ignition. (Ellis).

on a consideration of all imaginable reactions of such chain carriers as H, O, OH and HO_2, and the experimental data lead rather uniquely to the above sequence of reactions and the following chain-breaking reaction

$$H+O_2+M=HO_2+M,$$

where M is any third molecule. The radical HO_2 is removed by adsorption and self-neutralization at the wall before it can react appreciably in the gas phase.

The phenomenon of the upper explosion limit is thus seen to be one of the most important sources of information concerning the reaction mechanism. The knowledge gained there lends material aid in understanding the behavior of the system in other pressure ranges. For example, if in the present case the pressure is lowered very much, another chain-breaking process comes into prominence which consists of the destruction of H, O and OH at the wall. Therefore, a lower limit of the explosion region is established when β once more equals α. The position of this limit depends strongly upon vessel factors and gas motion. If, on the other hand, the pressure is increased above the upper limit, the chance of a gas-phase reaction of the radical HO_2 increases because of impeded diffusion and increased number of collisions, and a reaction whose rate depends on vessel factors and increases with

pressure is observed. If the pressure is increased sufficiently, a third explosion limit is reached which can again formally be described by the condition $\alpha=\beta$ but whose position depends not only on vessel factors and gas motion but probably also on thermal factors. Thus, from the mechanism of the upper explosion limit the mechanisms of both the lower and third explosion limits are deduced, which otherwise would be a difficult task because of complications introduced by vessel factors and thermal effects.

In other systems where no explosion limit exists that depends on reactions occurring exclusively in the gas phase, as in the combustion of hydrocarbons, the analysis of the reaction mechanism must draw largely on chemical facts. A detailed treatment of the subject of self-ignition is given elsewhere.[4]

2. *Ignition by Local Sources*

The dependence of the rate of the chemical reaction on the concentration of atoms and radicals provides an understanding of some interesting observations on ignition by electric sparks. It is a well-known fact that sufficiently small sparks do not produce ignition; but the nature of the minimum requirements for an igniting spark long remained obscure. According to an earlier prevailing concept derived from a purely thermal theory of ignition, this minimum requirement involved only the establishment of some critical temperature in the sparked volume, which in turn was governed by the amount and rate of release of energy. It has since been demonstrated, however, that an energy condition alone does not suffice but that the characteristics of the discharge play an important role. For example, in a carbon monoxide-oxygen mixture the addition of inductance to a high frequency spark lowers the amount of energy necessary to produce ignition. The explanation seems to be that essentially only that part of the energy that goes into the dissociation of molecules into atoms and radicals is available for chemical reaction, while energy of electronic excitation or of ionization is available for chemical reaction to a far lesser degree. As the average electron speed is lowered by the addition of inductance a larger percentage of the energy is used for molecular dissociations.

Local ignition by a heated surface, particle, or wire often requires temperatures much in excess of the temperature range in which self-ignition occurs. For example, mixtures of methane and air that ignite spontaneously in vessels below 750°C require local temperatures generally above 1000°C and up to 1500°C, depending on many factors, such as the nature of the surface and its position. Convection currents,

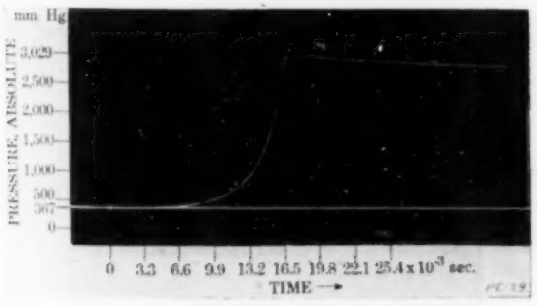

(a)

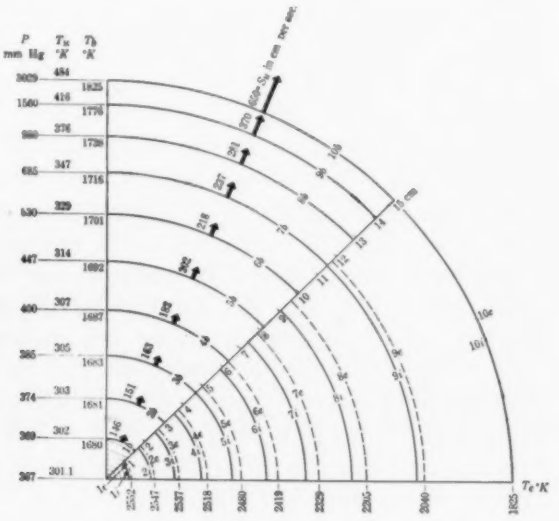

(b)

FIG. 4. Explosion of a mixture of 40 percent ozone and 60 percent oxygen in a spherical vessel with central ignition. (a) Time-pressure record of the explosion. (b) Analysis of the record shown in (a). Radius of the sphere 15 cm. Total explosion time 16.5×10^{-3} sec. Upper octant: Circles marked 1*b*, 2*b*, etc. indicate position of flame front in intervals of 1/10 of total explosion time. P = pressure throughout the vessel; Tu = temperature of unburned gas; Tb = temperature of burned gas adjacent to the flame front; Su = burning velocity. The values correspond to the indicated positions of the flame front. Lower octant: Solid circles 1*i*, 2*i*, etc. indicate volumes occupied before combustion by gas burned at intervals 1*b*, 2*b*, etc. Dotted circles 1*e*, 2*e*, etc. indicate corresponding volumes after the flame has reached the wall. Te = temperature at positions 1*e*, 2*e*, etc.

dilution and time of contact contribute to this difference.

The quantitative treatment of the problem of local igintion is not possible at this time[5] because of the complexity of the process, as is readily appreciated from a consideration of the various interdependent factors involved; namely, the reaction rate with its complicated dependence on temperature and concentration of active particles, the diffusion of the latter and the transport of heat by conduction and convection.

3. Flame Propagation

(a) Flame Front

There is a definite range of percentage of combustible gas below and above which a flame does not propagate in the mixture. In such mixtures the strongest source of ignition may cause a flame to form in its neighborhood, but the flame is extinguished on removing the source.

Flame propagation is always accompanied by gas movements which often lead to complicated disturbances such as the acceleration of flame in tubes. However, if the gas movement is known, as in Bunsen flames or spherical flames, the so-called burning velocity, which is defined as the rate of progress of the flame relative to the unburned gas, may be measured. It is difficult to investigate experimentally the structure of the zone of reaction or flame front which separates the unburned from the burned gas because of its extreme thinness. In this zone there must exist rather sharp gradients of temperature and concentrations of the reactants and the products of combustion, and the rate of reaction must be very rapid. If, for example, the thickness of the reaction zone is estimated to be not greater than 10^{-2} cm, then for a burning velocity of 5 to 10 meters per second the reaction is completed in the zone in less than 10^{-5} sec. Such reaction rates require high concentrations of atoms and radicals. Since the latter concentrations are for all purposes zero in the unburned gas and small in the burned gas where equilibrium conditions are substantially established, they must reach a maximum within the reaction zone. The well-known C−C or Swann bands and C−H bands in flames of organic gases and vapors furnish an example of the existence of such localized concentrations of radicals. Since the gases within the reaction zone are far from thermodynamic equilibrium, it is not surprising to find the radiation far more intense than corresponds to thermal radiation at the temperature of the burned gas.[6] A generalized qualitative representation of the structure of the reaction zone is shown in Fig. 2.

In the qualitative treatment of the burning velocity the reaction zone is placed at the zero position of a rectangular coordinate system with the unburned gas entering from one side at a rate equal to the burning velocity, all gradients of temperature and concentration remaining constant. The problem consists of solution of the steady-state equations of heat transfer and transport of all species present; in addition, the reaction mechanism and the probabilities of the elementary reactions must be known. In most cases the problem is at present far too complicated for solution. Using simplifying assumptions, the authors made calculations[4] for ozone flames which gave burning velocities of the order of those observed and led to values of the width of the flame front of the order of 10^{-3} cm and

Fig. 5. Flame with vertical wire obstruction in gas stream.

to maximum concentrations of oxygen atoms amounting to substantial fractions of the initial ozone concentrations.

In earlier treatments the problem was considered as one involving only heat flow. As the unburned gas enters the reaction zone it is heated up to a temperature called the ignition temperature at which the reaction becomes so fast that during the further travel of the gas element the percentage of heat evolution is commensurate with the percentage of distance traveled within the reaction zone. Somewhere along the temperature gradient in the reaction zone such a point exists, but it is evident from Fig. 2 and Section 1 above that values of the ignition temperature as defined here cannot be obtained from independent experiments on the self-ignition of gases. Nevertheless, this method, with further simplifying assumptions concerning the rate of heat evolution in the various layers of the reaction zone, leads to a simple equation of the burning velocity from which a number of conclusions can be drawn that are in semi-quantitative agreement with the facts.[4]

(b) Spherical Flames

A freely expanding spherical flame is obtained by blowing a soap bubble[7] with an explosive mixture and igniting near the center with a small spark. The strength of the soap film is insignificant; and, except for mixture compositions near the limits of inflammability, the flame is usually fast enough to prevent the formation of disturbing convection currents. The difference, Δp, of the pressure inside the flame and the atmosphere is found from hydrodynamical considerations to be

$$\Delta p = p\frac{3\gamma}{2}\frac{S_b^2}{c_u^2}\left(1-\frac{\rho_b}{\rho_u}\right)\left(1+\frac{\rho_b}{3\rho_u}\right), \qquad (3)$$

where p is the pressure of the surrounding atmosphere, γ the ratio of specific heats of the unburned gas at constant pressure and volume, S_b the speed of flame in space, c_u the velocity of sound in the unburned gas, and ρ_b and ρ_u the densities of the burned and unburned gases, respectively. In carbon monoxide-oxygen mixtures S_b seldom exceeds 12 meters per second. Using a value of $c_u = 330$ meters per second, Δp turns out to be less than 0.25 percent of the pressure of the surrounding atmosphere.

If the flame front is considered to be a geometric surface, which is a justifiable approximation, the mass of unburned gas entering it at any instant may be equated to the mass of burned gas leaving it. Thus

$$\rho_u S_u = \rho_b S_b, \qquad (4)$$

where S_u is the burning velocity. If the slight density changes that occur in the burned gas during the combustion process because of cooling and establishment of thermodynamic equilibrium are neglected, then

$$\frac{S_u}{S_b} = \frac{a^3}{A^3}, \qquad (5)$$

where a is the initial diameter of the soap bubble and A the final diameter of the flame. To measure A and S_b the mid-section of the bubble, preferably along the vertical axis, is focused on a film moving at right angles to it. A triangular flame trace is obtained, the angle of which determines S_b and the base of which, A.

A spherical flame is also obtained on igniting a quiescent mixture at the center of a spherical vessel. If the flame is not too slow, the convective rise of the hot gas is inappreciable, and it remains well-centered in the vessel, arriving at the wall practically simultaneously at all points. This is illustrated in Fig. 3 by a series of successive snapshots taken through a glass sphere. The slight imperfections may be attributed to the ignition rod and inhomogeneities in the glass. As the flame progresses the pressure increases but the flame speed is usually slow enough to insure substantial equalization of pressure throughout the vessel at any instant. In the faster burning mixtures, pressure waves appear toward the end of the process. Maximum pressure is established coincidentally with arrival of the flame at the wall.

In contrast to the case of freely expanding flames the burning velocity may always be expected to increase during the process because as the flame progresses the pressure and the temperature in the unburned gas increases because of adiabatic compression. A peculiar feature of the process is the establishment of a temperature gradient in the burned gas, the

temperature being highest where ignition occurred (at the center) and lowest at the flame surface. This is generally true for local ignition in closed vessels of any shape and may be understood from a consideration of the initial and final stages of the process. At the point of ignition a gas element expands at the initial pressure *Pi* and is subsequently compressed to nearly its original volume at pressures increasing from *Pi* to the final pressure *Pe* as the rest of the gas in the vessel burns. This latter work of compression exceeds the former work of expansion. On the other hand, a gas element near the wall is first compressed from *Pi* to *Pe* and then on burning expands at the pressure *Pe* to nearly its original volume. The latter work of expansion is larger than the former work of compression. Thus, the gas at the wall loses some of its energy while that at the center gains energy in excess of the chemical energy released within it. Calculations show that the difference in temperature between the gas at the center and at the wall always amounts to many hundred degrees centigrade. This has been verified experimentally.[8]

FIG. 6. Shadow photograph of gas stream emerging from a tube.

In deriving quantitative relations between the amount of gas burned, the pressure, and the temperature distribution in the vessel, use is made of the equation of adiabatic compression, the constancy of total volume, and of energy relations.[4, 9] Heat exchange between adjacent elements of gas may be neglected, an assumption consistent with experimental pressure records (see Fig. 4(a)), which show cooling to be a very slow process compared with the combustion itself. The treatment is simplified further by taking the heat capacity of the burned gas as constant and equal to the average value between the lowest and highest temperatures attained by it; a similar assumption is made for the unburned gas. The burning velocity at any instant can be determined from the observed rate of rise of pressure.

The results of the analysis of a pressure record of an explosion of a mixture of 40 percent ozone and 60 percent oxygen in a sphere of 15 cm radius is given in Fig. 4(b).

The high temperature established at the point of ignition toward the end of the explosion provides an explanation for the commonly observed re-illumination of the gas around the ignition source in the later stages of the process, while the gas that burned last remains dark.

(c) Stationary Flames

If an obstruction such as a wire is introduced into a gas stream, eddies or vortices are formed on the downstream side. If the stream is a combustible gas mixture, a flame that ordinarily

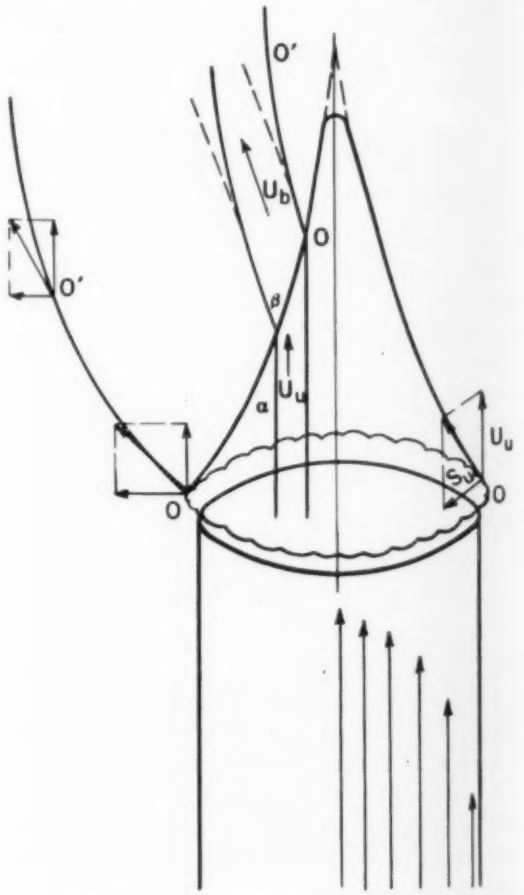

FIG. 7. Diagram of Bunsen-burner flame.

would be carried away by the stream often can attach itself to this zone of turbulent wake behind the obstruction, the downstream velocity of which is much less than that of the stream itself. The wake serves as a fixed source of ignition, maintaining combustion with fresh mixture drawn into it and igniting neighboring gas elements in the stream. The simultaneous movement of the flame to the outer boundaries of the stream and the movement of the stream itself result in the formation of a conical stationary flame front with its apex at the obstruction, as illustrated in Fig. 5. The burning velocity of the mixture in this example is small, and the flame is swept away when the wire is removed.

Another zone of eddies is always formed at the boundary of the stream with the surrounding atmosphere from the rim of the orifice upward. In this zone mixing of the gas with the atmosphere takes place. This zone increases in thickness and the diameter of the stream decreases as the latter moves upward. Fig. 6 is a shadow photograph showing this. Along this zone a flame may travel downward to the rim of the orifice, provided dilution of the gas in the boundary layer has not rendered the mixture noninflammable, as in the experiment shown in Fig. 5. In sufficiently rich mixtures the flame travels downward to the rim where it becomes permanently attached and serves as the base of the well-known Bunsen-burner cone. Fig. 7 is a diagrammatic sketch of a Bunsen-burner flame. Ignition occurs a little above the orifice along the circle 00. From here the flame travels inward with the burning velocity S_u and upward with the gas velocity U_u. The resultant movement of the flame front is along the surface of the cone terminating at the apex. U_u increases from the wall to the center of the tube according to some parabolic distribution indicated by arrows. The shape of the cone can be calculated from knowledge of the flow distribution and the condition that at the surface of the cone the normal component of the gas velocity equals the burning velocity. The latter condition is expressed by

$$\operatorname{ctn} \alpha = \pm \left(\frac{U_u^2}{S_u^2} - 1 \right)^{\frac{1}{2}}, \tag{6}$$

where α is the angle of the direction of the gas

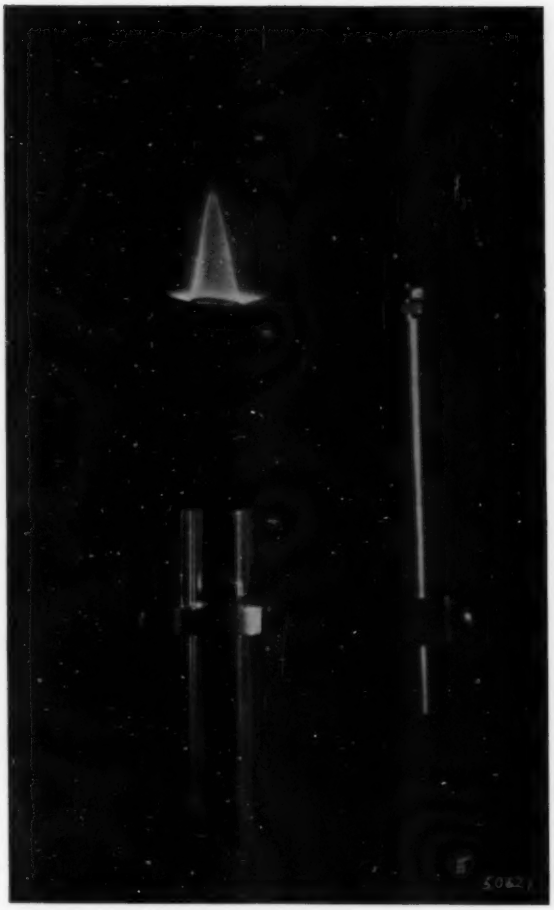

FIG. 8. Flame with ring obstruction in gas stream.

flow with the flame front. The negative sign describes the inverted cone demonstrated in Fig. 5. After passing through the flame front (cone surface) the gas flow undergoes a change in direction described by the equation of continuity

$$\rho_u U_u \sin \alpha = \rho_b U_b \sin \beta. \tag{7}$$

Since the thickness of the flame front is negligible,

$$U_u \cos \alpha = U_b \cos \beta, \tag{8}$$

which on combining with Eq. (7) gives the following simple relationship for the refraction of the gas stream in the flame front.

$$\frac{\rho_u}{\rho_b} = \frac{\tan \beta}{\tan \alpha}. \tag{9}$$

β may be measured by adding fine particles of carbonaceous material to the gas stream, which

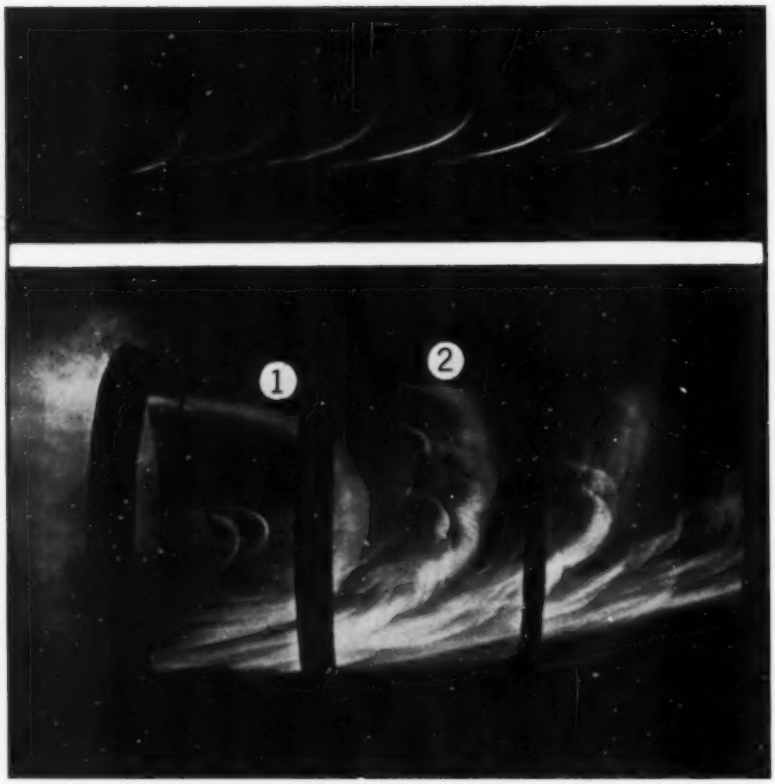

FIG. 9. Successive snapshots of flame of 10 percent CH_4-air mixture. (a) Horizontal propagation of flame in glass tube 5 cm in diameter. (b) Same as (a) in glass tube 24 cm in diameter. (Coward and Hartwell).

become incandescent. α is easily measured and ρ_u is known. It is then possible to determine ρ_b, thus obtaining information concerning the burned gas by comparison with thermodynamically calculated values. To date no use has been made of this method. The flow lines curve upward, as shown by the curves 0 0′, because an element of burned gas on moving away from the axis of the burner finds more room for expansion and thus suffers a decrease of its velocity component normal to the tube axis.

If the burning velocity were constant over the whole area of the cone, the tip would be sharp. However, a gas element at the tip receives heat and atoms and radicals from neighboring elements, thereby increasing its burning velocity, which causes a rounding off of the tip until equilibrium is established. At the highest point of the tip the gas velocity equals the burning velocity.

Although the burning velocity is not constant over the whole area (another disturbance occurs at the base of the cone by intermixing with the surrounding atmosphere), measurements of the total area and total gas flow are used to determine average burning velocities. The results are affected by experimental conditions, such as flow and orifice; but with reasonable precautions the discrepancies are not serious, and the method is a convenient one for comparative studies.

The stability of a Bunsen flame is greater the greater the burning velocity in the boundary layer. The rigidity of the flame increases with flow velocity. Particularly noteworthy for their stability and rigidity are fuel-oxygen torch flames.

If the boundary layer is nonexplosive an upright cone may still be obtained by placing a ring with a diameter smaller than the orifice concentrically within the gas stream, as illustrated in Fig. 8. In slow burning mixtures the flame is not in direct contact with the obstruction. The principle of forming cones by obstructions is used in the Méker burner which can maintain flames with far weaker mixtures than can be used in the Bunsen burner. A cone is formed over each opening of the mesh.

(d) Influence of Vessel Shape and Gas Motion

In vessels whose dimensions do not differ greatly in any direction, such as a cube or a wide short cylinder, essentially the same phenomena are encountered as in spheres, the flame being spherical initially and conforming to the shape of the vessel in the later stages. In tubes, however, a number of new phenomena are encountered. In tubes closed at one end, ignition at the open end frequently results in a flame that travels at a constant rate over some distance,

then accelerates, often giving rise to a vibratory movement, and, if the mixture composition lies between certain limits, ending in a detonation wave. The initial constant rate is found to differ according to the direction of flame travel, being larger for upward than for downward propagation, and to increase with increasing tube diameter. It is frequently difficult to reproduce in successive experiments. The basic cause for the different behavior of flame in tubes compared with spheres and similar vessels lies in the distortion of the flame front induced by the gas flow accompanying flame movement and by pressure waves which are reflected back and forth in the tube. This is illustrated in Fig. 9. Fig. 9(a) shows snapshots of the flame during the period of constant rate. The flame surface retains for a while an approximately constant shape and tilt, but this is not a stable condition. As the flame surface increases because of further distortion the combustion, and therefore the flame travel, is speeded up correspondingly. In 9(b) the same mixture is ignited in a larger tube. The snapshot in position 1 shows an almost hemispherical flame front, which in position 2 has become nodular, corresponding to an accelerated rate of travel. In subsequent positions the flame has become even more tilted and distorted. It has been demonstrated that very high rates of flame travel can be obtained even in normally slow burning mixtures if the tube diameter is large. This is of greatest importance for explosion hazards in confined and even vented passages such as in mines and tunnels. The speed may increase so that the pressure is no longer equalized, a phenomenon referred to as "pressure piling." Thus, it is often found that in disasters the greatest damage is done in a zone farthest from the ignition point.

An example of ignition in a closed tube is shown by the series of successive snapshots in Fig. 10. Ignition spreads from the top of the tube downward initially in the expected regular manner, compressing the unburned gas ahead. As the flame progresses expansion must take place predominantly into the volume occupied by the burned gas in the upper part of the vessel. The resulting gas flow is greatest in the center because of friction at the wall and thus leads to the formation of a cone of increasing steepness, similar to the Bunsen cone.

If the gas is set in turbulent motion as by a fan, the flame area becomes strongly distorted and very fast flames can be produced. This has been made use of in cylinder-head design in internal-combustion engines in order to produce a flame fast enough to keep up with the speed of the engine and to combat knocking combustion.

(e) Detonation

When highly reactive inflammable gas mixtures between certain limits of composition are ignited at one end of a tube, the ends of which

Fig. 10. Successive snapshots of a flame in a closed glass cylinder. Diameter 5 cm, length 19.5 cm. Ignition by spark on top. Moist 9.1 percent $CO-O_2$ mixture. (Ellis).

may be open or closed, the initial slow movement of the flame accelerates rapidly to a high speed which remains constant thereafter, regardless of the length of the tube. While it is possible to

induce temporarily faster flames by means of superimposed powerful shock waves, this constant rate represents the upper limit that a particular gas mixture can maintain. The reaction zone traveling at this constant speed is referred to as the detonation wave. Velocities of 1000 to 3500 meters per second are observed, depending on the gas mixture and independent of the tube diameter if this is larger than a small limiting value.

The formation of a detonation wave can be visualized by considering the mechanism of the formation of an impact wave in a neutral gas in tubes. Consider a long tube closed by a piston (Fig. 11a), and impart a small velocity dw to the latter. This movement produces a weak compression wave in the gas that travels from left to right with the velocity of sound. At a given instant (11b) the gas to the right of the wave is unchanged and at rest, while the gas between the wave front and the piston is compressed adiabatically by an amount $d\rho$ and has a velocity dw. The velocity of the piston is now increased by another increment dw, whereby a second compression wave is produced in the gas (11c) whose velocity is larger than sound velocity in the undisturbed gas since it is traveling in the compressed gas at a higher temperature. By frequent repetition of this procedure the velocity of the piston is brought to the final

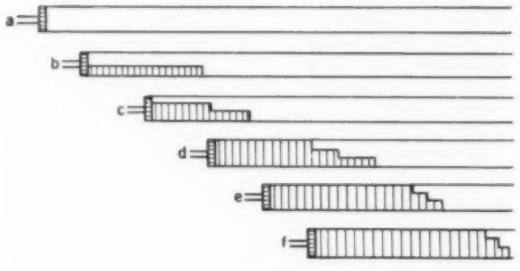

FIG. 11. Diagrammatic sketch of formation of impact wave. (Becker).

velocity w, and there is produced within the mass of gas a steplike set of waves, the particles in the upper step having the velocity w (11d). Since the upper steps have a greater velocity than the lower steps, they will draw together (11e and f). They finally merge to form an impact wave with extremely steep pressure and temperature gradients in its front. If the movement of the piston is continued at the velocity w a column of gas of ever-increasing length is pushed ahead at the same velocity w; work must constantly be performed by the piston in order to compress and set in motion this lengthening gas column; the impact wave forms the head of this column and travels with a constant but greater velocity than the column of gas behind it. To an observer moving with the wave the gas enters it with a velocity u_1 and leaves it compressed at the smaller velocity u_2. w is given by

$$w = u_1 - u_2. \tag{10}$$

If the piston were suddenly stopped, a zone of rarefaction would form at the face of the piston and gradually spread into the compressed gas ahead. The zone of rarefaction would itself have a definite front and would travel as a rarefaction wave pursuing the impact wave, which it would finally overtake. Both would then proceed forward together at decreasing speed and ultimately would degenerate to a sound wave.

If such an impact wave is formed in a highly reactive combustible mixture the extreme conditions in the wave will cause ignition and thus a reaction zone is coupled with the wave. The work for the maintenance of the wave will now be furnished by the expanding flame gases provided the reaction proceeds at a certain minimum rate.

The detonation wave may be initiated in various ways, as, for example, by the shock wave from a charge of high explosive, even if the charge is separated from the combustible mixture by a column of neutral gas. The acceleration of a flame in a tube as described above also ultimately produces a shock wave in a manner similar to the piston. In such experiments it is sometimes possible to induce a detonation wave some distance ahead of the flame. This is illustrated in Figs. 12(a), (b) and (c). Fig. 13 is an analysis of Fig. 12(c). Sometimes several such autoignitions ahead of the flame are observed in regular succession. In such instances there is a deceleration of the flame, probably caused by an insufficient reaction rate; the impact wave travels ahead, and a new ignition occurs within it. In most cases, however, the flame overtakes the train of compression waves ahead, merging them into the detonation wave. An example is given

in Fig. 14(a), (b) and (c), 14(c) being an analysis of 14(a).

In certain mixtures, particularly mixtures of oxygen with carbon monoxide or methane, a striking phenomenon accompanies detonation. A luminous zone appears in the wave front which occupies only a fraction of the cross section of the tube and describes a helical path in the latter along the surface, being able to mark its track in a film of deposited dust particles. Fig. 15 is a photograph showing such a track of spinning detonation traced in a film of lead dust. Fig. 16 is a direct photograph of the track of a spinning detonation wave. This picture is the continuation of the explosion shown in Fig. 12(c) after the stable detonation wave had been set up some 25 cm to the left of the latter picture in which the beginning of the spin is already observable. It shows not only the sinuous track of the spinning flame front (44,300 revolutions per sec.) but also two sets of striae crisscrossing and producing at their crossing points the impression of horizontal bands or "tails" emanating from the troughs of the undulations. This looks as though the detonation consisted of a number of partial explosions following each other with a frequency twice that of the spin. The striae in the forward direction could then be luminous particles traveling forward in the rear of the wave and the striae in the backward direction compression waves traveling against the flowing burned gas.

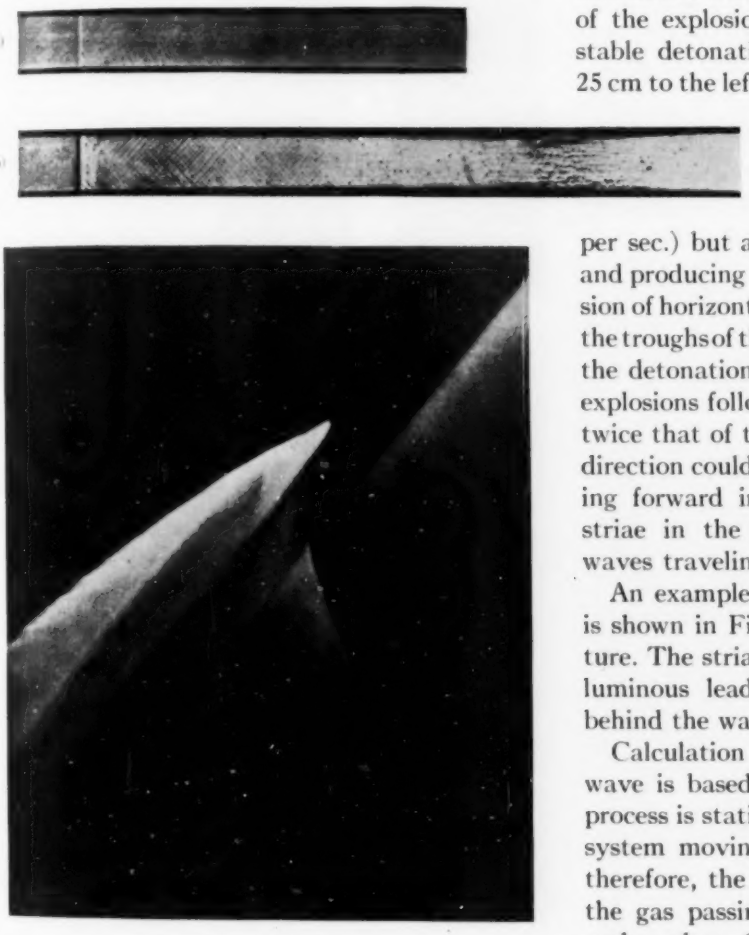

(c)

FIG. 12. Detonation of moist 2 $CO+O_2$ mixture in glass tube of 1.3 cm diameter. (a) Shadow photograph of a compression wave with flame about 1 meter behind it (toward the right and not shown in photograph). (b) Same wave, shortly before ignition, with flame about 10 cm behind it. (The criss-cross pattern is due to strains in the glass.) (c) Direct photograph of track of flame in (a) and (b). Film moving upward; flame moving right to left. Flame enters picture in upper right-hand corner with invisible slower traveling compression wave ahead. Ignition occurs in latter 6.37 cm ahead of flame. In the burned gas compression waves are visible as luminous tracks. (Bone, Fraser and Wheeler.)

An example of a common type of detonation is shown in Fig. 17 for a hydrogen-oxygen mixture. The striae in this instance are produced by luminous lead particles moving with the gas behind the wave front.

Calculation of the velocity D of the detonation wave is based upon the consideration that the process is stationary with respect to a coordinate system moving with the wave front and that, therefore, the masses, momenta and energies of the gas passing through a plane 1 in front of and a plane 2 behind the wave front must be equal. This leads to

$$D=v_1\left(\frac{p_2-p_1}{v_1-v_2}\right)^{\frac{1}{2}} \tag{11}$$

and the difference in internal energy ΔE of the gas in the planes 1 and 2 caused by compression

$$\Delta E=\tfrac{1}{2}(p_1+p_2)(v_1-v_2), \tag{12}$$

where v_1 and v_2 are the specific volumes and p_1 and p_2 are the pressures in the two planes.

Further,

$$\Delta E=\bar{C}_v(T_2-T_1)-\Delta E_c, \tag{13}$$

where ΔE_c is the energy released in the chemical reaction and $\bar{C}_v$ is the mean specific heat of the

burned gas at constant volume between T_1 and T_2. T_2 may be eliminated by the gas law

$$p_2 v_2 = n_2 R T_2, \tag{14}$$

where n_2 is the number of moles per unit mass of the burned gas.

v_1, p_1, T_1, ΔE_c, $\bar{C}_v$ and n_2 are known quantities. Eqs. (11) to (14) do not yet allow a solution because they contain five unknowns, D, p_2, v_2, T_2 and ΔE, but they may be used to construct a so-called Hugoniot curve (Fig. 18) which is the curve of all pairs of values of p_2, v_2 consistent with the known quantities. Point A corresponds to p_1, v_1; point G corresponds to a pressure p_2 obtained by burning the gas adiabatically in its own volume ($v_1 = v_2$), that is $\Delta E = 0$; and point F corresponds to combustion at constant pressure with an increase in volume corresponding to the work done $-\Delta E = -p(v_1 - v_2)$. The part of the curve between G and F is imaginary. In a neutral gas, that is, for $\Delta E_c = 0$ and $n_2 = n_1$, points G and F would merge with A. If B is a point on the Hugoniot curve and α the angle BAp_1, then according to Eq. (11)

$$D = v_1 (\tan \alpha)^{\frac{1}{2}}. \tag{15}$$

The point corresponding to actual detonation must lie on the branch from G upward because it represents an increase in pressure and decrease in volume. According to the generally accepted result this is the point of contact J of the tangent drawn from A. This was first demonstrated by Jouguet and Becker.[10] The former pointed out that point J corresponds to a maximum velocity because above this point any rarefaction wave would overtake and slow down the detonation wave. Becker supplemented this by showing that of the two points B and C, corresponding to a given α, the entropy of the gas is always smaller at C; and since the burned gas, in the moment of its formation, will tend toward the greatest probability in the statistical mechanical sense,

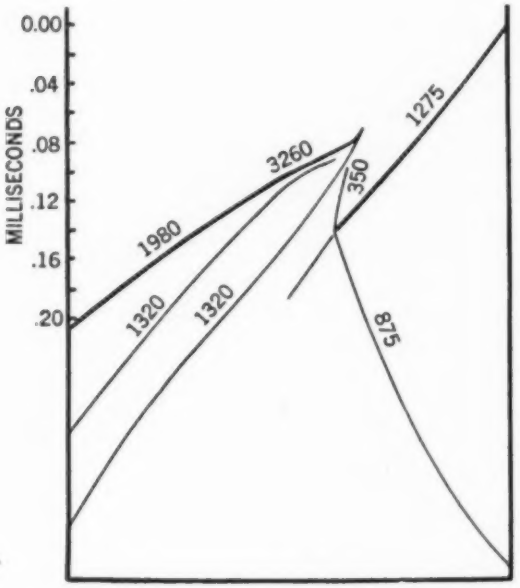

FIG. 13. Analysis of Fig. 12 (c). Flame enters at a speed of 1275 m/sec. At the point of ignition ahead, two new flames start; one moves forward at an initial speed of 2380 m/sec., which quickly rises to 3260 m/sec., and the other at an average speed of 350 m/sec. The latter shortly meets the original flame, giving rise to a compression wave traveling through the burned gas at 875 m/sec. Two other waves are set up, one at the point of ignition and the other just ahead of it, both eventually traveling at 1320 m/sec. The detonation wave slows down and passes out of the picture at a decreasing speed of 1980 m/sec., and eventually reaches its normal constant velocity of 1760 m/sec. This occurs *ca.* 25 cm to the left of the photographed tube section. (See Fig. 16 for later history of the detonation wave). (Bone, Fraser and Wheeler.)

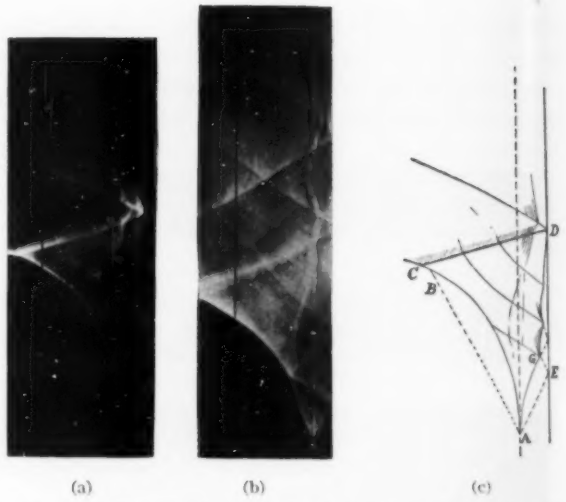

FIG. 14. Direct photographs of development of detonation in glass tubes. (Dixon.) Film moving downward. Ignition at a few inches from right closed end of tube. Flame moves to right and left, accelerating rapidly toward the left. Compression waves are visible in the burned gas. (a) 33 percent $C_2N_2 - O_2$ mixture. (b) 16.6 percent $CS_2 - O_2$ mixture. (c) Analysis of (a). From ignition source A two compression waves AE and AB travel through the unburned gas. AE is reflected at end of tube E and at the flame front G, slowing down the latter; this recurs several times. The compression wave EG is refracted at the flame front G, travels through the burned gas and overtakes and accelerates the flame front AC. It is again reflected at this point; cf. (b) The detonation wave develops at C near the point where the flame front meets the compression wave AB; at the same time, a recoil or "retonation" wave CD travels through the burned gas.

i.e., greatest entropy, it will tend to reach point B. The result is that the detonation wave, being mechanically unstable above J and thermodynamically improbable below J, will only find

FIG. 15. Helical path traced by spinning detonation wave in glass tube covered with lead dust. (Bone and Fraser.)

it possible to travel with a speed corresponding to point J. A different proof has been given by Scorah[11] who showed that at point J the wave proceeds at that speed which allows the greatest degradation of each unit of energy supplied to the wave, which makes point J the stable one from thermodynamic principles.

The theoretically calculated velocities of the detonation wave agree very well with the observed values.[4] This also applies to the flow velocity w of the gas behind the wave front, which can be measured from the path of luminous particles behind the wave front (see Fig. 17); w is given by the equation

$$w=(v_1-v_2)\left(\frac{p_2-p_1}{v_1-v_2}\right)^{\frac{1}{2}}, \qquad (16)$$

which is derived from the equations for conservation of mass and momentum.

While the mechanism of spinning detonation is not clear, a discontinuous progress of detonation can be visualized according to Becker as follows. A detonation wave started at point B of the Hugoniot curve will decrease in velocity to the normal detonation wave at point J. It may be possible that the reaction velocity suffices for the forced detonation at B but not for the normal one, the temperature and pressure being higher than at J. Under such circumstances the detonation would generally be terminated on approaching J. If now the termination point would be at a comparatively small distance above J it is conceivable that detonation ceases for a short moment but that the impact wave arising from the still rather fast reaction starts a new detonation a short distance ahead of the flame front, which again soon ceases and the process is repeated. This would be a rhythmic repetition of the process shown in Fig. 12(c).

(f) Diffusion Flames

If a flame is formed between the atmosphere and a stream of fuel gas, the process which determines the rate of combustion is the diffusion of the two gases into each other. The theory of such flames can therefore be given, without regard to reaction rates, purely on the basis of diffusion equations. In such an investigation which has been carried out by Burke and Schumann,[12] experiment and theory have been found to be in satisfactory agreement with regard to the size and shape of the flame as a function of gas flow, type of orifice, temperature, gas composition and concentration gradients of combustion products and fuel gas in the flame.

Diffusion flames are probably the most common type of combustion, the flame of a

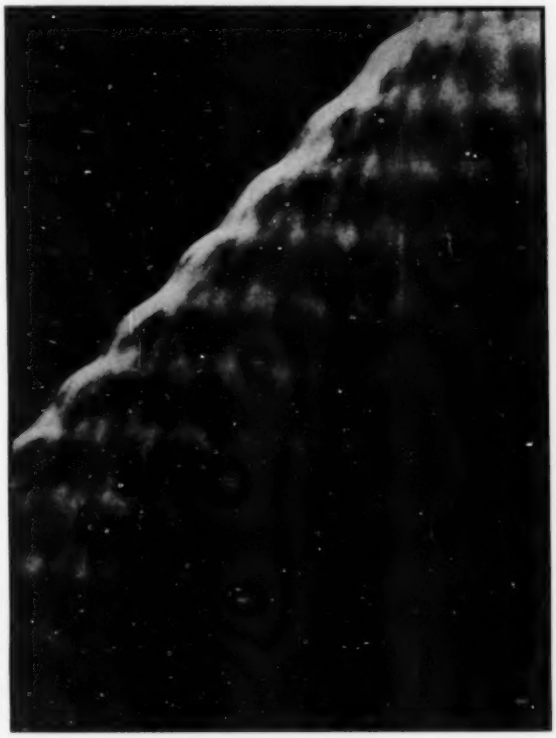

FIG. 16. Direct photograph of track of spinning detonation wave. Film moving upward, flame entering at upper right. See text for explanation. (Bone, Fraser and Wheeler.)

match or a candle being excellent examples. The reader is referred to the original paper for the mathematical treatment. Diffusion flames of hydrocarbons and air have found industrial application because they provide large surfaces

of intense radiation from the incandescent carbon formed in the flame.

4. State of the Burned Gas

Calculated explosion pressures* using energy contents and equilibrium data determined from band spectroscopy generally agree rather well with experimental explosion pressures determined in spherical vessels with central ignition. However, with some diluent gases, notably excess oxygen and nitrogen, pressures exceeding the theoretical by several percent are found which are outside the experimental error. In such cases,

FIG. 17. Direct photograph of detonation wave in $5H_2+O_2$ mixture. Film moving upward, flame moving from right to left. Speed of wave *ca.* 3500 m/sec. Striae are luminous lead particles moving with the gas behind the wave front. Note reflection of the wave at closed end of tube at the left and reversal of direction of the lead particles. Black strips are paper markers wrapped around tube. (Lewis and Friauf.)

therefore, thermodynamic equilibrium is not attained everywhere in the gas at the end of the explosion; there exists a momentary excess of translational energy and a corresponding deficiency of internal energy which is probably mostly confined to vibrational degrees of freedom. As the flame progresses the effect should die out in the central portions of the burned gas, and at the end of the explosion it should be strongest in the layers of gas close to the wall. If the rate of decay of the excess translational energy has a temperature coefficient it is conceivable that in mixtures having sufficiently low flame temperatures the decay in the central portions of the burned gas is slow at first and becomes very rapid in the later stages of adiabatic compression which, as mentioned above, increases the core temperature by several hundred degrees. The rapid decay can accelerate the volume shrinkage in the core and thus increase the mass movement of the gas and give rise to pressure waves. Such pressure waves are always observable in weak mixtures containing excess oxygen or nitrogen within certain concentration limits. An example is shown in Fig. 19. It is observed that the pressure waves begin long before maximum pressure is established during a period of comparatively slow rate of pressure rise. The absence of pressure waves in the much faster explosion shows that the pressure waves are not the result of flame movement *per se*. The temperature of this explosion being higher, the decay of excess translational energy occurs rapidly in the core already in the early part of the explosion. If the nitrogen in the two explosions is replaced by oxygen, the record of the fast explosion remains practically unchanged, but the pressure waves in the slow explosion now become so violent, start-

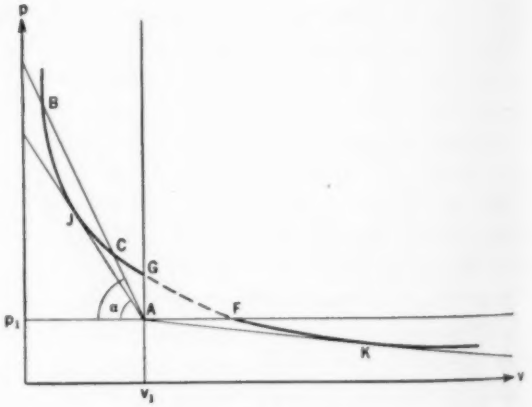

FIG. 18. Hugoniot curve.

* For method and details consult reference 4.

ing very early, that it is impossible to obtain a record and the recording system may be damaged.

In a number of investigations of flame temperatures using the sodium line-reversal method, temperatures higher than the theoretical have been measured.[4] Since the D levels of the sodium atom are excited by collision it is reasonable to assume that this effect is again caused by the momentary excess of translational energy.

5. *Incomplete Rotational Excitation in Diatomic Gases at Ordinary Temperatures and Pressure*

Some recent studies of flame propagation in closed vessels indicated that the adiabatically compressed unburned gas surrounding the flame attained a temperature higher than that corresponding to its normal specific heat and that it was necessary to assume that during the period of compression the rotational degrees of freedom did not receive their full amount of energy corresponding to equilibrium. This was verified[13] by rapidly compressing gases like oxygen, nitrogen, and carbon monoxide and measuring the change of volume and pressure with time. For an increase of pressure from 1 to 1.2 atmospheres in compression times ranging from 7.5 to 12 milliseconds deficiencies of rotational excitation ranging from 33 to 20 percent, respectively, were found depending on the rate of compression. For argon, on the other hand, the theoretical specific heat was found. This excitation lag effect had already been observed earlier for vibrational degrees of freedom in experiments with sound waves at room temperature. However, whenever rapid gas compressions occur, such as in internal-combustion engines, the above compression experiments show that not only the vibrational but also the rotational lag must be taken into account.

FIG. 19. Time-pressure records of explosions in hydrogen-air mixtures. Slower explosion, 15 percent of hydrogen; pressure waves start early in the explosion. Faster explosion, 20 percent of hydrogen.

We are indebted to the Cambridge Press for permission to reproduce a number of photographs and figures.

Bibliography

1. A. O. Allen and O. K. Rice, J. Am. Chem. Soc. **57**, 310 (1935).
2. H. C. Campbell and O. K. Rice, J. Am. Chem. Soc. **57**, 1044 (1935).
3. Rice, Allen and Campbell, J. Am. Chem. Soc. **57**, 2212 (1935).
4. B. Lewis and G. von Elbe, *Combustion, Flames and Explosions of Gases* (Cambridge University Press, 1938).
5. An attempt has been made recently by H. G. Landau (Chem. Rev. **21**, 245 (1937)) using simplifying assumptions among which is the independence of reaction rate on temperature.
6. N. R. Tawde and J. M. Patel, J. Univ. of Bombay 6, 29 (1937).
7. F. W. Stevens, Nat. Adv. Comm. Aer. Rep. No. 176 (1923); J. Am. Chem. Soc. **50**, 3244 (1938). E. F. Fiock and C. H. Roeder, Nat. Adv. Comm. Aer. Rep. No. 532 (1935).
8. B. Hopkinson, Proc. Roy. Soc. **A77**, 387 (1906); G. Rassweiler and L. Withrow, S. A. E. J. **36**, 125 (1935).
9. Flamm and Mache, Wien. Ber. **126**, 9 (1917); H. Mache, *Die Physik der Verbrennungserscheinungen* (Leipzig, 1918).
10. Cf. R. Becker, Zeits. f. Physik **8**, 321 (1922); Zeits. f. Elektrochem. **42**, 457 (1936).
11. R. L. Scorah, J. Chem. Phys. **3**, 425 (1935).
12. S. P. Burke and T. E. W. Schumann, Ind. Eng. Chem. **20**, 998 (1928).
13. B. Lewis and G. von Elbe, J. Chem. Phys. **7**, 197 (1939).

Other references to figures.

14. O. C. Ellis, Fuel, **7**, 247, 502 (1928).
15. H. F. Coward and F. J. Hartwell, J. Chem. Soc., 1996 (1932).
16. H. B. Dixon, Phil. Trans. Roy. Soc. **A200**, 315 (1903).
17. B. Lewis and J. B. Friauf, J. Am. Chem. Soc. **52**, 3905 (1930).
18. Bone, Fraser and Wheeler, Phil. Trans. Roy. Soc. **A235**, 29 (1936).
19. W. A. Bone and R. P. Fraser, Phil. Trans. Roy. Soc. **A228**, 197 (1929).

Recreating Geological History with Models

The Experimental Study of the Earth's Crustal Deformations

BY MILTON B. DOBRIN

Gulf Research & Development Company, Pittsburgh, Pennsylvania

Subjected to tremendous forces that act from the interior, the thin outer crust of the earth gives evidence of having suffered intense deformations throughout geological time. Because of the complexity of these movements, it is often impossible to deduce their mechanisms by the use of ordinary physical concepts.

Dimensional analysis shows, however, that the rigid rocks of the earth's crust deform, on their own large scale, in much the same way that very soft, plastic materials deform on a much smaller scale. This fact has been utilized with interesting results in the design of scale models to represent the formation of many observed geologic features such as mountains, ocean basins, and salt domes.

Introduction

IN the classification of knowledge, geology is listed among the natural rather than the exact sciences. However, there are many phases of the subject which can be studied to advantage through the application of physical principles. Since it is the province of geology not only to describe the present configuration of the earth's crust but also to trace the movements which gave rise to it, there have been many geologists who have invoked the principles of mechanics to solve their problems. Inasmuch as the mechanical phenomena involved in the earth's deformation are exceedingly complex, the experimental study of them has proved more fruitful than theoretical analysis.

The nature of the problems that would be encountered in such a study can be readily observed by examining the present condition of the earth's outer crust. The greater portion of the rocks that constitute it gives evidence of having undergone some degree of deformation or distortion. Originally laid down by sedimentary deposition through the agencies of water or wind, the strata which cover the granite foundations of the continents exhibit convolutions and fractures which testify to a continuous mobility within the earth. In some places these movements have resulted in spectacular topographic features such as mountain ranges and rift valleys. In others, a gently rolling, soil-covered surface may give no indication of intricate flexures in the sedimentary layers a few thousand feet below. There are canyons, however, where the incisive action of swiftly running water has laid bare the geological history of the past hundred million years; and along their walls one can often see the results of extensive folding and warping in the exposed strata.

The fact that these hard, rigid rocks have been stretched, compressed, crushed, sheared and bent points unquestionably to the existence of tremendous forces within the earth's crust. To postulate the nature of these forces by studying the visible evidences of the movements they have caused, the science of structural geology has been evolved. Since it deals essentially with the deformation of solid materials under stresses of various kinds, structural geology is fundamentally a study in the mechanics of deformable bodies. On this basis it should be theoretically possible to explain all observable geological structures by direct application of the principles of elasticity and plasticity to rock materials.

However, one need not search far to find geologic structures which seem to have been formed in violation of all mechanical laws. There are numerous regions where originally flat strata composed of rigid materials, which could be scarcely bent at all without breaking under ordinary circumstances, are folded to an extent almost beyond belief with *no apparent evidence of fracture whatever*. To reconcile these structures with everyday physical conceptions, the sug-

gestion has been offered that these deformations took place when the sediments were buried under several miles of overlying formations, so that the pressure of the overburden caused the rocks to bend under stress without rupture. While it has been demonstrated by the classic experiments of Adams[1] and Bridgman[2] that the ability of rocks to yield by plastic flow increases somewhat at high pressures, there are too many examples, particularly in the Jura Mountains of Switzerland, of strong folding in formations which geologists claim could not possibly have been buried under the requisite depth of sediments to make this explanation tenable.

Another problem which has thus far defied all attempts at solution by mechanical reasoning is that of the formation of the Alps. For three-quarters of a century some of the world's most able geologists have studied the fossils and stratigraphy of this region and on the basis of their observations have deduced what crustal motions must have taken place to account for the apparent structure of this mountain system. According to their concept, thick sheets of folded and fractured sediments were forced out of the earth and thrust forward for as much as a hundred miles over the surrounding country, resulting in a succession of the so-called overthrust faults which characterize the region. The extent of this action can perhaps be realized from the fact that such lofty peaks as the Matterhorn and the Weisshorn are remnants of the heads of such overthrust sheets. Erosion has carved the sheets into discontinuous masses of land, so that these mountains are separated by miles from their roots, resting on the surface over which the sheet was originally thrust. The mechanical difficulties of reconciling this manner of yielding to stress with the properties of materials established in the laboratory have baffled all students who have made the attempt. Even Albert Heim,[3] the great Swiss geologist who spent all his life unraveling the complex structures of the Alps, admitted that he had not succeeded in conceiving the mechanics of the overthrusting. But the evidence for it was so overwhelming that he had no alternative but to accept the concept and seek and wait for the understanding.

If we accept the postulate that the established laws of mechanics hold for geologic movements as well as for any other kind, we must conclude that materials of very large dimensions acted upon by forces exerted over very long periods of time do not exhibit the same behavior that small samples of the same material would exhibit when tested in the laboratory. While it has not been possible to make direct observations of geological movements which have required millions of years to take place, direct evidence exists that stresses exerted over a long time produce in many cases an entirely different kind of deformation from that caused by similar stresses acting only for a short period. For example, a century or more ago it was the custom to lay tombstones horizontally, mounting them on stone pillars at the ends. Today, many of these stones display a

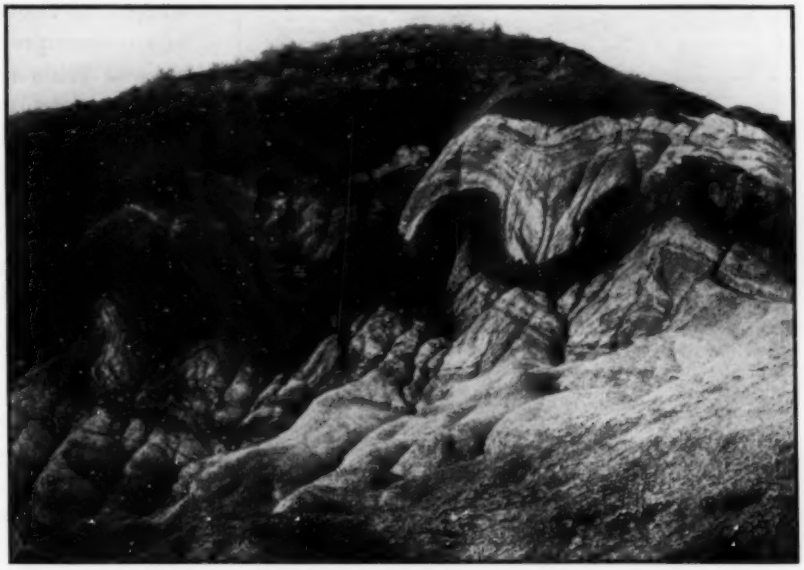

FIG. 1. Outcrop in the bad lands around Steveville, Alberta, which shows the great folding which has taken place in geological formations. Courtesy of the *Oil Weekly*.

pronounced sag in the middle, indicating that plastic flow has evidently taken place under the action of the tombstone's weight. The most notable example, perhaps, is a marble stone in Rock Creek Cemetery in Washington, D. C., that has sagged three inches at the center in 85 years: The bending of marble slabs was investigated experimentally by Lord Rayleigh[4] who, bearing geological applications in mind, measured the permanent elongation and inelastic flexure of samples baked in an oven at various temperatures. Bingham and Reiner[5] have shown that bars of cured cement mortar about one inch square by 33 inches long bend appreciably at the center when supported at their ends for only a few months. The time factor would be even more significant in determining how rocks in the earth's crust deform over millions of years.

Geologic Scale Models

The dynamics of geologic movements presents too many complications to be readily amenable to theoretical analysis, although several notable attempts[6] have been made to develop a mathematical theory of mountain building and basin formation by treating strata as elastic, homogeneous beams and making other simplifying, but sometimes questionable, assumptions. Our conceptions, therefore, of what actually takes place in the formation of mountains, basins, flexures, faults, and other geological features are embodied in several diverging hypotheses of a qualitative sort which have been propounded by geologists. Since it has, of course, been impossible to test these hypotheses by direct experimentation, the small scale dynamic model has been widely used for some time as the most promising substitute.

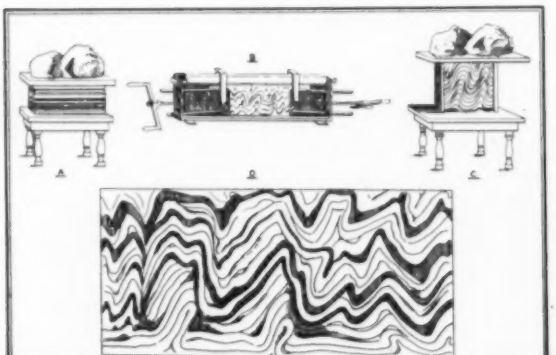

FIG. 2. The earliest recorded geologic model experiment, performed in 1812 by Sir James Hall. Layers of cloth were used to represent the sedimentary strata. A. Cloth weighted down to represent gravitational effect of overburden. B. Apparatus for compressing layers in operation. C. Layers convoluted by compression. D. Enlarged cross section of folded layers.

The earliest of the important papers on structural geology, read by Sir James Hall[7] before the Edinburgh Royal Society in 1812, describes a model experiment. Hall conjectured that the convolutions of the strata exposed along the Berwickshire cliffs of Scotland were caused by horizontal compression; and he proved this to his own satisfaction by laying a large number of pieces of cloth on top of one another to represent the strata and observing that when he pushed the opposite edges of the mass together he obtained folds of the same shape as those he had seen recorded in the rocks.

Almost half a century ago, Bailey Willis[8] investigated the mechanics by which the Appalachians were formed, making use of experiments with a model. Inside a box about a meter long he compressed alternating layers of beeswax mixed with plaster of Paris to represent the stronger beds and beeswax mixed with Venice turpentine to represent the weaker ones. Above these layers he spread lead shot to simulate the weight of the overlying sediments. Upon sufficient compression, the various wax layers showed folds and convolutions bearing a surprising resemblance to those which geologists had mapped after extensive field work in the Appalachian region.

Numerous subsequent workers have obtained interesting results with dynamic models. Tokuda[9] laid a piece of rice paper over some soft paste, pushed on the paper with his thumb and obtained a pattern that looks remarkably like a relief map of the Appalachian or the Jura Mountains. L. L. Nettleton[10] has illustrated his fluid mechanical theory of salt-dome formation by a model in which the sedimentary rocks are represented by a very thick syrup and rocksalt by heavy crude oil. Hans Cloos[11] experimented with models made of soft mud and obtained miniature structures closely resembling real ones observed in the field. Most recently, David Griggs[12] of Harvard constructed a model which supports the theory that

mountains are formed by the action of what may be called convection currents in the substratum below the earth's crust. This viscous medium was represented by water glass and the crust itself by a thin layer of mixed sand and machine oil. The convection currents were simulated by revolving drums toward one another inside the water glass. By varying the speed of the drums, Griggs was able to create many of the characteristic features of the world's mountain ranges.

It appears paradoxical that in all these experiments the materials of the earth's crust are represented not by rocks or substances of comparable strength, but by soft, weak materials ranging from beeswax to syrup. If the results of such experiments are to be accepted as valid it must first be proved that the relationships between the characteristics of the original material and those of the model material can be justified physically. Fortunately, a set of objective principles has been developed for analyzing the quantitative relationships that must obtain between a dynamic model and its prototype. For more than half a century these principles have guided designers of models to represent waterways, boats, airplanes, and static engineering structures. By the application of them it has been possible to derive information from measurements in wind tunnels and towing tanks that has been of inestimable value for the design of aircraft and ships. The theoretical background has been derived mainly from a branch of physics known as dimensional analysis.

However, it has been only recently that this analysis, so long in use by the engineer, has been applied to the study of geologic models, although some pioneering work in this direction, which, by the way, received little notice at the time, was done in 1912 by Koenigsberger and Morath.[13] In 1935, Maillet and Blondel[14] made some application of this method in devising a model of the earth; while, more recently, M. King Hubbert[15] of Columbia University published the most complete paper that has yet appeared on the subject. Unfortunately, as Hubbert shows, the principles of dimensional analysis have been frequently violated in the design of geologic models and consequently the majority of such model experiments have been of questionable value.

Dimensional theory enables us to derive quantitative relationships between the physical properties of the model and the corresponding ones of the original. That the apparent characteristics of any body ought to vary as its size varies can be illustrated qualitatively by considering a familiar example. In *Gulliver's Travels*, Jonathan Swift imagined a race of people, called Brobdingnagians, whose linear dimensions were of the order of ten times the corresponding dimensions of ordinary human beings. In the story, these giants were constructed of the same materials

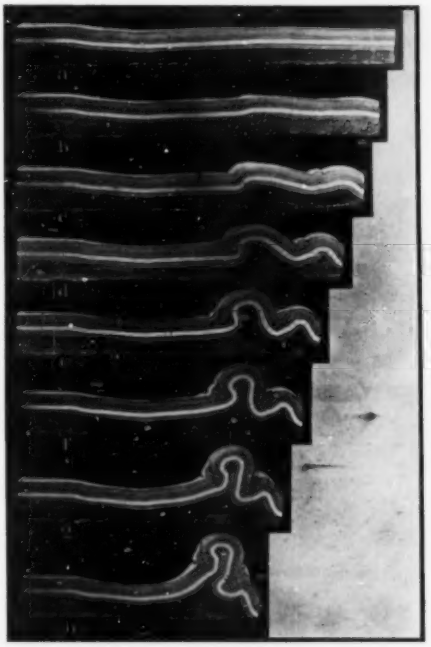

FIG. 3a. Various stages of mountain folding as represented by a model made by Bailey Willis in 1893. Courtesy of Bailey Willis.

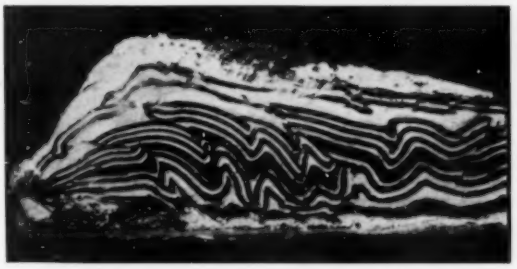

FIG. 3b. An example of the ability of Willis' model to produce in a wax model realistic mountain folding by compression.

as ordinary sized people and carried on their lives in just the same way; but an analysis of the situation might leave us cause to wonder whether they really could.

A typical Brobdingnagian, ten times as tall and ten times as broad as one of us, would have a volume a thousand times as great, and with the same density should weigh a thousand times as much. To support this weight, however, he would have available only a hundred times the cross-sectional area of bone; and hence each square inch would have to bear ten times the load. Since the strength of a structure is measured by the force per unit area that it can bear without yielding, it would either be necessary for the bones of these giants to have been built of a material with several times the strength of our bones, or else they would have to have been of

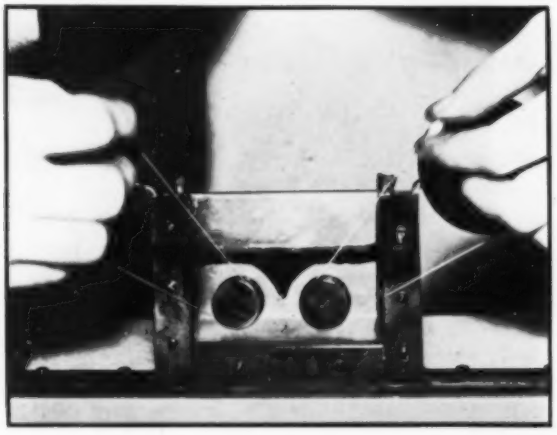

FIG. 4. Model illustrating formation of mountains by action of convection currents (simulated by rotating drums) in viscous substratum (water glass) beneath earth's crust (mixture of sand and machine oil). Courtesy of David Griggs.

greater diameter in proportion to their length, thus departing from Swift's original conception of geometric similarity to ordinary humans.

Conversely, if some hypothetical Brobdingnagian satirist were to conceive of a race whose representatives are of our own size, he might just as easily fall into the error of endowing its members with bones and muscles of such strong materials that they would be able to support loads which no actual human weight lifter ever attempted. In other words, he would fail to allow for a proper reduction in the strength of his model, just as many geologists have failed to observe similar considerations in building small scale models of geologic structures.

Principle of Dynamic Similarity

A correct scale model of any physical system must not only be geometrically similar to its prototype; but, in addition, the physical characteristics of the model must be such that the forces, motions, and deformations are similar as well. Dynamic similarity is the principle specifying the conditions that must be satisfied in order that all motions and deformations in the original be correctly represented by corresponding motions and deformations in the model. There are two such conditions. First the mass of each volume element in the model must bear a constant ratio to that of the corresponding volume element in the prototype. This ratio will be designated by μ. Secondly, all forces acting upon the model must individually and collectively bear a constant ratio to the corresponding forces acting upon the prototype. In practice, this will mean that the various types of force that act on the original must be represented in the model by forces of the same type that correspond in direction and in relative magnitude. For models of solid bodies we must consider separately the gravitational, inertial, and elastic forces. With models of systems containing fluids there may be, in addition to gravitational and inertial forces, viscous resistance and forces caused by hydraulic pressures. To illustrate, let us consider the problem of representing the acceleration of a boat by an experiment with a geometrically similar model in a towing tank. In this case there is the force of gravity (bouyancy); there is the resistance of the water to the boat's motion; and there is the inertial force, a fictitious force equal and opposite to the mass times the acceleration, by which the rest are balanced. Dynamic similarity requires that the ratio of the gravitational forces acting, respectively, on the model and on the prototype be equal to the ratio of the two inertial forces and equal also to the ratio of the two viscous resistances. If it is impossible to satisfy all of these conditions simultaneously in the model, the validity of the experiment will be in doubt.

To put these relationships into their most useful form, the various kinds of force are expressed in terms of quantities associated with the system that are directly measurable. It is at this stage of the procedure that dimensional analysis enters.

Dimensional Analysis

If any physical magnitude is determined, not by direct measurement, but by measurements upon other quantities, we ordinarily obtain its value by substituting the measured values of the primary quantities, as they are called, in some mathematical formula. If, by two separate sets of measurements on primary quantities in two different but similar physical systems, we determine two corresponding values for the secondary quantity, as the one in which we are mainly interested is called, this formula should give the same ratio between the two absolute magnitudes of the secondary quantity, no matter what units we use to express the primary quantities. Bridgman[16] shows that this will be the case only if the formula employed can be expressed as a constant multiplied by arbitrary powers of the primary quantities. The exponents indicating these powers are defined as the dimensions of the secondary quantity in the respective primary quantities associated with it.

Thus, a velocity, which is measured by dividing the number measuring a certain length by that measuring a certain time, has the dimensional formula LT^{-1}. An acceleration, the time rate of change of velocity, has the dimensions LT^{-2}; and a force, mass times acceleration, is expressed dimensionally as MLT^{-2}. The choice of primary quantities to be used in a dimensional formula is in no way restricted to the arbitrarily defined fundamental units of the English or metric systems, such as mass, force, length or time. Any measurable magnitude, such as density, viscosity, electric charge, or temperature, may be employed for this purpose.

Model Ratios

From Bridgman's relation it is evident that the ratio of any two values of a secondary quantity can be expressed as the product of the ratios of the primary quantities raised to the powers indicated in the dimensional formula. In dealing with dynamic models we make use of this fact to obtain ratios between the physical properties of the model and the corresponding properties of the prototype from the ratios of readily measurable primary quantities of the model and the prototype. Following Hubbert, let us designate all ratios of primary quantities in the model to the corresponding ones in the original by the Greek letter equivalents of the English symbols representing their dimensions. Thus, the scale factor of length (the ratio of corresponding lengths in the model and its original) is λ; that of time (the ratio of the time required for a motion in the model to the time required for the corresponding motion in the original) is τ; the ratio of mass is μ. It follows that the model ratio of velocity will then be $\lambda\tau^{-1}$; of acceleration $\lambda\tau^{-2}$; of force $\mu\lambda\tau^{-2}$, etc.

Ratio of Elasticity

If we should construct a model of a system where only elastic and inertial forces are important (a steel wire in vibration would be such a system), it would be necessary to calculate the correct elastic modulus of the model material in terms of the linear and other reduction factors. In the case under consideration, we apply the criterion that the elastic force, dimensional formula EL^2 (where E is the dimension of elasticity) in the model must bear the same relationship to the elastic force in the prototype that the inertial force, with dimensions MLT^{-2}, in the model bears to that in the prototype. Expressing the two model ratios by the dimensional symbols written in Greek letters, equating them, and solving for ϵ, we find that the model ratio of elasticity becomes $\mu\lambda^{-1}\tau^{-2}$. Now the dimensions of elasticity are the same as those of stress, since both are measured by a force divided by an area. Moreover, the elastic strength, measured usually by the stress at which the elastic limit is reached, also has the dimensions of stress. Therefore, the model ratios worked out for ϵ apply equally to stress, modulus of elasticity, and elastic strength.

For the case where an equilibrium is reached between the elastic and gravitational forces so that the system is either static or else has negligible acceleration, a different expression can be

derived for the elasticity. A static structure would be an example of such a case. The ratio of the elastic forces must here be equal to that of the gravitational forces to satisfy the criterion of dynamic similarity. The model ratio of gravitational attraction is $\mu\gamma$, where γ is defined as the ratio of the acceleration of gravity for the model to that for the prototype. This latter ratio, for experiments conducted on the earth's surface, does not deviate from unity by any significant amount. Hence, by setting $\epsilon\lambda^2$, the model ratio of elastic force, equal to μ, we find that the ratio of elasticity is now $\mu\lambda^{-2}$ or $\delta\lambda$, where δ, the ratio of the densities, can be expressed as $\mu\lambda^{-3}$.

For a model whose material has the same density as that of the original, the elastic modulus, as well as the elastic strength, must therefore be reduced by the same ratio as the linear reduction factor, λ.

Ratio of Viscosity

The same reasoning is applied to obtain the model ratio of viscosity both for the general case where accelerations exist and for the static case. The dimensional formula for the viscosity coefficient follows from its definition as the force exerted by viscous drag per unit area per unit velocity gradient. However, if we wish to consider the viscosity a primary quantity, of dimension H, we can express the force of viscous resistance by the dimensional formula HL^2T^{-1}. The corresponding model ratio is $\eta\lambda^2\tau^{-1}$.

The case where inertial forces and viscous forces predominate is frequently met with in engineering problems, such as in the flow of fluids through pipes. The criterion of dynamic similarity requires that the viscous forces in the model and original must bear the same ratio to one another as the inertial forces. We can therefore equate the model ratios for the two types of force and solve for the model ratio of viscosity. This is $\mu\lambda^{-1}\tau^{-1}$.

Where static equilibrium exists between viscous and gravitational forces, such as in the case of a body falling at a constant speed in a viscous liquid, we set the model ratio of viscous force equal to that of gravitational force, μ. The ratio of viscosity obtained by solving this equation is $\mu\lambda^{-2}\tau$ or $\delta\lambda\tau$.

Reynolds Number

By applying the principles of dynamic similarity to the case where viscous and inertial forces act with a somewhat different choice of primary quantities, one obtains one of the most important relations in modern fluid mechanics,

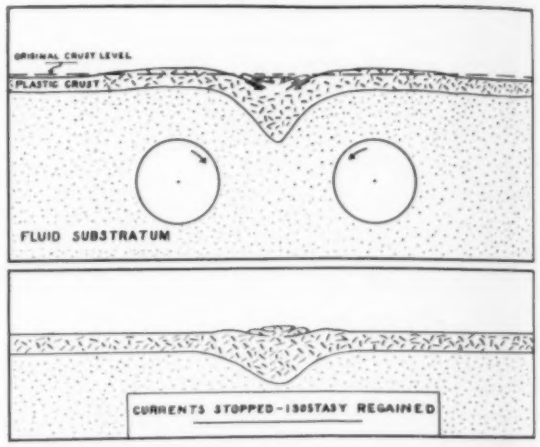

Fig. 5. Diagram illustrating action of Griggs' model of mountain formation by convection. Root of mountain pulled down into viscous substratum by convection currents. After currents have stopped, mountains rise to restore isostatic equilibrium.

the formula for a dimensionless constant called Reynolds number. Using velocity, LT^{-1}, as a primary quantity instead of time, we can transform the dimensions of viscous force to HVL, and those of inertial force to MV^2L^{-1}, or DL^2V^2, where D is the dimension of density. The ratio of these forces can be written dimensionally $LV/(H/D)$. By the principles of dynamic similarity this must be a constant. When numerical values are substituted for L, any characteristic length; V, the velocity of the fluid; and H/D, the kinematic viscosity of the fluid, the ratio is known as Reynolds number.

It is Reynolds number that sets the conditions that must be observed in conducting experiments on model airplanes in wind tunnels. As long as its value is the same for the model and the prototype dynamic similarity is observed and the behavior of the model in the tunnel will be a reliable indication of the performance of the actual airplane built according to the same design. If the model should be constructed on the scale of 1 : 10 with respect to the original, the

velocity of the air in the tunnel must be ten times that of the airplane, or else a gas or liquid of one-tenth the kinematic viscosity (viscosity coefficient divided by density) must be used, in order to keep Reynolds number the same for both cases. In some wind tunnels the kinematic viscosity is lowered by compressing the air to raise its density.

Acceleration under Gravity

For a system where acceleration takes place in the presence of gravitational forces, the model ratios of length and time can no longer be chosen independently of one another. For, if we equate the model ratio of inertial force, $\mu\lambda\tau^{-2}$, to that of gravitational force, μ, we obtain

$$\mu\lambda\tau^{-2}=\mu, \quad \lambda=\tau^2.$$

With a geological model experiment such a restriction upon our choice of reduction factors can be exceedingly cumbersome. For example, if a geologist constructed a model to a scale of 1 : 100,000 of an original structure which is believed to have formed by a series of accelerative movements over a period of ten million years, he would have to entrust his experiment to the continuous care of a hundred future generations of geologists to be sure that the results will be correct. The reason can be seen from the relationship above. With a scale constant, λ, of 10^{-5},

Table I.

Quantity	Model Ratio General Case	Model Ratio Static Case
Stress Elastic Modulus Elastic Strength	$\mu\lambda^{-1}\tau^{-2}$	$\mu\lambda^2$ or $\delta\lambda$
Viscosity Coefficient	$\mu\lambda^{-1}\tau^{-1}$	$\mu\lambda^{-2}\tau$ or $\delta\lambda\tau$
Density	$\mu\lambda^{-3}$	

the corresponding value of τ would have to be $10^{-2.5}$ and the time required to represent a deformation occurring in 10,000,000 years would have to be 3160 years. Fortunately, most geological movements take place at a very slow and constant speed so that the accelerations are negligible and inertial forces do not control the conditions of similarity.

In recapitulation, the model ratios thus far derived which are of importance in the design of geologic models are shown in Table I.

Application to Geological Models

Using these and other model ratios, Hubbert has worked out the mechanical properties of the materials from which geological models of various kinds should be constructed. Sometimes, as he points out, it may be difficult or impossible to obtain materials having all the requisite properties. But even where this is the case, it can often clarify our conceptions of geological movements if we can figure out just what these properties should be.

Mountain Formation

It is probable that the majority of all geological model experiments on record have been carried on to illustrate theories of how mountains are formed. On account of the highly divergent nature of the theories that, according to their proponents' claims, have been proved by various model experiments, one cannot help but be suspicious of the validity of any of them. Fortunately, dimensional analysis affords a reliable criterion for determining the plausibility of any such experiment.

Since mountains are formed with negligible acceleration, except for occasional earthquakes, we can calculate the strength that the model material representing the earth's sedimentary rocks should have from the model ratio of elastic strength for the static case. To do this it is necessary to know the strength of the original mountain material. This quantity is not known with any degree of certainty, for although the elastic strength of rocks at and near the earth's surface has been measured in testing laboratories, we know that the ultimate strength of rock increases with increasing depth because of the higher pressure, but decreases with the increased temperatures that are met with at any considerable depth. However, the error is not likely to be great if we consider the ultimate strength of the mountain material to be the same as that of granite, which is 2×10^9 dynes/cm^2.

If the model material is specified to have the same density as that of the original, then δ is unity and the model ratio of strength, ϵ, is the same as that of linear reduction, λ. A convenient size for a model representing a mountain range 100 kilometers long would be 100 centimeters, in

which case λ, and hence ϵ, would be 10^{-5}. The model would thus have to be constructed of a substance with a strength of $10^{-5}\times 2\times 10^{9}$ or 2×10^{4} dynes/cm^2. Such a material would be very weak. Vaseline, or very soft clay, would have a strength of this order of magnitude, and

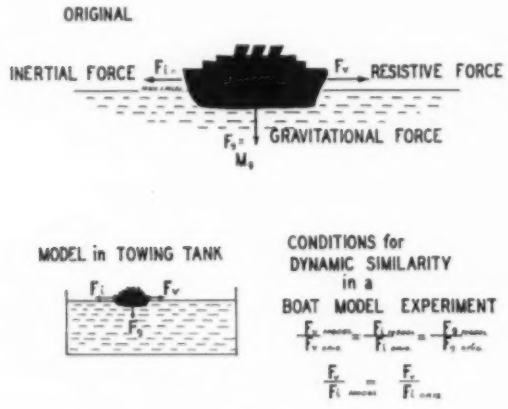

FIG. 6.

hence should constitute the proper material for an experiment on mountain building.

In his experiment to illustrate the formation of mountains by the action of convection currents in the fluid substratum underlying the outer crust, Griggs[12] has used dimensional analysis to choose the proper materials for his model and to determine the correct time and velocity relationships. The model ratios of length, strength, density and viscosity were so chosen that the model is dynamically similar to the earth's crust. When these are chosen the time and velocity ratios are fixed. Two models have been built, one 24 inches long, the other three inches. In the larger an event requiring a million years is reproduced in one minute. In the smaller, the same process may be represented in one second. The drums are used merely to simulate the convection currents that are believed to exist, in the substratum, it being impossible to reproduce these currents by thermal means in a model of this size.

SALT DOMES

Along the Gulf Coast of the United States, in Rumania, and in Persia, great plugs of rocksalt up to several miles in diameter have pushed their way up through thousands of feet of sedimentary rock, forming dome shaped masses whose tops often come within a short distance of the earth's surface, even piercing it in some places. Along the flanks of these salt domes and in the sediments directly above them, the strata have become so distorted by the intrusion of the salt that they form excellent traps for oil. Indeed, many of the world's great oil fields are located over or against domes of this type. The problem of just how salt domes form has never been completely solved. However, several hypotheses have been proposed to explain their occurrence, and the most generally accepted is the mechanical theory of Nettleton,[10] based on the concept that the domes were formed by viscous flowage of the salt and the sediments under gravitational forces only. As stated before, he has illustrated this theory by a model experiment.

Offhand, it might appear absurd that rocksalt could ever flow as a viscous fluid; but considerable evidence has accumulated through observations in the laboratory and elsewhere that many rigid materials deform by plastic or elastico-viscous flow under the action of great stress, or even of a small stress over a very long period of time. According to Nettleton's hypothesis, the salt was originally in horizontal beds buried far

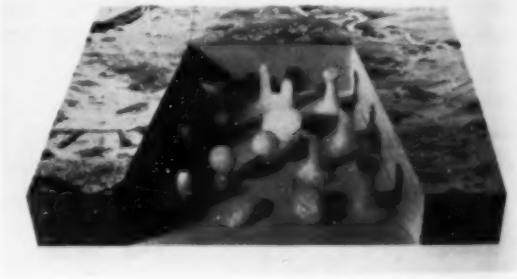

FIG. 7. Silhouette photographs taken from Nettleton's model.

below the earth's surface. The diagrams illustrate how the material rose from these beds to its present position. After an initial uplift of one portion of the bed, at C', caused possibly by a buckling of the salt layer under compressive forces, a differential pressure was set up in the salt between points B and C. This was a consequence of the difference in the weights of the overlying masses at those two points, since the

density of the salt, ρ_s, is less than that of the sediments at this depth. The differential pressure gave rise to a lateral flowage of salt from B to C, which caused the surface at B to sink and that at C' to rise. As the salt dome thus began to take form, the differential pressure increased and the process continued until the supply of salt from below was exhausted.

In the model that illustrates this theory, the salt is represented by heavy crude oil of density close to unity and the overlying sediments by a thick syrup of density about 1.4. In the apparatus

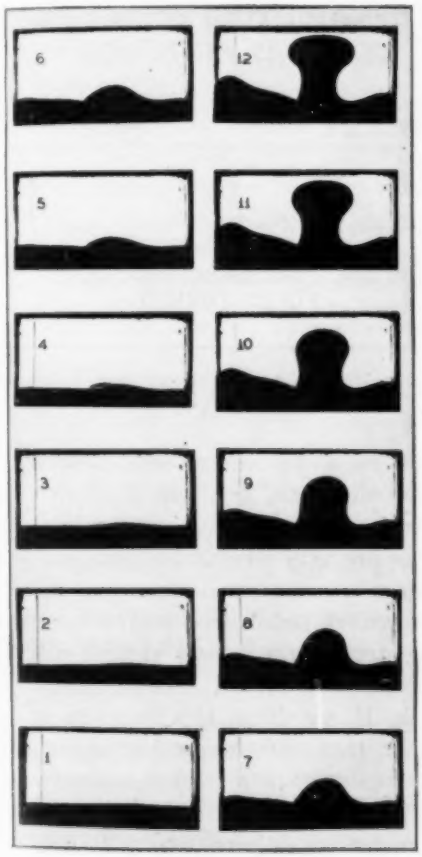

FIG. 8. Stages in the formation of a miniature salt dome in Nettleton's model.

the syrup is above the layer of oil. This is an unstable condition, on account of the lower density of the oil, and if an initial uplift is made in the layer of oil a column of it will rise up through the syrup, simulating the postulated action of the rocksalt.

Hubbert considers the problem of relating the physical properties of these model materials with those of the original salt mass and overlying sediments, on the basis of dimensional theory. The constants of interest are the viscosity of the rocksalt and the shearing strength of the sediments. This would be a case of viscous flow where equilibrium exists between bouyant forces acting upwards and viscous resistance acting downwards. For it we can use the model ratios of viscosity and elastic strength applying to a static system. These are $\delta\lambda\tau$ for viscosity, and $\delta\lambda$ for shearing strength.

Gutenberg[17] has tabulated values for the viscosities of a number of solids, as determined in the laboratory. For rocksalt he gives a value of 2×10^{18} c.g.s. units at 18°C and 2.5×10^{17} c.g.s. units at 81°C. Geologists can tell us the order of magnitude of the time required for the domes to rise; it is something like 60,000,000 years. And enough information has been obtained from drilling around salt domes to delineate the shapes and dimensions of a large number of them. The model ratios λ and τ can be readily obtained from these data and from observation of the time necessary for a model dome to form; and the requisite viscosity of the model material representing the salt can be computed by use of the model ratio for viscosity. The value obtained by Hubbert for this is 5×10^{2} c.g.s. units, which is of the same order or magnitude as the viscosity of the crude oil actually used to represent the salt. Hubbert concludes that of all models of salt domes, Nettleton's comes closest to being dimensionally correct.

Impacting Meteorite

Using similar reasoning, Hubbert designs a model experiment to determine the nature of the hole made by a falling meteorite upon hitting the earth's surface. By making appropriate assumptions about the elastic constants of the earth and the speed of the meteorite, he finds that the impact could best be represented by shooting a lead-amalgam pellet about five millimeters in diameter with a velocity of 350 meters per second into a barrel of soft clay. The effect would be about the same as that of firing a shot-gun into a mud bank. In this case, each shot makes a hole about as large as a man's fist. If such an experi-

ment is a correct representation, we might conclude that the huge crater in Arizona, 4000 feet in diameter, where a meteorite is believed to have struck several thousand years ago was created by a projectile only one-tenth that size.

Conclusion

These are but a few examples of how dimensional theory can be applied to models of geologic interest. It would appear from the foregoing analysis that most of the well-known experiments with such models have had the common defect that the materials representing the sediments of the earth's crust have been too strong. Bailey Willis, in his experiments on Appalachian type structures, realized that the strength of his strata should be less than that of the original; nevertheless, he failed to make them sufficiently weak. As a result, he found it necessary to load down his beeswax and plaster layers with enough buckshot to represent a sedimentary overburden a hundred miles thick. Actually, he was achieving dynamic similarity by exaggerating gravitational forces in the same measure in which elastic forces were being unwittingly exaggerated. Even then his more competent beds yielded by fracturing rather than by folding. Had he used a weaker material than beeswax or plaster, this excessive loading would not have been necessary.

In a number of model experiments, notably those of Mead[18] and R. T. Chamberlin,[19] the earth's crust has been represented by layers of paraffin and plaster, materials which dimensional reasoning shows to be much too strong. However, the results thus obtained did not seem to bear much resemblance to any structures actually observed in nature.

It is noteworthy that all models in which structures have been produced bearing a strong resemblance to those seen in the field have been made of the softest and weakest materials imaginable. Tokuda used paste; Cloos, soft mud; and Griggs, a mixture of sand and machine oil, to represent the earth's crustal rocks; and all three obtained an uncanny similarity to observed geologic or topographic features. This is just what would be expected from the results of dimensional analysis.

Thus, as Hubbert points out, we reach a resolution of the paradox of an earth whose

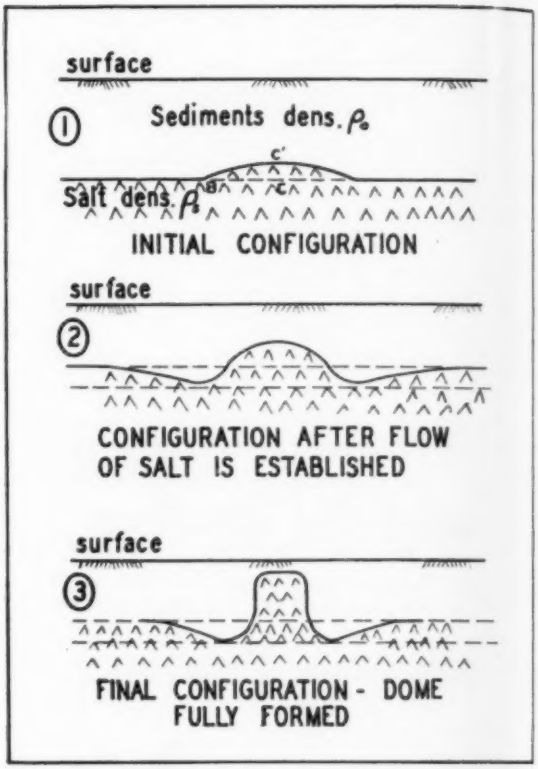

FIG. 9. Model showing the salt dome formations in an East Texas oil field.

materials by all laboratory tests seem to possess enormous strength, but which shows deformations that could only have taken place in materials that are very weak. Strength and weakness are only relative terms, possessing no absolute significance. A small specimen of any material may be strong, but a large sample will deform, under sufficient stress, like a much weaker material. If we bear this fact in mind and remember that the stresses acting within the earth's crust are of almost inconceivable magnitude, it is no longer difficult to understand how strong rocks can deform, like taffy, by intricate folding, or how the Alps were created by the squeezing of great sheets of rock over the surrounding country, in the same way that tooth paste is squeezed out of a tube over a brush.

An analysis on the basis of dimensional considerations, while indispensable in the design of model materials, has a more general applicability to geological problems. By the use of it we are able to bring both the large and the small structural features of the earth's crust to a size at

which we can conveniently visualize them. It is difficult for anyone to reason objectively on any mechanical system of a larger size than his field of vision can cover. And when, consciously or unconsciously, the geologist reduces vast areas to the size of a table model in his imagination, he is liable to arrive at entirely erroneous conclusions if he does not also visualize his model to possess the physical properties corresponding to his scale of reduction. Maillet and de Ceccatty[20] have examined various structural theories bearing in mind correct dimensional concepts. They reach the conclusion that most of these theories are of little validity because they were not formulated with proper regard to dimensional theory.

It has not been long since physics and geology joined hands and the science of geophysics evolved. Although geophysical methods have been widely employed to study the subcrustal constitution of the earth and to outline the structures near the earth's surface in the search for oil and precious minerals, it has seldom been applied in more than a rough, qualitative way to study the structural mechanics of the earth's deformations. A real opportunity exists, therefore, for further work in the quantitative study of structural geology. The use of dimensional and structural analysis to accomplish this end presents one more almost untraversed frontier for applied physics, one which can be widened to the mutual advantage of both sciences.

Acknowledgments

The author wishes to express his appreciation to the following members of the Geophysics Division of the Gulf Research and Development Company for their help in the preparation of this article: to Dr. E. A. Eckhardt, Mr. G. B. Lamb, Mr. C. H. Dresbach and Dr. L. L. Nettleton for reading the manuscript and offering valuable suggestions; and to Mr. J. L. Scott for assisting with the drawings. He is indebted also to Professor Bailey Willis, of Stanford University; Dr. David Griggs, of Harvard University; Mr. Warren L. Baker, Editor of the *Oil Weekly*; and Dr. Nettleton for the loan of illustrations.

Bibliography

1. F. D. Adams, "The Action of Differential Pressure on Certain Minerals and Rocks," J. Geol. **18**, 489 (1910).
2. P. W. Bridgman, *The Physics of High Pressure* (Macmillan Company, 1931). "Shearing Phenomena at High Pressure of Possible Importance to Geology," J. Geol. **44**, 653 (1936). "Reflections on Rupture," J. App. Phys. **9**, 517 (1938).
3. Albert Heim, *Die Schweiz* (Tauchnitz, 1921) Vol. II, 1, p. 30.
4. Lord Rayleigh, "The Bending of Marble," Proc. Roy. Soc. London **144**, 266 (1934).
5. E. C. Bingham and Markus Reiner, "Rheological Properties of Cement and Cement Mortar-Stone," Physics **4**, 88 (1933).
6. Ross Gunn, "A Quantitative Study of Mountain Building on an Unsymmetrical Earth," J. Frank. Inst. **224**, 19 (1937).
7. Sir James Hall, "On the Vertical Position and Convolutions of Certain Strata and Their Relation with Granite," Trans. Roy. Soc. Edinburgh **7**, 79 (1815).
8. Bailey Willis, "The Mechanics of Appalachian Structure," U. S. Geological Survey 13th Annual Report, part 2 (1892–93), p. 231.
9. Bailey Willis and Robin Willis, *Geologic Structures* (McGraw-Hill, 1934), third edition, pp. 480–482.
10. L. L. Nettleton, "Fluid Mechanics of Salt Domes," Bull. Am. Assoc. Petrol. Geologists **18**, 1175 (1934).
11. Hans Cloos, "Artificial Mountains," Nat. u. Mus. Senckenbergische Naturforschende Gesellschaft, part 1, 225 (1929); part 2, 258 (1930).
12. David Griggs, "Convection Currents and Mountain Building," Bull. Geol. Soc. Am. **49**, 1884 (1938). Abstract of paper given at 51st Annual Meeting, New York.
13. G. Koenigsberger and O. Morath, "Theoretical Foundation of Experimental Tectonics," Zeits. Deutsch. Geol. Gessell. **65**, 65 (1913).
14. R. Maillet and F. Blondel, "On Similitude in Tectonics," Bull. Soc. Geol. France, [5] **4**, 599 (1934).
15. M. King Hubbert, "Theory of Scale Models as Applied to the Study of Geological Structures," Bull. Geol. Soc. Am. **48**, 1459 (1937).
16. P. W. Bridgman, *Dimensional Analysis* (Yale University Press, 1931) revised edition, p. 21.
17. Beno Gutenberg, *Handbuch der Geophysik*, Vol. 2, part 1 (1931), p. 539.
18. Warren J. Mead, "Notes on the Mechanics of Geologic Structures," J. Geol. **28**, 505 (1920).
19. Rollin T. Chamberlin, "The Wedge Theory of Diastrophism," J. Geol. **33**, 755 (1925).
20. R. Maillet and R. P. de Ceccatty, "The Physicist Looks at Tectonics," *Second World Congress of Petroleum, Paris, 1937*, Vol. I, Sec. I, p. 383.

Resumés of Recent Research

Phase Diagram of Na-K Alloys at High Pressures

The familiar phase diagrams, which describe the thermodynamical equilibrium between the phases which appear on mixing several components, are concerned with only two quantities; namely, temperature and composition. Largely because of difficulties in experimental technique, the fundamentally important variable, pressure, has not been given much consideration. C. H. Kean,[1] working at Harvard University, succeeded in mapping out the three-dimensional phase diagram of alloys of sodium and potassium covering the pressure interval, 1–10,000 kg/cm².

His experimental technique was simple and direct. An alloy of known composition was placed in a glass tube into which convenient wires had been sealed and then placed in a high pressure chamber held at a fixed temperature. The relative resistance was measured as a function of pressure. Usually, discontinuities of the first derivative, or discontinuities of the resistance occur which were associated with two-phase and three-phase equilibrium, respectively. He found the phase diagram to consist essentially of three surfaces on which two phases were in equilibrium. Through two lines of intersection of these surfaces were found two developable surfaces which represented the equilibrium between three phases. Without exception the five surfaces increased along the temperature axis as the pressure increased. All phases found were identified with phases existing at atmospheric pressure.

Two interesting properties of the alloys were manifest in the experimental work. Resistance measurements of the liquid phase gave strong indications that the minimum of resistance at high pressures appeared to be a property of the liquid alloys as well as the pure metals. Also, the appearance of one phase was brought about only by a pressure hundreds of kg/cm² above the true equilibrium pressure and the amount of excess pressure varied according to the previous history of the alloy.

[1] C. H. Kean, Phys. Rev. **55**, 750 (1939).

Measurement of Reverberation Time

The methods and apparatus that have been used in the past for the measurement of reverberation time, or more specifically for the measurement of the rate of decay of sound energy in a room, provide many combinations of convenience, flexibility, precision, and cost. Their applications vary from measurements in reverberation chambers, where precision is of utmost importance, to surveys of occupied rooms, where speed and convenience of operation are the principal considerations. Although it is not to be expected that any one system will be ideal for all applications, the need for a simple, portable, precise, inexpensive, direct-reading instrument has been felt for some time.

Apparatus which is an approach to this ideal has been developed by W. M. Hall of the Department of Electrical Engineering at the Massachusetts Institute of Technology.*

In this instrument, two relays which operate at predetermined sound levels start and stop the charging of a condenser through a resistance. The time interval required for the sound to decay from the first to the second level determines the voltage built up on the condenser. This time interval is read directly on a meter. The rate of decay of sound energy in a room can be determined by a single reading of this sort, or a plot of the decay of sound can be made by changing the level at which the second relay operates and

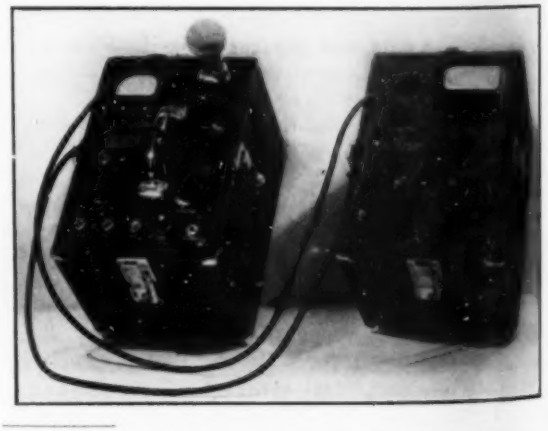

* W. M. Hall, J. Acous. Soc. Am. **10**, 302 (1939).

repeating the measurement of the time interval. The unit is battery-operated, and is thus made independent of any external power supply, timing element, or sound source. An interlocking mechanism prevents improper operation of the relays, and a simple calibrating means is provided.

Advances in the Application of Radioactivity for Geological Age Measurements

It is well known that practically all terrestrial materials contain at least measurable traces of the parent radioactive elements, uranium, actino-uranium and thorium. The accumulation of the decay products, helium and radiogenic lead, resulting from the slow, spontaneous disintegration serves as a means of estimating the time which has elapsed since crystallization of the rock or mineral in which the radioactive elements occur.

In the last quarter century a fairly complete time scale, extending over most of the recognized range of geological time, has been built up on this basis. During the development of a direct, physical method for measuring the helium and radioactive content of igneous rocks, a serious discrepancy was discovered when these new observations were compared with the published ages of rocks from the same geological horizons. A cooperative investigation, with two independent methods of measurement, was undertaken to determine the source and magnitude of these differences. The results of these researches have been reported in detail[1] recently and indicate that a large downward revision of ages in the helium time scale is necessary. The radium determinations involved in most of the earlier helium ages have been shown to be incorrect by more than a factor of two. However, an uneven revision in the helium time scale must be made, because rocks vary widely in the relative proportion of helium produced by the thorium and uranium series.

The recording section of Evans' apparatus used in establishing precision radium standards at low concentrations. Left to right, control panel a.c. operated through Telechron driven switch, camera for photographic recording, and double, temperature-controlled housing for string-electrometer.

[1] R. D. Evans, C. Goodman, N. B. Keevil, A. C. Lane and W. H. Urry, Phys. Rev. **55**, 931 (1939).

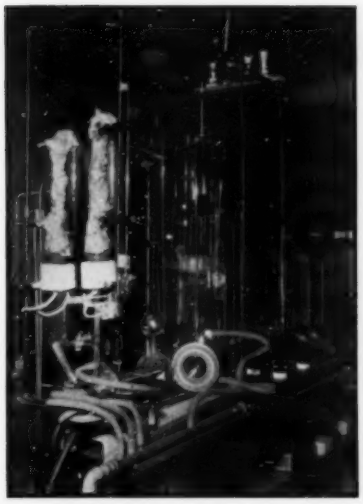

Direct-fusion helium apparatus showing water-cooled vacuum furnace in foreground with purification and measuring apparatus in background.

Not only in connection with age measurements but also in a large share of the numerous determinations of the radioactivity of terrestrial materials reported in the literature, too little attention has been given to the reliability of the standards and techniques employed. As a result, much of the research on the radioactivity of rocks cannot be considered quantitative. In order to place this important phase of geophysics on a firmer foundation, an international intercalibration program has been initiated under the joint sponsorship of the National Bureau of Standards and the National Research Council, Division of Physics. The purpose of this program is to provide reliable standards, both in the form of solutions and as analyzed rock samples, for the various investigators throughout the world. By referring all measurements to this common basis, it should be possible to obtain a more accurate estimate of the radioactivity of the various rock types comprising the earth's crust.

A New Million-Volt X-Ray Outfit

By E. E. Charlton, W. F. Westendorp, L. E. Dempster and George Hotaling

Research Laboratory, General Electric Company, Schenectady, New York

I. Introduction

THIS new x-ray unit incorporates some of the features of the early 800-kv peak[1] and of the more recent 500-kv peak[2] outfits. In the main, however, it is so radically different from them as to merit a rather detailed description.

It consists of a low frequency resonance transformer with a coaxially mounted multi-section x-ray tube within, both contained in a grounded steel tank and employing compressed gas insulation. The x-rays are generated from a target mounted in the end of an extension chamber projecting out from the bottom of the grounded tank.

The most attractive features of this type of outfit are its compactness, simplicity, reliability and freedom from exposed high voltage together with the ready accessibility of the target.

II. The Transformer

The transformer shown in Figs. 1 and 2 has a low voltage coil (12) of flat copper strip and a high voltage coil (11) consisting of 120 thin flat sections spaced apart for ventilation.

In order that the x-ray tube may be placed within the coils to facilitate making connections from suitable voltage taps to the various tube electrodes, and to get for the tube the benefit of the electrostatic shielding thus afforded by the transformer, no iron is used within the latter.

The lower end of the high voltage coil is grounded, and, to shield the upper high voltage end, a hemispherical radially slotted brass spinning is used.

The number of turns chosen for the high voltage winding is such as to make its natural period of oscillation 180 cycles per second, a frequency obtained from the 60-cycle, three-phase power supply lines through the intermediary of a static frequency tripler unit.

To avoid the energy loss which would ensue were the magnetic flux of the transformer to penetrate the surrounding steel tank, the latter is provided with an inner lining (1) consisting of narrow overlapping strips of silicon steel electrically insulated from one another, and at the bottom with a ring of similar strips.

The multi-section high voltage coil serves a quadruple purpose, to generate the voltage, grade the potential so as to prevent creepage over the solid dielectric between coils, to electrostatically shield the x-ray tube from the grounded tank and to mechanically support the hemispherical shield.

III. The X-Ray Tube

The tube envelope (Figs. 1 and 3) consists of eleven sections of molded Pyrex glass tubing sealed to Fernico rings which carry the intermediate accelerating electrodes, of stainless steel.

The cathode spiral consists of 6½ convolutions of 8.5-mil tungsten wire mounted in the electrostatic focusing cup (6). The tube is supported by a metal flange bolted to the grounded metal tank. This flange has been copper-brazed to the Fernico ring which is sealed to the bottom glass section of the tube. An exhaust manifold is bolted to the tube envelope with metal gaskets.

The target (17) of copper-backed tungsten is mounted in the lower end of the extension chamber and both the target and the walls of the extension chamber are water cooled. The metal flange on the extension chamber is bolted to the exhaust manifold of the tube envelope with metal gaskets.

IV. The Exhaust System

This consists of an oil diffusion pump (22) backed up by a rotary oil pump (25). Apiezon oil has been used in the diffusion pump. Oil vapors are kept from the tube by the charcoal trap (21) placed directly over the diffusion pump.

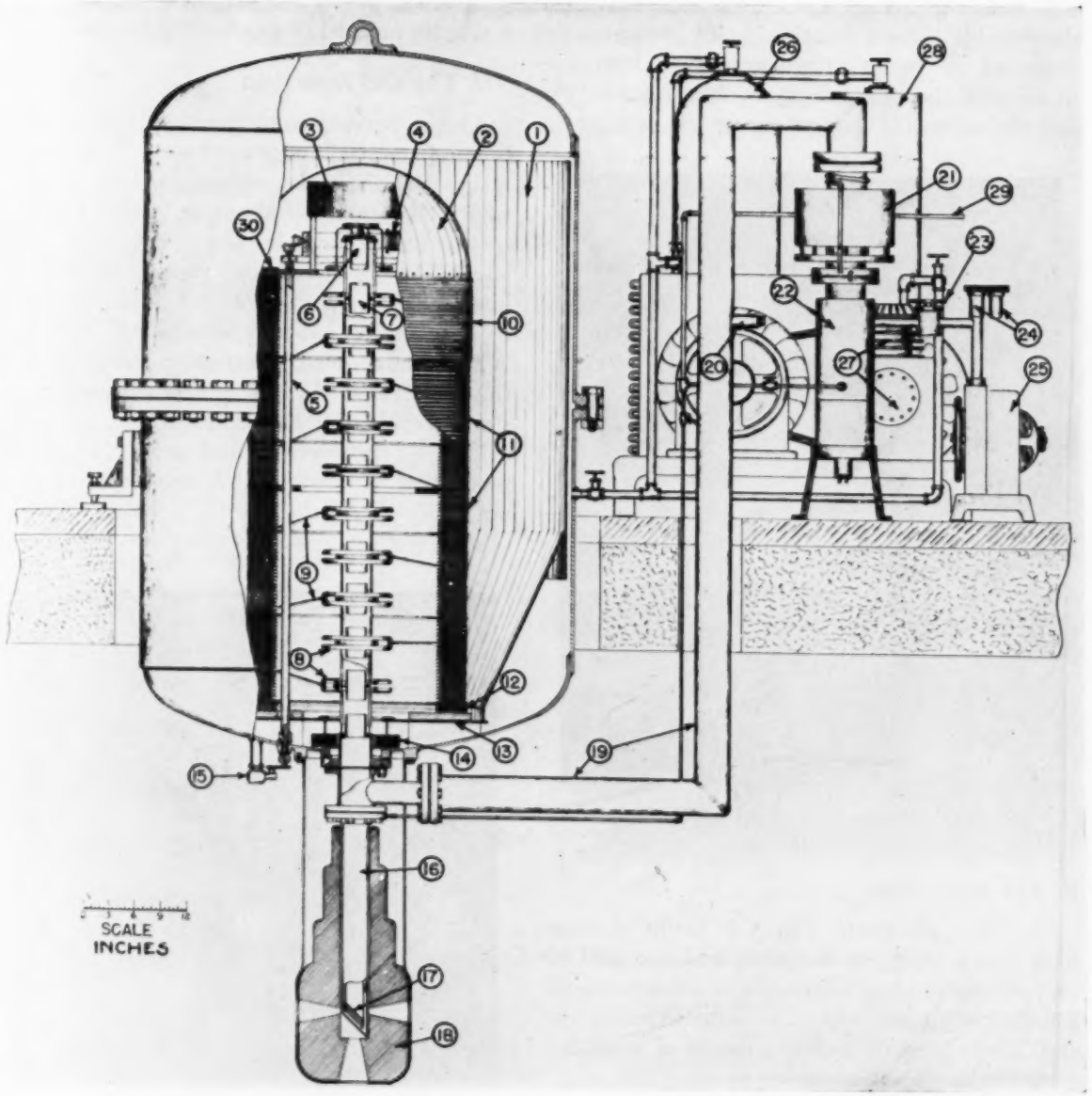

1. Laminated steel shell
2. Slotted brass shield
3. Lead shield
4. Variable reactor
5. Insulating shaft
6. Cathode assembly
7. First intermediate electrode
8. Shields around the seals
9. Tapleads
10. Secondary coils with copper-tube shields
11. Secondary coils
12. Primary winding
13. Laminated steel bottom
14. Focusing coil
15. Filament control motor
16. Extension chamber with waterjacket
17. Target
18. Lead shield
19. Vacuum line
20. Ionization gauge
21. Charcoal trap
22. Oil diffusion pump
23. Vacuum shut-off valve
24. Hale-Pirani gauge
25. Rough vacuum pumps
26. Freon supply tank
27. Freon compressor
28. Freon storage tank
29. Cooling water inlet, drain omitted
30. End-turn filament-coil

FIG. 1. Drawing of million-volt x-ray outfit.

The charcoal in this trap can be baked out when desired by Calrod heating units permanently mounted in metal tubes extending into the interior of the charcoal mass. Pirani-Hale (24) and ionization (20) gauges record the vacuum.

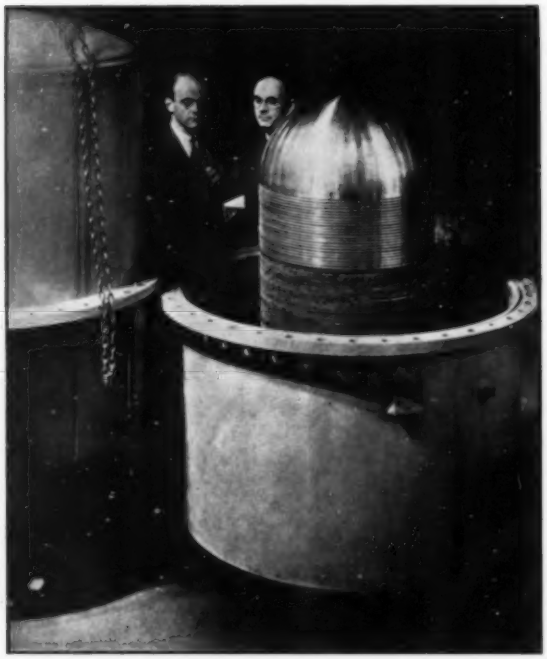

FIG. 2. Million-volt resonance transformer.

V. The Steel Tank

The tank shown in Fig. 4 is made of sheet steel $\frac{3}{8}$ inch thick, 48 inches in diameter and 80 inches long and has been tested to a pressure of 200 lb. per square inch. The joint between the two halves is made tight by means of a rubber gasket bolted between heavy flanges.

VI. X-Ray Protection

To provide x-ray protection a lead shield (18) with an equivalent wall thickness of five inches has been used around the extension chamber. A lead disk (3) placed back of the cathode inside the hemispherical cap is used to absorb the x-ray beam which passes back through the axis of the tube. The small dimensions of the outfit permit this amount of primary protection to be provided with about 1000 lb. of lead. Lead shot can be used in place of cast lead for this same protection with an increase of about 35 percent in volume. In certain instances it may provide a simpler method of mechanical handling.

VII. The Gas Insulation

This is derived from the supply tank (26) of liquid dichloro-difluoro methane, "F-12." Before filling, the air is first exhausted from the main tank to a vacuum of about 28 inches. The valve to the supply tank is then opened and heat is applied to the latter until enough gas has been liberated to raise the pressure in the main tank to about 40 lb. gauge, when the valve is closed. When it subsequently becomes necessary to open the main tank, the gas is first returned to the storage tank (28) by means of the compressor (27). F-12 is odorless and nontoxic, but one precaution in handling it is necessary:—it must not come in contact with a naked flame as otherwise poisonous phosgene gas is produced.

FIG. 3. The tube envelope for million-volt multi-section x-ray tube.

VIII. The Electrical Circuit

This is shown in Fig. 5. From the 220-volt three-phase 60-cycle power supply, current is fed to the frequency tripler "*H*" which converts it

into 230-volt single-phase 180-cycle current which in turn is supplied to the primary, F, of the x-ray transformer and controlled by means of the saturable core reactor, J, L and the auto transformer, N.

The x-ray tube filament current is supplied from end turns B and remotely controlled by means of the adjustable inductance A, operated mechanically from without, as shown in Fig. 1, by means of a reversible motor (15), a shaft passing through a packing gland, an insulating rod (5), and a pair of bevel gears.

IX. Discussion of Design Features

1. The Transformer

There are several advantages to be derived from the use of the resonance rather than the conventional type of transformer.

(a) The removal of the iron core, permitting the tube to be placed in the axis, Fig. 6, eliminates the space otherwise required for insulation between primary and secondary and results in a reduction in the required tank diameter to something like 62 percent with a corresponding volume decrease to 38 percent. All electrical connections between tube and transformer are made inside the transformer and its hemispherical cap and are thus completely shielded.

(b) The wave form in the high voltage circuit is always essentially sinusoidal regardless of that supplied to the primary. Furthermore, the oscillating current in the secondary is so large, 76.0 milliamperes at 1000 kv peak, that the useful and inverse voltages remain essentially equal even when the tube is drawing as much as 10 milliamperes of rectified current.

(c) The subdivision of the secondary into so many thin coils results in a very uniform gradient along its length thus facilitating its adequate internal insulation. It facilitates the placing of taps at equal voltage intervals, for connection to the various intermediate electrodes of the tube. Then, through the spacing apart of these thin coils it facilitates their cooling through circulation of the gas. Finally, it permits of random winding.

For convenience in assembly, the ends of the individual coils of the secondary are not soldered together but, with the coils stacked on top of one another, connections are made through flat phosphor-bronze springs.

The number of turns in the secondary is so chosen as to make its natural period of oscillation match that of the supply circuit, 180 cycles.

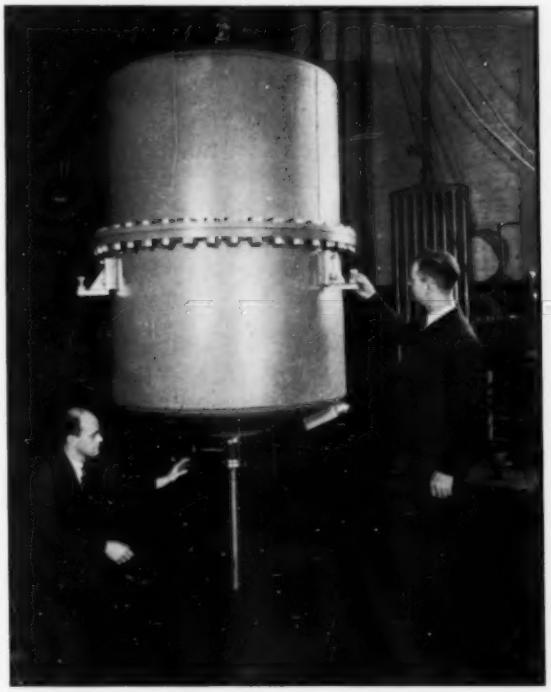

Fig. 4. Million-volt x-ray unit.

The total height of the secondary could have been chosen materially less for 1000 kilovolts peak were it not for the fact that it is more convenient in making connections to the tube to have it of about the same length as the latter. It is the tube which determines the height of the outfit as a whole.

The split rings of copper tubing placed around the upper sections of the secondary and connected each to the outer end of its coil are intended to protect the upper sections in case arc-over should occur from one of them to the tank. Such an arc-over might otherwise result in damaging the insulation locally.

The distribution of volts generated per turn in the secondary at different levels is shown in Fig. 7.

2. Gas Insulation

The data of Fig. 8 on the arc-over voltage as a function of gas pressure were obtained by operating the transformer without the tube. Curves *A* and *B* are for F-12 and nitrogen, respectively.

Corresponding data obtained with an earlier, 60-cycle, transformer are shown in Fig. 9. In this case the spacing between the high voltage terminal and the tank was considerably less, about five inches. The arc-over voltages for three different insulating media, F-12, 10-C transil oil and nitrogen as a function of pressure are shown.

Figures 8 and 9 show for both designs, throughout the voltage range, a strength ratio of more than 2.5 to 1.0 in favor of F-12 over nitrogen.[3]

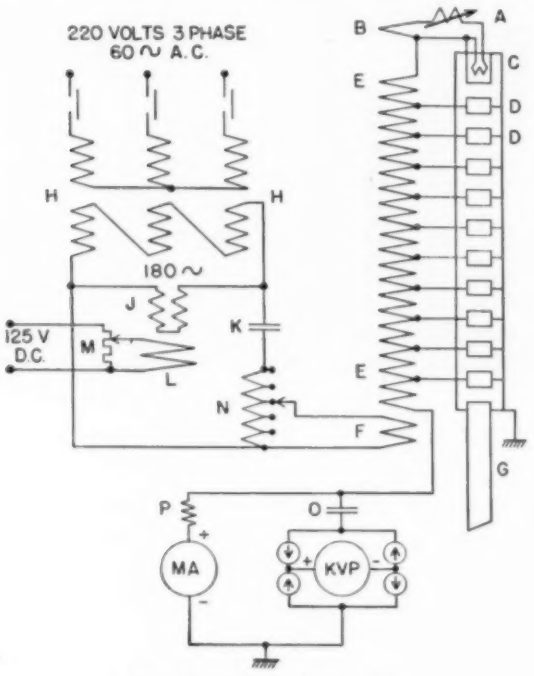

Fig. 5. The circuit diagram.

Fig. 9 shows the strength superiority at the higher pressures of F-12 over 10-C transil oil. For voltages of not more than 1200 kv peak, 40 pounds gauge pressure seems to afford an ample factor of safety. This calls for a weight of F-12 of only about 100 lb. It is interesting to note that about 12,000 lb. of oil would be required to give the same insulation in a necessarily larger tank.

F-12 decomposes under the action of corona, setting free chlorine and fluorine, and experience was required to determine whether enough such decomposition would take place under the conditions pertaining in this outfit to cause troublesome deterioration of any of the insulating or other materials present. We have so far been unable to observe any deterioration due to this cause, indicating that, at least up to 1200 kv, the amount of corona must be very small.

3. The X-Ray Tube

Because of the fact that the tube is symmetrically placed with respect to the transformer, the magnetic flux passing through it does not interfere with electron focusing.

Toroidal shields, surrounding and connected to the various electrodes, electrostatically shield the electron beam. The size of the electron beam is determined largely by cathode geometry and by the ratio of the voltage used in the first to that in the remaining sections. With an extension chamber 24 inches long, and without magnetic focusing, the focal spot is $1\frac{1}{4}$ inches in diameter but can be changed if desired by use of the magnetic focusing coil (14) in Fig. 1. The cathode design is so chosen as to give an electron beam small enough to clear all of the intermediate electrodes and the upper portion of the extension chamber without necessitating at the same time too high a filament temperature, for it is clearly desirable that the filament shall have a very long life. The entire cathode assembly may be readily removed and replaced by a new one, by heating its supporting flange Fig. 1 electrically by means of an attached electric heater to melt the tin which solders it to the topmost Fernico ring.

4. The Insulating Shaft for Adjusting the Filament Current

This consists of a heavy-walled Pyrex glass tube which has been carborundum blasted and coated with a resistance paint to avoid creepage over its surface.

This control shaft (5) mounted inside the transformer stack and driven by a reversible motor, provides remote control for the variable inductance (4) in the filament circuit to give the desired milliamperage.

FIG. 6. Assembly of million-volt x-ray unit.

5. THE SATURABLE CORE REACTOR

A saturable core reactor, J, L, Fig. 5, connected across the frequency tripler controls its power output to the x-ray transformer. The power that can be obtained from the frequency tripler is very strongly limited by the high internal reactance for 180-cycle current. Actually the short circuit current of a frequency tripler is only about two-thirds of the rated output current. To make possible a high power output the internal reactance is neutralized by means of a series capacitor K. With a properly chosen series capacitor K, the voltampere rating of which is of the same order as that of the unity power factor load, the amount of 180-cycle power is limited only by the heating of the copper. To obtain low voltage on the resonant transformer the reactor is saturated and forms very nearly a short circuit across the terminals of the tripler proper. This results in a current smaller than the rated amount of the tripler and the output voltage is low. Reduction of the direct current in the saturating winding L by means of the potentiometer M, lowers the alternating current in the saturable reactor and raises the output of the frequency tripler.

X. Control of Voltage and Current

Once calibrated, the control of the outfit is very simple. The current is adjusted by operating the reversible motor activating the insulating shaft which controls the variable inductance in the filament circuit. If the outfit is to be operated always with the same voltage and current and the proper adjustment of the impedance in the filament circuit is made, the autotransformer, N, is permanently set to the desired voltage tap. The only control then that is finally used for normal operation after the main switch is closed is the potentiometer M controlling the direct current in the saturating winding of the saturable reactor to bring the x-ray tube quickly and smoothly from 300 kv peak to 1000 kv peak and 3.0 milliamperes.

XI. Operating Data

1. MILLIAMPERAGE AND VOLTAGE MEASUREMENTS

The voltage generated in the secondary coils without x-ray tube load is a linear function of the charging current—the current required to

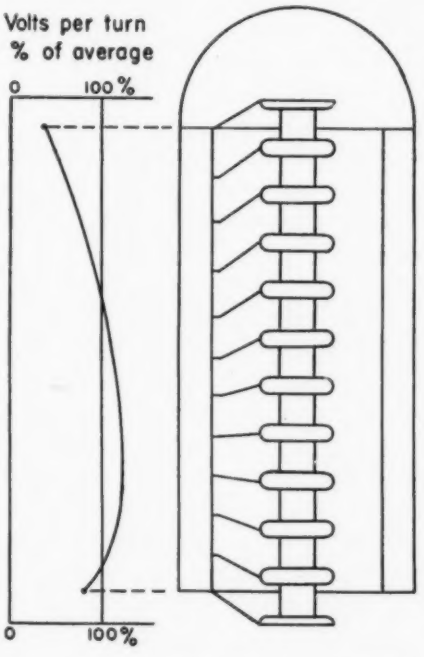

FIG. 7. Voltage distribution per turn along secondary coils of resonance transformer.

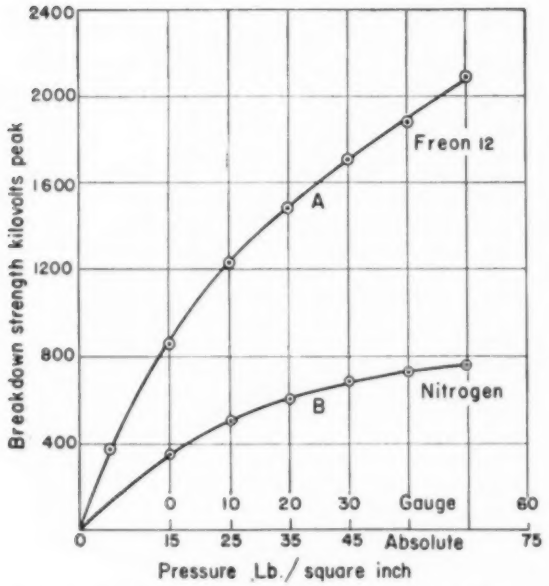

FIG. 8. Breakdown strength of nitrogen and Freon 12 when used as insulation for the resonance transformer as a function of pressure.

charge the secondary to the potential in question with respect to the tank. As shown in Fig. 5 the lower terminal of the winding E.E. is connected to ground through a measurement circuit. The reactor P allows the direct-current component to pass through a milliammeter which registers the electron current flowing to the anode. The alternating charging current is blocked by the reactor P and passes through the capacitor C and a vacuum tube rectifier bridge. The rectified charging current passes through a d.c. milliammeter which is calibrated in terms of kilovolts peak. This calibration is secured at 100 kv peak by the use of a sphere gap temporarily placed in the top of the tank.

A 12.5-centimeter irradiated sphere gap set for 100 kv peak is placed on top of the hemispherical cap of the transformer, and the unit assembled as usual, air being left inside. A motor generator is used to supply power at the proper frequency for tuning to resonance at a frequency f_2, a few cycles lower than f_1 (180 cycles per second), due to the added capacity of the spheres. The voltage is raised till the spheres arc, which is audible and also visible on the cathode-ray oscillograph and on the charging current meter. The charging current of the secondary is recorded at this sparking potential. After removal of the sphere gap the true calibration is found by making a small correction for the increased frequency. The correction is based on the fact that the inductance L in both cases is the same although the capacitance differs by the capacitance of the spheres. Since at f_1 the reactance is $2\pi f_1 L$ and at f_2, it is equal to $2\pi f_2 L$ the current required to produce 100 kv peak at f_1 is $i_1 = i_2 \times f_2/f_1$. This value i_1 for the charging current at 180 cycles per second is then used as a basis for the no load calibration beyond 100 kv peak, a linear relationship being assumed between voltage and charging current. This assumption is reasonable since in a unit of fixed geometry both the inductance and the capacitance are independent of voltage. The reluctance of the magnetic circuit is affected very little by the small amount of iron which operates at a very low flux density. The relationship between voltage and charging current is expressed by

$$V_p = i_p \omega L = i_p/\omega C,$$

i_p, L and C representing equivalent values of peak current, inductance and capacitance for a circuit with integrated or lumped inductance and capacitance.

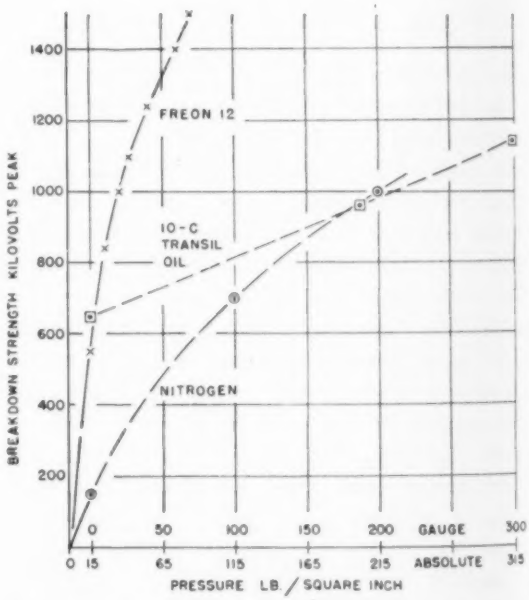

FIG. 9. Breakdown strength of different insulating media used to insulate an earlier 60-cycle transformer as a function of pressure.

For example, with the sphere gap connected,

the resonant frequency is 174 cycles per second and the current recorded at spark-over on the meter in the vacuum tube rectifier circuit is 7.85 ma. After removing the sphere gap, 100 kv peak should then be obtained at 180 cycles with (174/180×7.85 ma=) 7.60 ma and hence for 1000 kv peak the charging current is 76.0 ma.

This method of no load calibration has been experimentally justified by other methods involving the use of an insulated pick-up ring temporarily placed in the top of the tank nearly flush with the inner wall. This ring is connected to ground through a capacitor to keep the picked up voltage reasonably low. The system thus formed consists entirely of capacitance elements. In such a system the voltage of any one floating potential is a linear function of one potential varied at will.

A connection between the pick-up ring and a cathode-ray oscillograph gives a visual record of the high voltage and an indication of the proportionality between the charging current and the secondary voltage at no load. By connecting a peak volt meter across the pick-up ring-grounding capacitor, one can obtain an accurate proof of the linear relationship between secondary charging current and secondary voltage. The a.c. component of voltage on the pick-up ring is exactly proportional to the x-ray tube voltage on the peak voltmeter circuit as shown in Fig. 10. The vacuum tube does not allow the pick-up ring to drop below ground potential. Hence the ring assumes a d.c. component of voltage proportional to the peak, useful voltage of the x-ray tube, as can be seen from the curve of Fig. 10; this d.c. component of voltage is read on the microammeter which has a five-megohm resistor in series.

When the unit is operating at 1000 kv peak at no load the charging current is 76.0 ma average current. A correction must be made in the charging current for the x-ray tube load current. The reason for this is a slight redistribution of the charging current in the distributed capacity of the coil to ground when the load is applied. Under load conditions the charging current is slightly higher and the correction can be determined by the use of the vacuum tube peak voltmeter attached to the pick-up ring in the top of the tank. In the calibrated unit with constant geometry, the voltage measurement by means of the charging current is independent of variations in the line frequency of ±10 percent. The normal fluctuations of frequency of power systems, less than ±0.2 percent, have no effect on the output voltage or x-ray tube current.

With the tube drawing 10 ma the wave

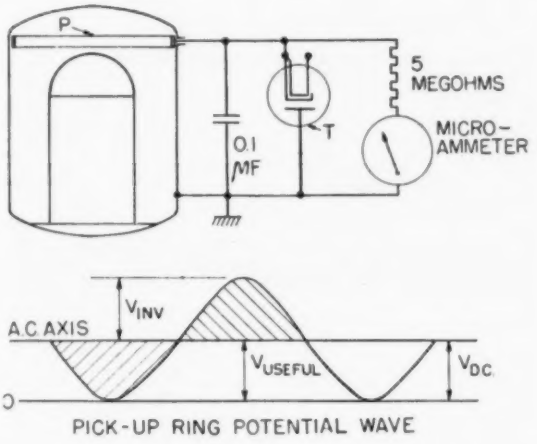

FIG. 10. Circuit diagram of peak voltmeter.

distortion produced is still less than one percent difference between useful and inverse voltage as observed on a peak voltmeter. There is negligible wave form distortion from a pure sine wave of voltage when the tube is operating over a wide range of voltage and current values. The wave form of the secondary of the high tension transformer is essentially independent of the wave form of the supply circuit. Fig. 11 shows the oscillographic record of tube voltage wave and the voltage wave of the tripler unit supplying power to the primary winding. When operating at 1000 kilovolts peak and three ma the oscillating power in the secondary coil is approximately 50,000 volt-amperes while the half-wave load of the x-ray tube amounts to about 2000 volt-amperes. This large ratio illustrates the fly wheel action of the tuned circuit which tends to maintain the perfect sine wave shape of voltage impressed on the x-ray tube.

The voltage measurement has also been checked, so far as order of magnitude is concerned, calorimetrically by a measurement of the amount of target cooling water used, together with the temperature at inlet and outlet.

2. Determination of Filament Temperature

To determine the filament current a thick glass window was introduced in the top of the tank at a point commanding a view of an

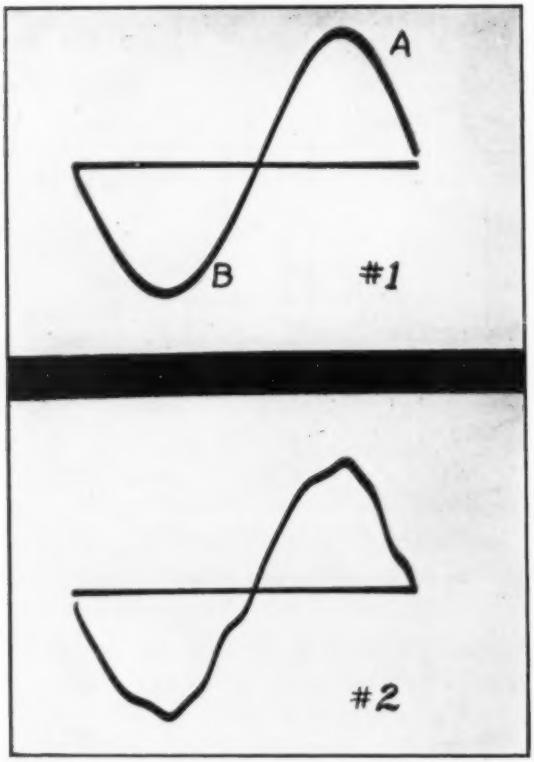

Fig. 11. Oscillographic records of the x-ray unit operating at 1000 kv peak and 3 ma. No. 1 secondary voltage, *A* being the useful half-cycle and *B* the inverse half-cycle. No. 2 primary voltage.

ammeter connected in the filament circuit and set in a hole in and screened flush with the surface of the hemispherical shield at the top of the transformer. Upon operating the outfit at 1000 kv peak the filament currents and temperatures for different tube milliamperages were as indicated in Table I.

According to tungsten lamp data this x-ray cathode delivering three ma of electron current should have a life of several thousand hours before normal burn-out. Positive ion bombardment resulting from tube operation at a poor vacuum will probably be the determining factor in filament life rather than normal tungsten evaporation. There are no inherent difficulties in sealing this million-volt tube off the pump. It is merely a question of economics whether it is cheaper to operate sealed-off tubes at this voltage or take on pump equipment with replaceable cathodes and anodes. The life of sealed-off tubes operating at this voltage is unknown.

3. Electrical Data

The energy losses in the system are mainly due to heating of the secondary by the oscillating current, and are proportional to the square of the voltage generated.

A characteristic set of operating data is given in Table II.

No special precautions were taken to dry the coils. The shields around the Fernico edges of the x-ray tube are made of a graphite-phenolic resin compound with a resistivity of about ten ohm-centimeters and therefore give negligible losses. At no load the power factor is high and leading. As the load is increased the power factor becomes lagging and goes down. The cause of this change, is the primary leakage reactance which may be considered as a lumped reactance in series with the primary. As the primary current increases the reactive drop increases and the power factor drops. The wattages correlate approximately as follows

$$W = 1200\,V^2 + 800\,Vi,$$

where W = wattage, V = peak voltage in millions, and i = the tube current in milliamperes. The term $1200\,V^2$ accounts for the no load losses, the second one for the electron beam power and a third term proportional to the square of the load current is omitted since the primary winding has small losses and the load current in the secondary is in quadrature with the much larger charging current. A more accurate formula would also have to contain a constant term of about

Table I.

Tube Current ma	Filament Current Amperes	Filament* Temp. Degrees K
3	4.15	2155
5	4.28	2180
8	4.40	2215
10	4.50	2245

* The brightness temperature of the x-ray filament as measured by an optical pyrometer.

40 watts for the losses in the filament circuit when the filament is being used.

The primary voltage and current cannot very well be expressed in a simple formula since they are the result of vector summations. The primary voltage and the power factor are influenced by small changes in line frequency, but the primary current, the secondary voltage and x-ray tube current are very stable during operation.

The frequency tripler was designed for a maximum continuous power output of 10 kilowatts. Since the actual 180-cycle load at 1000 kv peak and three ma is only 3600 watts, it is clear that for this load a smaller and more economical tripler could be designed which would draw less power and less current from the three phase 60-cycle line.

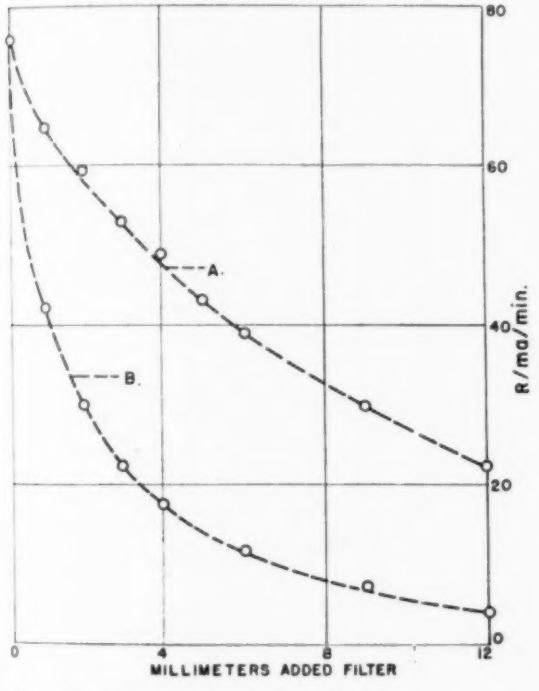

FIG. 12. X-ray measurements. Absorption curve for 1000 kv peak and 1 ma 90 degrees to electron beam axis. 50 cm target-thimble distance. Inherent filtration 1.65 mm of iron, 1 mm of brass, 4 mm of water. Curve *A*: added copper filter. Curve *B*: added lead filter.

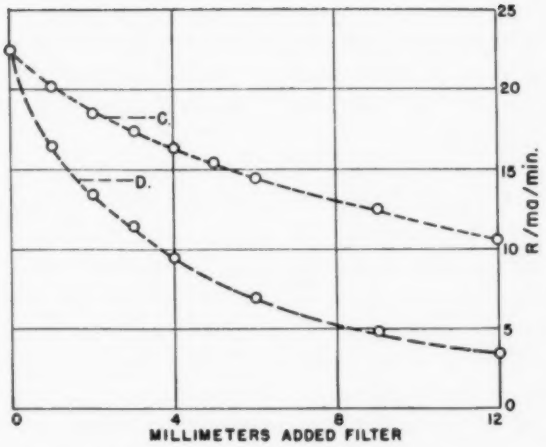

FIG. 13. X-ray measurements. Absorption curve for 1000 kv peak and 1 ma. Zero degrees to electron beam axis transmitted x-ray beam. 50 cm target-thimble distance. Inherent filtration 1.5 mm tungsten, 4.75 mm nickel, 15.7 mm of brass and 4 mm of water. Curve *C*: added copper filter. Curve *D*: added lead filter.

4. X-RAY OUTPUT

A measurement of the intensity of the x-ray beam was made in two positions (1) 90 degrees to the main tube axis and (2) 0 degrees to the main tube axis parallel with the electron beam.

These measurements were made with a Victoreen "*R*" condenser meter with the chamber positioned in free air. For the measurements of the 90-degree beam, the chamber was placed five feet or more from all walls. Later experiments indicated that these wall distances could be reduced 50 percent without appreciably changing the value of these measurements. With

TABLE II. *Input power data as a function of output power for high voltage unit.*

3-PHASE 60-CYCLE LINE			180-CYCLE POWER FROM TRIPLER					CHARGING CURRENT	TUBE VOLTAGE	TUBE CURRENT
VOLTS	AMP.	KVA	WATTS	VOLTS	AMP.	KVA	WATTS	*PF* %	MA AVG	KV PEAK	MA
218	40	15.0	2300	143	8.8	1.25	1200	96	76.0	1000	0
217	45	17.0	4900	190	19.8	3.75	3600	96	81.2	1000	3
216	51	19.2	6700	220	27.2	6.00	5200	87	84.5	1000	5
213	80	29.5	12300	330	43	14.2	9800	69	86.6	1000	10
218	41	15.5	2880	172	10.5	18.0	1730	96	91.2	1200	0
216	49	18.2	6040	224	21.5	4.81	4620	96	96.2	1200	3
215	60	22.5	8380	245	30.0	7.35	6530	89	99.5	1200	5

the 0 degree transmitted beam, the back wall could be brought as close as 12 inches to the thimble chamber without producing any great error in the intensity measurements due to back scatter.

Figure 12 shows the absorption curves at 1000 kv peak and one ma for the 90-degree x-ray beam at 50 cm target-thimble distance. The inherent filtration of the extension chamber was 1.65 mm iron, 1.0 mm brass and 4.0 mm water. Curve *A* is the copper absorption curve and curve *B* the lead absorption curve. Fig. 13 shows the absorption curves at 1000 kv peak and one ma for the transmitted x-ray beam measured at 0 degrees to the electron beam axis. The inherent filtration through this target was 1.5 mm tungsten, 4.75 mm nickel, 15.7 mm brass and 4 mm water. Curve *C* is the copper absorption curve and curve *D* the lead absorption curve.

Table III shows the change in intensity of the x-ray beam per milliampere with kilovoltage.

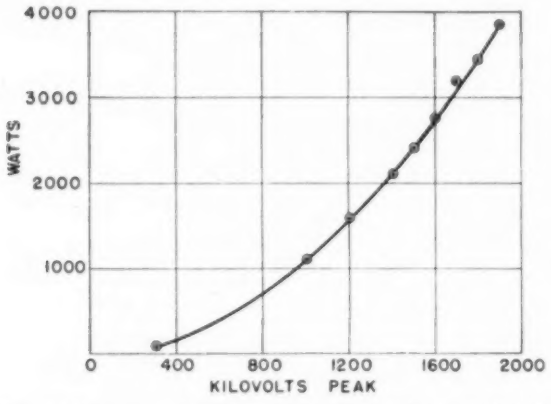

FIG. 14. Losses of transformer without tube as a function of kilovolts peak.

The intensity of the beam in the forward direction parallel with the tube axis is practically three times the value of the 90-degree beam[4] for the same equivalent filtration.

Since the voltage wave form of the generator does not change with load, the x-ray output at constant voltage changes linearly with x-ray tube current as shown in Table IV.

XII. Heat Losses in the Resonance Transformer

The cooling of the transformer windings for operation at 1000 kv peak is accomplished by spacing the secondary coils $\frac{3}{32}$ inch apart and

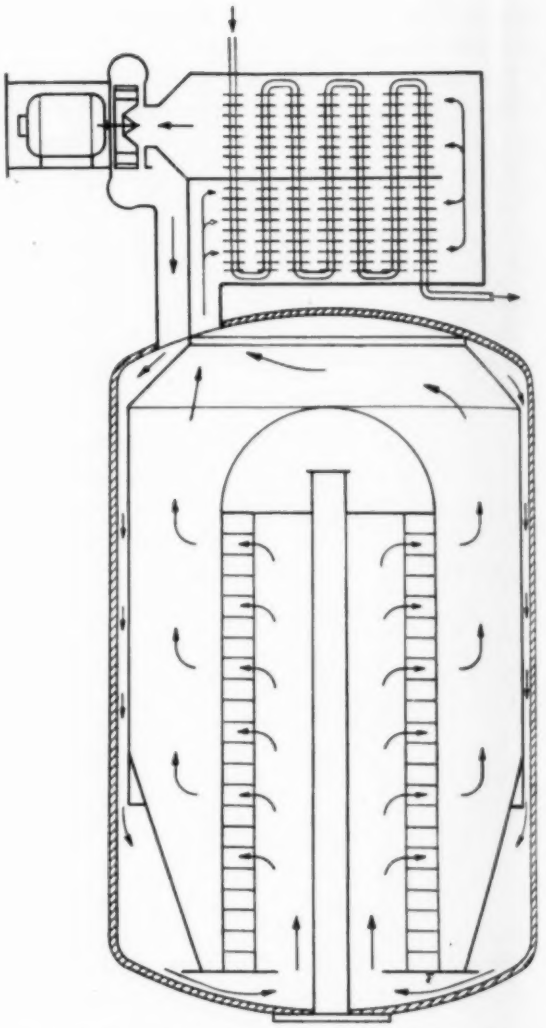

FIG. 15. Forced circulation of Freon gas in tank for more effective cooling of the unit when operated continuously at voltages in excess of 1000 kv peak.

permitting the gas to circulate through them by normal convection. The spark-over data of the curve of Fig. 8 demonstrate clearly the large factor of safety against spark-over, for operation at one million volts with 40 pounds per square inch gauge pressure. A limitation to continuous operation of the transformer at a higher voltage is the power dissipation and the consequent temperature rise. Fig. 14 shows the wattage loss in the transformer alone for different operating voltages. The wattage loss of the transformer without load is proportional to the square of the voltage within experimental error over the full range of measurements.

The million-volt unit reaches a maximum temperature rise in the hemispherical cap, of 35 degrees C, when operated for eight hours at 1000 kv peak. With a blower which propels the gas through the transformer at the rate of 20 cubic ft. per minute the unit has been operated continuously at 1250 kv peak for eight-hour periods and reached a maximum temperature rise of 45 degrees C. A later unit has been constructed with a space of $\frac{3}{8}$ inch between the shell supporting the laminated steel and the tank wall, thus allowing circulation of the gas downward through this space and providing better natural cooling by free convection.

For continuous operation at voltages very much higher than 1000 kv peak, a simple water-cooled heat exchanger with a blower to circulate the gas can be designed to keep the unit to any desired maximum temperature (Fig. 15).

In x-ray units, of the same basic design as the 1000-kv peak outfit, which are built for operation at lower voltages and hence of smaller dimensions, it may be desirable in some instances to use oil insulation in place of gas to facilitate the cooling problem.

In one x-ray unit, built to operate at 250 kv peak and 30 ma, housed in a tank 21 inches in diameter and 32 inches high, 10-C transil oil can be used to meet the necessary insulating and cooling requirements.

Resonant transformer x-ray units for voltages higher than one million can readily be designed to operate at lower resonant frequencies. With resonance at 60 cycles, the need of frequency changing equipment would be eliminated.

TABLE III. *Change in intensity of the x-ray beam per milliampere with kilovoltage, as measured along the axis parallel with the electron beam and at 90 degrees to it. 50 cm target-thimble distance.*

KV PEAK	0-DEGREE BEAM INHERENT FILTRATION* R/MA/MIN.	90-DEGREE BEAM		X-RAY BEAM RATIO 0°/90° THROUGH EQUIVALENT FILTRATION
		INHERENT FILTRATION† R/MA/MIN.	EQUIVALENT FILTRATION‡ TO 0-DEGREE BEAM R/MA/MIN.	
800	10.0	44.0	3.8	2.6
900	15.6	58.5	5.7	2.7
1000	22.5	76.0	8.0	2.8
1100	32.0	92 0	11.0	2.9
1200	43.5	108.0	14.5	3.0

* Inherent filter 0-degree beam—1.5 mm tungsten +4.75 mm nickel +15.7 mm brass +4.0 mm water.
† Inherent filter 90-degree beam—1.65 mm iron +1.0 mm brass +4.0 mm water.
‡ Equivalent filter 90-degree beam—inherent filter +1.5 mm tungsten +4.75 mm nickel +12.7 mm copper.

TABLE IV. *Change in intensity of the x-ray beam with milliamperage at constant voltage as measured along the axis parallel with the electron beam and at 90 degrees to it. 50 cm target-chamber distance.*

KV PEAK	MA	0-DEGREE BEAM INHERENT FILTRATION* TOTAL R PER MIN.	90-DEGREE BEAM EQUIVALENT FILTRATION† TO 0-DEGREE BEAM TOTAL R PER MIN.
1000	1.0	22.5	8.0
1000	3.0	62.4	21.6
1000	9.0	196.7	68.8

* Inherent filtration 0-degree beam—1.5 mm tungsten +4.75 mm nickel +15.7 mm brass +4.0 mm water.
† Equivalent filtration to 0-degree beam—1.65 mm iron +1.0 mm brass +4.0 mm water +1.5 mm tungsten +4.75 mm nickel +12.7 mm copper.

Acknowledgments

We are happy to make grateful acknowledgment to Dr. W. D. Coolidge for his inspirational leadership and invaluable suggestions in carrying out this investigation. We are also much indebted to Mr. Harry Mesick for his assistance in the development of the x-ray tube.

Bibliography

1. W. D. Coolidge, L. E. Dempster and H. E. Tanis, Jr., Physics **1**, 230 (1931).
2. E. E. Charlton, G. Hotaling, W. F. Westendorp and L. E. Dempster, Radiology **29**, 329 (1937).
3. E. E. Charlton and F. S. Cooper, Gen. Elec. Rev. **40**, 438 (1937).
4. K. E. Corrigan and B. Cassen, Am. J. Roentgenology **37**, 811 (1937).

Here and There

Professor Bergen Davis and Professor Daniel D. Jackson, of the Department of Physics of Columbia University, have leave of absence for the present semester.

★

Dr. Harold C. Urey, Professor of Chemistry at Columbia University, has been appointed executive officer of the Department of Chemistry for a term of three years beginning on July 1. He will succeed Dr. Henry C. Sherman, Mitchill Professor of Chemistry, who has been head of the department for the last twenty years. Dr. Sherman will devote his time to research and teaching. Dr. J. Enrique Zanetti, Professor of Chemistry, has been named to the newly established position of Director of Laboratories.

★

Dr. Samuel C. Lind, Dean of the Institute of Technology of the University of Minnesota, previously Director of the School of Chemistry, has been chosen President-elect of the American Chemical Society.

★

Professor Frank E. Richart, Professor of Engineering Materials at the University of Illinois, was elected President of the American Concrete Institute at the recent annual meeting in New York City.

★

The John Simon Guggenheim Memorial Foundation announces the following fellowship awards in the field of physics:

Dr. Maurice Ewing, Assistant Professor of Physics, Lehigh University, his second fellowship, for deep-sea investigations by gravitational and seismic methods.

Dr. Hubert M. James, Professor of Physics, Purdue University, to make a study of the application of wave mechanics to the computation of intensities in band spectra.

Dr. Rose C. L. Mooney, Associate Professor of Physics, Newcomb College and Tulane University, for research into the structure of crystals by methods of x-ray analysis.

★

Nature reports that at the meeting of the Royal Society, held on March 16, the following were among those who were elected fellows of the Society:

A. J. Bradley, Assistant Director of Research in Crystallography, Cavendish Laboratory, Cambridge, distinguished for his methods of applying x-ray crystallography to elucidate the structure of metals, and particularly the gamma-phase and order and disorder in alloys.

G. W. C. Kaye, Superintendent, Physics Department, National Physical Laboratory, distinguished for his pioneer work in x-ray measurements and for his studies on acoustics and physical constants: has rendered valuable service to the Radium Protection Committee and the National Radium Commission.

I. Masson, Vice Chancellor of the University of Sheffield, formerly Professor of Chemistry, University of Durham, distinguished for his researches in physical chemistry, particularly on the physical interaction of mixed gases and on new aspects of the chemistry of iodine.

C. E. K. Mees, Vice President of the Eastman Kodak Company, Rochester, New York, distinguished for his influence on the technology of photography, thereby assisting advance in many branches of science.

E. J. Williams, Professor of Physics, University of Wales, Aberystwyth, distinguished for his researches on the passage of electric particles through matter, and on individual collision processes, which have provided evidence for the existence of the heavy electron.

★

The Board of Trustees of the Lalor Foundation has announced the following awards:

Dr. Robert Byron Jacobs, of the Research Laboratory of Physical Chemistry of the Massachusetts Institute of Technology, to continue work with Dr. F. G. Keyes on the fundamental properties of materials at low temperatures.

Dr. William Earl Roseveare, Assistant Professor at the University of Wisconsin, to work with Dr. Henry Eyring at Princeton University on the determination of intermolecular forces in binary gaseous mixtures.

★

The title of the Pilgrim Trust Lecture delivered by Sir William Bragg at 8:30 P.M., on Monday, April 24, at the Washington meeting of the National Academy of Sciences was "History in the Archives of the Royal Society."

★

The James Arthur Lecture on Time and its Mysteries at New York University was given in the auditorium of Gould Memorial Library, University Heights, on April 26 by Dr. A. H. Compton, Professor of Physics at the University of Chicago. The subject of the lecture was "Time and the Growth of Physics."

★

A new Hall of Optical Science, part of the Division of Light, Vision and Optics, was opened on April 20 at the New York Museum of Science and Industry in Rockefeller Center. The opening of the exhibition was marked by an anniversary luncheon in honor of William Bausch, Vice President of Basuch and Lomb Optical Company, whose experiments in optical glass manufacture, begun just twenty-five years ago, have resulted in notable achievements in this branch of American industry. Following the luncheon, the guests inspected the new exhibition, after which it was opened to the public.

ASTM Annual Meeting

The American Society for Testing Materials will hold its annual meeting at the Chalfonte Haddon Hall, Atlantic City, New Jersey, from June 26 to 30. The technical program will include, among other topics, round table discussions on quantitative spectrochemical analysis, effect of subatmospheric temperatures on the properties of metals, and fatigue of metals. In addition, an exhibit will be held on testing apparatus and related equipment.

★

Society of Automotive Engineers

An extensive program is being developed for the 1939 World Engineering Congress of the Society of Automotive Engineers. Some sixty technical papers by well-known authorities are given on the preliminary program; over one-third of the speakers are Europeans. The Congress opens on May 22 in New York for a five-day session, will be in Indianapolis from May 29 to May 30, in Detroit from May 31 to June 2 and closes with a three-day session in San Francisco, ending on June 8. Advanced engineering design problems of aircraft, automobiles, trucks, buses, railcars, the role of tractors in our national economy, operating problems of fleet owners and reports on fuel and lubricant developments will be covered by the Congress.

★

American Geophysical Union

The twentieth annual meeting of the American Geophysical Union and its seven sections (Geodesy, Seismology, Meteorology, Terrestrial Magnetism and Electricity, Oceanology, Volcanology and Hydrology) was held in Washington, D. C., on April 26, 27, and 28. At the regular sessions of the sections, scientific papers were presented. The principal feature of the general assembly, which was held in the auditorium of the National Academy and Research Council Building on the afternoon of April 28, was a symposium on geophysical prospecting. At this symposium papers were presented as follows: geophysical methods in petroleum exploration, by J. Brian Eby; electrical and magnetic exploration in the mining industry, by Sherwin F. Kelly; and geophysical prospecting by the Federal Government, by F. W. Lee, J. H. Swartz and Irwin Roman. On the evening of April 27, a smoker was held in Building D of the George Washington University, 2013 G Street, N.W.

★

Symposia in Physics at the University of Chicago

Two symposia of interest to physicists are to be held at the University of Chicago from June 23 to 30, as follows:

I. Symposium on Liquids and Polyatomic Molecules, a joint symposium of the chemistry and physics departments, to be held on June 23 and 24 and on June 26 and 27.

The first part of the symposium is devoted to the liquid state (structure of liquids, viscosity, condensation of liquids, the fusion process, two-dimensional liquids, infra-red absorption and hydrogen bonding). The second part includes discussion of visible and ultraviolet spectra of complex molecules, the color of dyes, refractivity, optical activity and liquid and molecular viewpoints in nuclear structure. The speakers include K. F. Herzfeld, B. E. Warren, J. G. Kirkwood, O. K. Rice, F. A. Ogg, Jr., J. E. Mayer, H. Eyring, W. D. Harkins, W. H. Rodebush, L. Pauling, R. S. Mulliken, E. Teller, J. Franck, T. R. Hogness.

II. Symposium on Cosmic Rays, June 27 to 30. The subjects to be discussed include:

The Intensity and Absorption of Cosmic Rays.
Geographic and Geomagnetic Effects.
Time Variations of Cosmic Rays.
Composition of Cosmic Rays.
Energy Distribution of Cosmic Rays.
Showers and Bursts.
Mesotrons and Other Heavy Particles.

The expected participants include:

P. Auger from Paris; W. Bothe and W. Heisenberg from Germany; P. M. S. Blackett and B. Rossi from England; J. Clay from Holland; G. Herzog from Switzerland; C. Anderson, V. F. Hess, T. H. Johnson, R. A. Millikan, W. F. G. Swann, M. S. Vallarta from elsewhere in the United States, and A. H. Compton, W. P. Jesse, M. Schein and V. Wilson from Chicago.

★

Fellowship in Electrochemistry

The Electrochemical Society has just awarded the eleventh Weston Fellowship of $1,000 to Mr. Waldemar P. Ruemmler of St. Louis, Missouri. Mr. Ruemmler will continue his research at Columbia University, investigating the electrodeposition of antimony. The work will be done under the direction of Professor Colin G. Fink.

★

Calendar of Meetings

May	
22–June 8	World Automotive Engineering Congress, New York, Indianapolis, Detroit, San Francisco.
June	
19–24	American Association for the Advancement of Science, Milwaukee, Wis.
23–24	American Physical Society, Princeton, N. J.
26–30	American Society of Testing Materials, Atlantic City, N. J.
27–30	Institute of Radio Engineers, San Francisco, Cal.
28–30	American Physical Society, Stanford University, Cal.
July	
6–8	Sixteenth Colloid Symposium, Stanford University, Cal.
10–14	American Society of Mechanical Engineers, San Francisco, Cal.
10–13	American Institute of Mining and Metallurgical Engineers, San Francisco, Cal.
September	
4–12	International Congress of Mathematicians, Cambridge, Mass.
4–15	International Union of Geodesy and Geophysics, Washington, D. C.
11–15	American Chemical Society, Boston, Mass.
20–23	Institute of Radio Engineers, New York, N. Y.
October	
5–7	American Institute of Mining and Metallurgical Engineers, Coal Division, Columbus, Ohio.
12–14	Optical Society of America, Lake Placid, N. Y.
23–25	American Institute of Mining and Metallurgical Engineers, Metals Division, Chicago, Ill.
23–27	American Society for Metals, Chicago, Ill.
November	
2	U. S. Institute for Textile Research, New York, N. Y.
2–4	American Institute of Mining and Metallurgical Engineers, Industrial Minerals Division, Tuscaloosa, Ala.
15–17	American Institute of Chemical Engineers, Providence, R. I.
December	
1–2	American Physical Society, Chicago, Ill.
27–Jan. 2	American Association for the Advancement of Science, Columbus, Ohio.
28–30	American Physical Society, Coumbus, Ohio.
28–30	Geological Society of America, Minneapollis, Minn.

Contributors to This Issue

M. B. Dobrin

Milton B. Dobrin received the S.B. degree in Physics at the Massachusetts Institute of Technology in 1936 and spent the following year at Columbia University on a Graduate Residence Scholarship. Since 1937 he has been connected with the Geophysics Division of the Gulf Research and Development Company.

G. von Elbe

Guenther von Elbe was born in Germany in 1903. He studied physics and chemistry at the Universities of Kiel and Berlin and received his Ph.D. from the latter in 1929. From 1928 to 1930 he was a Liebig and Notgemeinschaft Fellow at the University of Berlin, and from 1930 to 1932 a duPont Research Fellow and research associate at the University of Virginia. In 1932 he became a member of the Coal Research Laboratory, Carnegie Institute of Technology. Since 1934 he has been engaged in a study of gas reactions and the properties of flames and explosions in cooperation with the United States Bureau of Mines. He is a United States' citizen.

L. P. Winsor

Lauriston P. Winsor was born in Johnston, Rhode Island, in 1914. He received the degree of Sc.B. from Brown University in 1936, and M.S. in Electrical Engineering from the Graduate School of Engineering at Harvard University the following year. At the present time, he is an Assistant in Electrical Engineering at Harvard, where he is continuing his work in preparation for the degree of Sc.D.

B. Lewis

Bernard Lewis was born in London, England, in 1899. He received his B.S. in Chemical Engineering in 1923 from the Massachusetts Institute of Technology and his M.A. in 1924 and Ph.D. in 1926 in Physical Chemistry from Harvard and Cambridge Universities, respectively. He held a National Research Fellowship at the Universities of Minnesota and Berlin from 1926 to 1929. Since 1929 he has been studying the self-ignition of gases, flame propagation and the properties of explosions at the United States Bureau of Mines at Pittsburgh. He is a co-author with Guenther von Elbe of a book *Combustion, Flames, and Explosions of Gases* published in 1938 by the Cambridge University Press and Macmillan Company.

L. E. Dempster

W. F. Westendorp

L. E. Dempster was born in Leicester, England. After two years in high school there he came to America and since 1898 has been with the General Electric Company, at first in the Schenectady Works, and since 1901 in the Research Laboratory, except for three years from 1907 to 1910 when he was with the incandescent lamp department. His work in recent years has been with x-ray apparatus.

W. F. Westendorp, born in Amsterdam, Holland, received his E.E. degree from the University of Delft, Holland, in 1928, and immediately went to Schenectady, New York. Following work in the Testing Department and in the Advance Engineering Course, he joined the Research Laboratory staff in 1930. Since then he has been a research engineer in x-ray work.

G. Hotaling

George Hotaling entered the Schenectady Works of the General Electric Company in 1901, and five years later was transferred to the Research Laboratory. He has been particularly interested in x-ray equipment developments.

R. D. Richtmyer

Robert Davis Richtmyer was born in Ithaca in 1910. He received his A.B. from Cornell in 1931, his M.A. in 1932 and his Ph.D. from Massachusetts Institute of Technology in 1935. Since 1935 he has been Instructor in Physics at Stanford University.

G. Fonda

Gorton R. Fonda, a graduate of New York University, received the degree of Dr. Ing. from Karlsruhe, Germany, in 1910. He is employed in the Research Laboratory of the General Electric Company at Schenectady.

E. E. Charlton

E. E. Charlton, in charge of the section of the General Electric Research Laboratory, Schenectady, devoted to x-ray tube and generating apparatus developments, received his A.B. degree from Grinnell College in 1913, and his M.S. and Ph.D. degrees from the University of Illinois in 1915 and 1918, respectively. He has been a research engineer with the General Electric Company since 1920.

Letter to the Editor

Centrifugal Stresses in Rotating Disks

In recent experiments at this laboratory the photoelastic method has been successfully applied to the determination of centrifugal stresses in rotating disks. The new technique depends upon the double structure of Bakelite BT-61-893.[1] Bakelite consists of two phases, one of which (the *A* phase) fuses at relatively low temperatures. If a sample is heated the viscosity of the *A* phase is rapidly lowered until it becomes virtually negligible at about 115°C, whereas the *C* phase is little affected. At this temperature the modulus of elasticity is reduced to 1/640 of its value at room temperature and the stress-optic coefficient is increased 25 times. If the specimen is subjected to external load at this temperature and allowed to cool slowly to room temperature while still under load the deformation and photoelastic optical effect are "frozen" in. This is brought about by the solidification of the liquid *A* phase within the space lattice formed by the *C* phase. Subsequent removal of load leaves the deformation and optical pattern virtually unaltered.

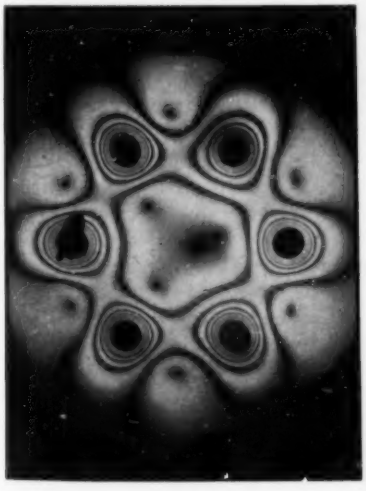

These properties are taken advantage of by spinning (at constant speed) a Bakelite model of the rotor to be studied, raising its temperature to about 110–115°C, and slowly cooling to room temperature. The specimen may then be removed from its mounting and studied while at rest. This technique eliminates the tremendous handicaps of the stroboscopic method which has the disadvantage of requiring high speeds, high intensity of illumination, and extremely accurate synchronization. A stroboscopic study also requires the construction of a mounting which permits viewing the central portion of the disk during rotation—a great hindrance because the axis of the polariscope and the axis of rotation must be practically coincident. The increased optical sensitivity at an elevated temperature makes possible the use of relatively low speeds and small models (the accompanying photograph was made of a model 5½" in diameter and one inch thick having 6 quarter-inch holes located at 60° intervals on a circle of one-inch radius; speed—1800 r.p.m.). The technique is applicable to all problems of centrifugally-induced stress distributions where the speed of the rotor is constant.

A more detailed account of these investigations will be published upon completion of the current experiments.

R. E. Newton

Washington University,
St. Louis, Missouri,
April 22, 1939.

[1] For a complete account see M. Hetenyi, "The Fundamentals of Three-Dimensional Photoelasticity," J. App. Mech. December (1938).

New Books

Fundamental Electronics and Vacuum Tubes. A. L. ALBERT, Professor of Communication Engineering, Oregon State College. Pp. 422+ix, Figs. 284, 15×23 cm. Macmillan Company, New York, 1938. Price $4.50.

The aim of this book is obviously to give a *simple* and *balanced coverage* of the large amount of detail underlying the field of electronics. It does so, in a technically-descriptive manner. This means that a figure or a diagram is given, of a tube or of a circuit, together with the characteristic curves, charts, wave forms, an occasional equation or two, and a clear, but brief, statement of the important definitions, features and principle of operation. The book is only "fundamental" in the sense that it deals with the tubes and their immediate circuits, avoiding the multiplicity of applications in the communication and power fields. There are relatively few equations and these, in general, are not derived. Carefully chosen references, mostly to engineering books and magazines, are given at the end of each chapter and are referred to frequently in the text as an aid to a more profound study of the subject. The various topics are well balanced, without undue emphasis of any one branch of the material.

The book proceeds in a logical sequence from the simple to the more complex. Thus the early chapters, which deal with electrons and their emission, are followed by chapters on two-, three- and multi-electrode tubes. Thereafter, the tube-plus-circuit combinations are treated in the following order: rectifiers, voltage and power amplifiers, oscillators, modulators and demodulators. The last two chapters deal with photoelectric and cathode-ray tubes and their circuits.

There are comparatively few mistakes in this first edition, but it might be mentioned that the constitution of the nuclei of atoms, as given in the first chapter, does not agree with modern theory.

J. BARTON HOAG
University of Chicago

The Mobility of Positive Ions in Gases. A. M. TYNDALL. Pp. 93, Figs. 35, 14×22 cm. Cambridge Physical Tracts. Cambridge University Press and Macmillan Company, New York, 1938. Price $1.75.

This tract is the second in the series on current physics which is being issued by the Cambridge Press. It deals with the results on positive ionic mobilities in gases which have been primarily obtained by Tyndall and his coworkers at Bristol. This is however justifiable for the reason that the work at Bristol in this field has been so effective that it has rendered obsolete much of the earlier work. Due recognition is however given to results obtained elsewhere which have been able to stand the test.

Aside from experimental skill the effectiveness of the work at Bristol rests on the development of an effective method which has permitted a thorough baking out of the apparatus, thereby reducing the chance of impurities. This was the defect in much of the earlier work.

The mobility of metallic ions in nitrogen has received special attention, although the mobilities of several of the metallic ions in the inert gases as well as CO, CO_2 and H_2O have been obtained.

Naturally the results have been checked against Langevin's theory and the agreement in nitrogen and in the inert gases is gratifying.

Very striking results are given showing the relation between mobility, field and pressure. The study of polar impurities and the effect of temperature are also of interest.

This tract should be of special interest to those interested in chemical interactions. It is quite nonmathematical and well illustrated by means of figures.

This tract will prove to be a very helpful unit in the very useful series the Cambridge Press has undertaken to issue.

HENRY A. ERIKSON
University of Minnesota

Modern Atomic Theory. An Elementary Introduction. J. C. SPEAKMAN. Pp. 207, Figs. 10, 13×19 cm. Longmans Green & Co., New York, New York, 1938. Price $2.00.

This book is intended as a supplement to ordinary first-year college textbooks of physics and chemistry. A student really interested in physics and chemistry might find it useful to read during the vacations in his freshman and sophomore years. However there are other books, for instance Millikan's *The Electron*, which he would probably find more exciting and stimulating.

The book could have been improved by including many more interesting pictures such as those of expansion chamber particle tracks. Also a fuller description with diagrams of the more important experimental methods would have helped the reader to get a better grasp of the subject. Room for these could have been found by omitting some questions difficult to discuss adequately in an elementary way.

There are some errors in the book. For example, it is stated that the ionizing effect of a particle increases with its mass so that the mass can be estimated from the ions per cm of path and secondary beta-rays are attributed to the Compton effect of nuclear gamma-rays on the *K* and *L* electrons.

The writer's general impression is that this book is at about the average level of elementary textbooks written by authors who have mainly derived their information from other textbooks. It has the merit of containing some information about nearly everything in modern atomic theory and it is readable by anyone with an elementary knowledge of physics and chemistry.

H. A. WILSON
The Rice Institute

Contributed Original Research

Dielectric Resonators

R. D. Richtmyer
Stanford University, California
(Received December 14, 1938)

We show that suitably shaped objects made of a dielectric material can function as electrical resonators for high frequency oscillations. We develop the theory of such resonators very briefly and compute their resonant frequencies and losses in some very simple cases. The paper concludes with an observation on the behavior of dielectric wave guides.

1. General Discussion

It was shown by Rayleigh[1] that an "infinitely" long cylinder of a dielectric material can serve as a guide for electromagnetic waves of certain frequencies. That means that the dielectric has the effect of causing the electromagnetic field (except for a small part which decreases exponentially with increasing distance from the cylinder) to be *confined* to the cylinder itself and the immediately surrounding region of space. More recently Southworth and collaborators[2] at the Bell Telephone Laboratories have studied the properties of such wave guides from the point of view of electrical communication.

On the basis of this phenomenon W. W. Hansen has suggested (unpublished) that if a long dielectric cylinder were bent into a ring and the ends joined together, it would guide the waves round and round indefinitely, so that they would be confined to a finite region of space (again except for an exponentially decreasing part outside). Such an object would act as an electrical resonator, the resonant frequencies being determined by the fact that the field must have the same phase at the two ends which are joined together to make the ring. This paper develops some of the theory of this resonator and similar ones having other shapes finite in extent, and will refer to them as dielectric resonators.

Hansen's conclusion will be found to be essentially correct, although a slight modification is required. If the part of the field outside of the resonator could decrease exponentially with increasing distance from the resonator, and continue to do so as the distance is increased indefinitely, there could be no loss of energy by radiation, and neglecting dielectric losses oscillations once set up would continue indefinitely. However we shall see that according to the laws of electrodynamics the field *cannot* decrease in quite the manner required, and that it is in fact impossible to confine electromagnetic waves to a finite region of space with the aid of dielectric material alone. Nevertheless in certain cases the energy will escape only very slowly, so that the resonator will exhibit only slightly damped oscillations. Sections 4 and 5 below describe certain cases of this sort and give their resonant frequencies and rates of damping.

The paper lastly considers the effect of bending dielectric wave guides around corners, and concludes that in many cases a certain fraction of the energy will escape in going around the corner. This fraction will be smaller, the larger the radius of bending in comparison to the wave-length. We give order-of-magnitude formulas for the attenuation due to this cause.

2. Proof that a Dielectric Resonator Must Radiate

We deal here with periodic solutions of Maxwell's equations for the dielectric resonator surrounded by empty space, and we consider a system of spherical polar coordinates, r, θ, φ,

[1] Rayleigh, Phil. Mag. **43**, 125 (1897).
[2] See G. C. Southworth, Bell Sys. Tech. J. **14**, 330 (1936); 15, 284 (1937); J. R. Carson, S. P. Mead and S. A. Schelkunoff, *ibid.* **15**, 310 (1937).

whose origin is in or near the resonator. Since the resonator is considered finite, it will be contained entirely within some sphere of radius R. Outside this sphere the field can be expanded in terms of a fundamental set of solutions, obtained by separating the vector wave equation in polar coordinates. The radial dependence of these solutions will be given essentially by various Hankel functions of the first and second kind, whose orders are half-odd-integers, and whose arguments are kr with $k=2\pi/$wave-length.[3] The Hankel functions of the *second* kind represent waves coming in toward the origin from infinity, and since in a physical case such waves would not be present, we must assume that only the Hankel functions of the first kind have nonvanishing coefficients in our case. Under these circumstances the total power radiated is proportional to the sum of the squares of the absolute values of the coefficients.[3] If the power radiated is zero, all the coefficients must vanish, and the field vanishes identically outside the sphere of radius R. By the principle of analytic continuation of solutions of the wave equation we see that the field must vanish identically everywhere outside the resonator, and in particular it must vanish just outside the surface of the resonator. At this surface the boundary conditions are that the tangential components of the electric intensity E and the normal component of the electric displacement D must be continuous. The dielectric constant is assumed finite, and so the field must vanish everywhere just inside the outer surface of the resonator. Continuing in this fashion we finally conclude that the only nonradiating solutions are zero everywhere.

It is quite essential for this proof that the wave equation is of the second order in the time derivative. Were it of the first order (as is the Schrödinger equation), the quantity k could assume pure imaginary as well as real values (for periodic solutions), and then the Hankel-function solutions would not lead to loss of energy by radiation.

An alternative method of proof, suggested to the author by Professor Hansen, shows very clearly the nature of the electromagnetic fields involved. It starts by observing, as before, that the field cannot vanish identically outside the resonator, if there are oscillations present, and then considers the nodal surfaces of the vector potential. The field outside can be thought of as caused by a certain current distribution inside the resonator; this current in fact consists of the motions of the ions of the dielectric. The vector potential can be obtained by multiplying the current density by the Green's function e^{ikr}/r and integrating over the current distribution. Here r is the distance from point P_1 (integration point) to point P_2, and the value of the integral is the vector potential at P_2. The nodal surfaces consist of points P_2 for which contributions to the integral from one part of the current distribution just cancel those from the remainder; and from the nature of the Green's function it follows that if the distance r is very large compared to the dimensions of the resonator, the conditions for such canceling will depend only on the *direction* of P_2 from the resonator, and not on its distance. In other words, the nodal surfaces are asymptotic at large distances to a family of cones (of course, not necessarily circular) whose apexes are, for example, at the center of the resonator. As point P_2 is moved about keeping its distance from the resonator fixed and large, the vector potential varies very slowly since the nodes are far apart, and to make up for this it must be an oscillatory function of the distance of P_2 from the resonator. The oscillations represent outgoing waves and, therefore, radiated energy.

3. Resonant Frequencies and Modes of Oscillation

As a consequence of this theorem, in order to investigate the oscillations of a dielectric resonator, we must imagine it to be continually supplied with energy from some outside source. From the mathematical point of view it is simplest to suppose that this energy is supplied in the form of electromagnetic waves coming from infinity in toward the origin, or in other words to remove the prohibition of Hankel functions of the second kind in the solution of Maxwell's equations for the system. Then for any given frequency the most general solution will involve an infinite number of arbitrary

[3] W. W. Hansen and J. G. Beckerley, Proc. I. R. E. **24**, 1594 (1936).

parameters, in addition to the frequency itself. For example, if the field outside the resonator be expanded as described in the theorem, the amplitudes and phases of all the incoming waves will be arbitrary. The extent to which the resonator "resonates" to excitation of this kind is conveniently characterized by the quantity

$$Q=\omega\frac{\text{energy stored}}{\text{power radiated}}. \tag{1}$$

By "power radiated" we mean the energy radiated per second, as computed from the outgoing waves only. This is, of course, equal to the energy supplied the resonator per second, as computed from the incoming waves only. By "energy stored" we mean the total electromagnetic energy within the resonator itself, averaged over a complete cycle.[4] ω is 2π times the frequency. Q is a finite, positive quantity and is a continuous function of all the parameters, including the frequency, which characterize the solution, and therefore will have maxima for certain values of the parameters. Such a set of values of the parameters define what we will call a resonant mode of oscillation. It will appear below that in some cases these maxima may be very sharp and high. These resonant modes are analogous to the metastable states of a heavy particle in certain radioactive nuclei according to wave mechanics.

In the specially simple cases amenable to calculation it is possible to determine the resonant frequencies and modes quite accurately without actually maximizing Q with respect to the infinitely many parameters, but in spite of this we believe it advisable to formulate the definition as we have done.

[4] This definition of energy stored in the resonator is to some extent arbitrary. In general the field *immediately* outside the resonator will be comparable with that inside, and it might seem that we should include the energy of this part of the field. The reason we do not is that one cannot say just how much of the field outside to include; certainly one should not include it all, since the incoming and outgoing waves, even though they be extremely feeble, contain an infinite amount of "stored" energy spread out over all space. Perhaps one should include all the energy out to the point where the field stops decreasing exponentially and starts oscillating. In the cases we have calculated this would produce only a small change in our estimate of the stored energy. The change is small, partly because the exponential decrease is rapid, and partly because the dielectric constant, which enters into the energy expression, is smaller outside the resonator than inside.

4. Some Resonant Modes of a Dielectric Sphere

We treat the case of a solid spherical resonator first because of its simplicity, and again use polar coordinates with the origin at the center of the sphere. We will confine our attention to a solution involving Hankel functions of just one order (assumed quite large), and we will express it in terms of the Bessel and Neumann functions of that order. Inside the sphere only the Bessel function is allowed, because of the requirement of finiteness at the origin, but outside we will generally have a linear combination of the two, adjusted to satisfy the boundary conditions at the surface of the sphere. We can draw conclusions from the radically different behaviors of the two functions. For arguments larger than the order, they are very much alike in general characteristics—they are both oscillatory, and with roughly the same period and amplitude. But when the argument is less than the order and is allowed to approach zero, the Bessel function approaches zero very rapidly while the Neumann function becomes infinite very rapidly. In some cases we can satisfy the boundary conditions in such a way that the value of the argument corresponding to the surface of the sphere is considerably less than the order. Then the Bessel function part of the solution corresponds to a very large amount of radiated power and a very small amount of stored energy, whereas just the reverse is true for the Neumann function. Then the maximum values of Q will occur for those frequencies such that only the Neumann function is present outside the sphere. We wish to compute these frequencies and the corresponding values of Q.

The vector potential, which, in a gauge such that the scalar potential vanishes, is proportional to the electric field,[3] can be taken to be

Inside:

$$A=\frac{1}{(k_1r)^{\frac{1}{2}}}J_{l+\frac{1}{2}}(k_1r)e^{im\phi}\left[\mathbf{k}_\theta\frac{im}{\sin\theta}P_l^{|m|}-\mathbf{k}_\phi\frac{d}{d\theta}P_l^{|m|}\right],$$

Outside: (2)

$$A=\frac{a}{(k_2r)^{\frac{1}{2}}}N_{l+\frac{1}{2}}(k_2r)e^{im\phi}\left[\mathbf{k}_\theta\frac{im}{\sin\theta}P_l^{|m|}-\mathbf{k}_\phi\frac{d}{d\theta}P_l^{|m|}\right]$$

with $P_l^{|m|}=P_l^{|m|}(\cos\theta)$, $k_1/\sqrt{\epsilon}=k_2=\omega/c$.

ϵ is the dielectric constant of the sphere. The constant a and the frequency are to be determined by the condition that at the surface of the sphere the tangential components of A and of its curl must be continuous. This requires that the frequency satisfy the equation

$$\frac{J'_{l+\frac{1}{2}}(k_1r_0)}{J_{l+\frac{1}{2}}(k_1r_0)}+\frac{\frac{1}{2}}{k_1r_0}=\frac{N'_{l+\frac{1}{2}}(k_2r_0)}{N_{l+\frac{1}{2}}(k_2r_0)}+\frac{\frac{1}{2}}{k_2r_0}. \quad (3)$$

The frequency is involved implicitly through the k's. r_0 is the radius of the sphere. To determine the energy stored one integrates the electromagnetic energy density over the volume of the sphere; to determine the power radiated he separates the Neumann function of (2) into incoming and outgoing Hankel functions, computes Poynting's vector from the outgoing one and integrates this vector over the surface of a large sphere. The complex field strengths must of course first be replaced by their real parts. This gives

$$Q=\left(\frac{k_1r_0}{2}\right)^2\left[1-\left(\frac{l+\frac{1}{2}}{k_1r_0}\right)^2+\left\{\frac{J'_{l+\frac{1}{2}}(k_1r_0)}{J_{l+\frac{1}{2}}(k_1r_0)}\right\}^2\right]\times\{N_{l+\frac{1}{2}}(k_2r_0)\}^2. \quad (4)$$

Below are some typical values computed from these formulas. Eq. (3), which was solved by a numerical procedure, requires that the argument k_1r_0 fall just slightly short of one of the roots of the Bessel function. The quantities given below all refer to the case in which this is the *first* root of the Bessel function. We have expressed the frequency in terms of the vacuum wave-length λ.

For $\epsilon=5$, $l=7$; $\lambda/r_0=1.37$, $Q=206$;
$\epsilon=5$, $l=10$; $\lambda/r_0=1.035$, $Q=3100$;
$\epsilon=5$, $l=20$; $\lambda/r_0=0.571$, $Q=27\cdot10^6$.

To see what the functions look like, we have plotted a quantity proportional to $r^{\frac{1}{2}}A_\theta$ or $r^{\frac{1}{2}}A_\phi$ as function of r for constant θ, ϕ, for $l=10$, in Fig. 1. It is seen that the wiggles of the Neumann function, representing radiated energy, are almost too small to show.

In the computation it was found convenient to make extensive use of the first term of Debye's asymptotic expansion[5] for the Neumann function.

[5] See G. N. Watson, *Theory of Bessel Function* (Cambridge University Press, 1922), or Courant Hilbert, *Methoden der Mathematische Physik*, second edition (Julius Springer, Berlin, 1931), p. 456.

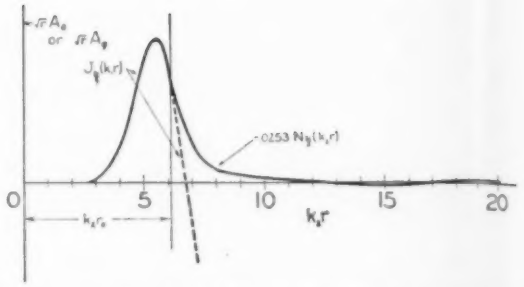

FIG. 1. Distribution of field in dielectric sphere operating in the tenth mode of oscillation with no radial nodes inside the sphere. Along any radius the vector potential has a constant direction and varies in magnitude as shown in the graph.

It should be remarked that in practice such high Q values would not be found, because dielectric losses would cause further damping of the oscillations. It is found experimentally that for a given maximum field strength the dielectric loss per cycle per unit volume is more or less independent of the frequency. For fused quartz, one of the best dielectrics now known for high frequencies, this amounts to about one-thousandth of the energy stored per unit volume, so that on this account alone one would be restricted to Q values lower than can be obtained with *hohlraum*-type resonators. Therefore dielectric resonators using materials now known are not likely to be of much practical importance, although at much higher frequencies than are now in use they might be comparable with the *hohlraum*-type, whose Q is, for given material and shape, inversely proportional to the square root of the frequency.[6]

The largeness of the Q values given above can be at once understood by transition from wave "optics" to geometrical optics. When the waves are confined to a thin outer layer of the sphere, as indicated in Fig. 1, the rays which they represent must strike the surface of the sphere from the inside always at a small grazing angle, and therefore suffer total internal reflection. The fact that the energy nevertheless always leaks out to a certain extent is essentially a phenomenon of wave optics and cannot be explained by ray optics. But if the radius of curvature of the surface is everywhere large compared to the wave-length, the conditions of geometrical optics will very nearly hold and a large Q is the result.

[6] See W. W. Hansen, J. App. Phys. **9**, 654 (1938).

5. Circular Ring Resonator

In this section are discussed some modes of a resonator in the form of a circular ring of small cross section (Fig. 2). This case cannot be treated exactly, as can the sphere, but it merits consideration for the following reasons: it is the case originally envisaged by Hansen; it is a case in which one of the principal radii of curvature of the surface is *not* small compared to the wavelength; it has fewer resonant modes in the frequency range we consider, so that in use it would be easier to tell in what mode it is actually operating; and leads to conclusions on the effect of bending a wave guide.

We first find approximate expressions for the field within the material of the ring itself and nearby outside. We take this field to represent the simplest kind of guided wave going around the ring. Since exact expressions for such a field are not known, we use those functions of the coordinates ρ', ϕ', z' (see Fig. 2), which would correctly represent the field if the guide were straight, so that ρ', ϕ', z' were actually cylindrical coordinates:

$$\begin{aligned}\text{Inside}: \quad E=&e^{i\sqrt{\epsilon}k z'\cos\theta}[\mathbf{k}_{\rho'} i\cos\theta(d/d\rho)\\ &\times J_0(\sqrt{\epsilon}k\rho'\sin\theta)\\ &+\mathbf{k}_{z'}\sqrt{\epsilon}k\sin^2\theta J_0(\sqrt{\epsilon}k\rho'\sin\theta)]A_0\\ \text{Outside}: \quad E=&e^{ikz'\cosh\alpha}[\mathbf{k}_{\rho'} i\cosh\alpha(d/d\rho)\\ &\times H_0^{(1)}(ik\rho'\sinh\alpha)\\ &-\mathbf{k}_{z'}k\sinh^2\alpha H_0^{(1)}(ik\rho'\sinh\alpha)]C_0.\end{aligned} \tag{5}$$

The bold-faced k's are unit vectors in the directions indicated. For simplicity in printing, the top line has been omitted from the square-root sign, but in all cases appearing here this sign is to be considered as applying to the ϵ only. The boundary conditions require that the parameters θ, α, be connected by the relation

$$\sqrt{\epsilon}\cos\theta=\cosh\alpha, \tag{6}$$

that the constants A_0, C_0 be connected by

$$\begin{aligned}&\sqrt{\epsilon}\sin^2\theta J_0(\sqrt{\epsilon}ka\sin\theta)A_0\\ &\qquad=-\sinh^2\alpha H_0^{(1)}(ika\sinh\alpha)C_0\end{aligned} \tag{7}$$

and lastly that θ, α, and the frequency be connected by the further relation

$$\frac{\sqrt{\epsilon}J_1(\sqrt{\epsilon}ka\sin\theta)}{\sin\theta J_0(\sqrt{\epsilon}ka\sin\theta)}=\frac{-iH_1^{(1)}(ika\sinh\alpha)}{\sinh\alpha H_0^{(1)}(ika\sinh\alpha)}. \tag{8}$$

In order that this be a good approximation we must assume that (see Fig. 2)

$$a\ll b. \tag{9}$$

We must also assume that α is not too small, to insure that the field does not extend to distances comparable with b. The condition is

$$kb\sinh\alpha\gg 1. \tag{10}$$

To get the field at larger distances we now assume that these formulas give correctly the components of E and their normal derivatives on the surface of the cylinder $\rho=R$ shown dotted in Fig. 2. For the space outside this cylinder we find an exact solution of the vector wave equation which fits these boundary values on the cylinder. This can be done by expanding in the true cylindrical coordinates ρ, ϕ, z, and making use of

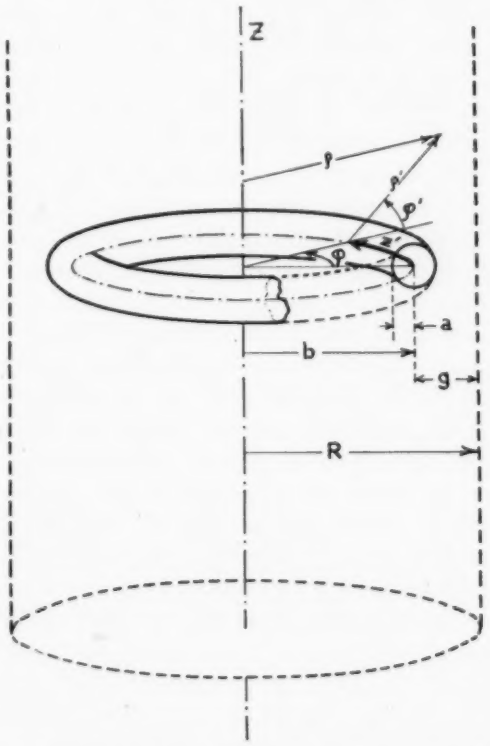

Fig. 2. Dielectric ring resonator, and various quantities used in the analysis: true cylindrical coordinates ρ, z, ϕ; pseudo-cylindrical coordinates ρ', z', ϕ'; and dimensions.

known Fourier transformations. Support is given to our belief that (5) is an approximate solution of the wave equation by the fact that under assumptions (9) and (10) the field outside is very nearly independent of the particular value of R chosen so long as R is only slightly greater than b, or more specifically so long as g, the difference of R and b, is comparable with a; and also by the fact that the resulting field outside the cylinder is very nearly divergence-free. We would like to use this field for the calculation of the radiated power. However we find that if we fit the boundary values exactly, although the field decreases rapidly with increasing ρ until quite large distances are reached, the field eventually starts getting large again, in fact so as to give an infinite amount of radiated power. This is where application of the definition of Section 3 comes in. This "radiated" power is of course not really radiated from the ring at all, but is due merely to waves coming in from infinity, missing the ring almost entirely, and going off to infinity again, and by a very slight change of the boundary conditions we could greatly reduce this part of the field which becomes large again at large distances, thus minimizing the radiated power or maximizing Q. The alteration of the field which this would require is very small near the ring, so that although (5) is not quite the field corresponding to a maximum of Q, it can be used for computing the wave-lengths and energy stored.

The actual minimizing of the radiated power for this case would involve practically insuperable mathematical difficulties, because the wave equation cannot be separated in any coordinate system in which the surface of the ring is a coordinate surface. Therefore we are forced to be satisfied with a qualitative estimate of Q, to which we will return later. The problem of determining these resonant modes exactly is somewhat analogous to that of calculating the current distribution in a radio antenna operating on a high harmonic. The analogy appears if one thinks in terms of the electromagnetic field surrounding the antenna, considered a perfect conductor, and again assumes for the sake of mathematical simplicity that the energy required to maintain the oscillations is furnished in the form of incoming waves. Here again the general solution of Maxwell's equations will contain an infinite number of parameters; and the actual field will be one for which Q, *qua* function of the parameters, is near a maximum; in a real antenna the current will automatically adjust itself so that this is the case. The "energy stored" is again somewhat indefinite but can be approximately defined in the limiting case of an antenna operating on a high harmonic, in which case the radiation field and the quasi-static field are clearly separated. In this limiting case, also, the radiated power, as calculated directly from the current, depends in a very sensitive way on the details of the assumed current distribution.

To obtain the wave-lengths we observe that when the field (5) is expressed in terms of the true cylindrical coordinates ρ, ϕ, z, the quantity $kb \cosh \alpha'$ must be an integer so that the functions will return to their initial values when the angle ϕ is increased by 2π. This is the same as Hansen's condition that the field must be in the same phase at the two ends which are joined together to make the ring and is the circumstance which determines the resonant frequencies. We call

$$kb \cosh \alpha' = m. \tag{11}$$

By use of Eqs. (6) and (8) we then get, for example, for $\epsilon = 5$, $b/a = 10$,

$$\begin{aligned} m &= 13, \quad kb \sinh \alpha' = 2.2, \quad \lambda/a = 4.90, \\ m &= 15, \quad kb \sinh \alpha' = 4.8, \quad \lambda/a = 4.43, \\ m &= 20, \quad kb \sinh \alpha' = 10.6, \quad \lambda/a = 3.71, \\ m &= 30, \quad kb \sinh \alpha' = 21.5, \quad \lambda/a = 3.03. \end{aligned}$$

λ is as before the vacuum wave-length; $m = 13$ gives the lowest mode of oscillation.

To obtain a qualitative estimate of Q we first solve the corresponding two-dimensional problem, obtaining a formula for Q, and then show that the qualitative predictions of this formula hold for the three-dimensional case as well.

The two-dimensional problem is defined as follows: (see Fig. 3). The part of the plane between the concentric circles of radii $b-a$ and $b+a$ contains the dielectric material. One seeks solutions E of the two-dimensional scalar wave equation subject to the condition that E and its two-dimensional curl be continuous at the boundary lines (circles). This is equivalent to the three-dimensional problem of finding certain electromagnetic waves in a thin cylindrical shell of infinite length parallel to the z axis. E is then

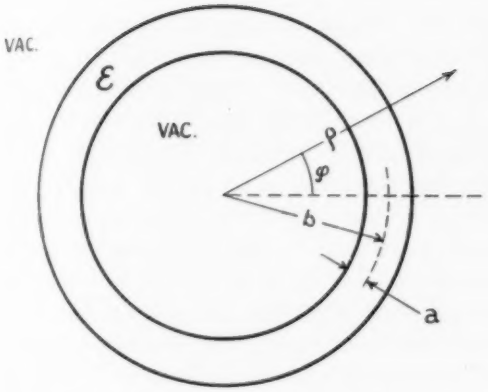

FIG. 3. Two-dimensional dielectric ring resonator.

the z component of the electric field for a solution independent of z.

The solution which interests us contains solutions of Bessel's equation of some order m, multiplied by $\exp(im\phi)$. The Bessel function will appear inside the inner circle, the Neumann function outside the outer circle, and both between the circles. The argument for these functions will be $k\rho$ outside the dielectric, and $\sqrt{\epsilon}k\rho$ in the dielectric. It is convenient as before to express m as

$$m = kb \cosh \alpha,$$

and then if conditions (9) and (10) are satisfied, and we assume again the simplest type of guided wave, it is quite easy to calculate approximately the energy stored and the power radiated, from which we get

$$Q = 4e^{2m(\alpha - \tanh \alpha)} \times \left\{ \frac{\epsilon ka(\epsilon - 1) + \cosh^2 \alpha \sinh \alpha}{\sinh \alpha(\epsilon - \cosh^2 \alpha)} \right\}. \qquad (12)$$

Perhaps the most striking thing about this result is the manner of variation with m. For a given resonator α is a function of m, increasing from near zero for the lowest allowed value of m to $\cosh^{-1}\sqrt{\epsilon}$ for $m = \infty$. But this variation of α is extremely slow, so that practically all the variation of Q is contained in the exponential factor. Just as in the case of the sphere it is in principle possible to get indefinitely large Q, neglecting dielectric losses, by suitable choice of the mode of oscillation.

The manner in which the radiation escapes from the two-dimensional ring is essentially the same as from the three-dimensional one. It escapes because the ϕ-nodes[7] of the function get farther apart with increasing distance from the axis. The initial rapid decrease of the field just outside the dielectric can continue only until the distances between these nodal planes becomes about equal to the wave-length, and beyond that the field must oscillate. The transition point comes at very nearly the same distance for the two- and three-dimensional cases, for a given value of m, while the rate of decrease of the field up to the transition point will be nearly the same for the two cases, for a given value of α. Therefore, if for each value of m one takes the corresponding value of α appropriate to the three-dimensional case, formula (12) should give roughly the correct variation of Q with m for this case.

For example, if $\epsilon = 5$, $b/a = 10$ again, formula (12) gives Q equal to about 140, 300, and $3.7 \cdot 10^6$ for $m = 15$, and 20, 30, respectively.

6. Effect of Bending Dielectric Wave-Guides

The ring-resonator of Fig. 3 may be thought of as equivalent to the bent wave guide of Fig. 4, with the difference that m is no longer restricted to integer values, since the ring is not complete.

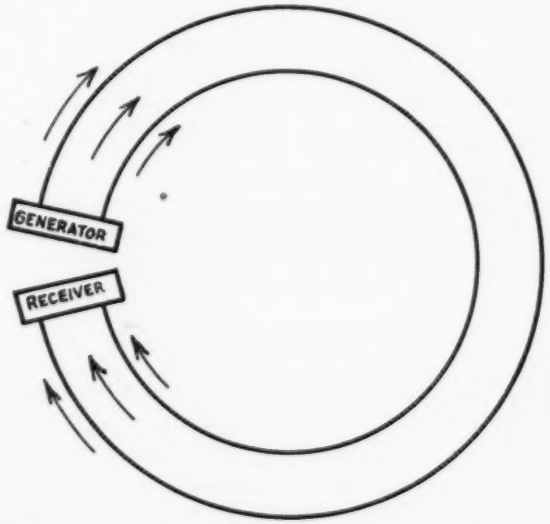

FIG. 4. A special case of a bent wave guide derived from the ring resonator.

[7] We should really speak of wave-fronts in this case instead of nodes, since we have used running waves in the ϕ-direction, represented by $\exp(im\phi)$.

The remarks of this section are purely qualitative, and apply also to the three-dimensional case. We have already computed the power lost by escape of radiation, and it is a simple matter to compute the power transmitted by such a guide, from which we get:

$$\frac{\text{Power lost in distance } \lambda_g \text{ along guide}}{\text{Power transmitted}} = \frac{\pi \tanh \alpha(\epsilon - \cosh^2 \alpha)}{2 \cosh \alpha[ka(\epsilon-1)+\sinh \alpha]} e^{-2m(\alpha - \tanh \alpha)}. \quad (13)$$

λ_g is the wave-length, as measured along the guide. m may be thought of as expressing the degree of straightness of the guide; it is in fact equal to 2π times the radius of bending divided by λ_g. Eq. (13) is, of course, strictly speaking, valid only for a guide bent into the arc of a circle, but no doubt some similar formula would hold for a guide bent into any other curve, so that we are led to the following conclusion: The attenuation of a dielectric wave guide which goes around a corner is always finite, but approaches zero (neglecting dielectric losses, etc.) more or less exponentially as the radius of bending is made large compared to the wave-length, and can therefore very easily be made negligible

Studies in Lubrication

V. The Theory of the Thick Film Lubrication of Flooded Journal Bearings and Bearings with Circumferential Grooves

M. Muskat and F. Morgan
Gulf Research & Development Company, Pittsburgh, Pennsylvania
(Received December 20, 1938)

The successive approximation theory for the thick film lubrication of flooded journal bearings and bearings with circumferential grooves is developed through the fourth approximation, that is, including the fifth power of the journal eccentricity. The analysis applies to bearings of arbitrary length, the boundary conditions at the ends of the bearings being satisfied rigorously. It is found that the journal eccentricities and friction coefficients, for fixed Sommerfeld variable, are greater for bearings of finite length than for that of infinite length, the difference increasing with decreasing bearing length. On the other hand the load-carrying capacities, for fixed eccentricity, of the bearings of finite length are much less than that for the infinitely long bearing. The general theory for the bearing with a central circumferential groove is also developed and it is shown that the only hydrodynamic effect of such a groove is to cut the bearing into two separate end fed bearings, each of half the original bearing length. The load-carrying and friction properties of these end fed bearings are identical with those of flooded bearings of the same length. The main advantages of such grooving must lie in the maintenace of the lubricant viscosity by the cooling effect of the lubricant flow and in overcoming the negative pressures and possible film rupture that would develop in a flooded bearing without internal lubricant sources.

Introduction

In THE previous papers[1–4] of this series results were presented on both theoretical and experimental investigations of full journal bearings operating in the thick film region and subjected to forced pressure lubricant feeds. A general theory was developed[3] which is applicable to arbitrary positions of the source of lubricant and valid for journal eccentricities less than or equal to $\frac{1}{2}$. Experiments[4] with the journal bearing machine have verified the essential features of this theory, and confirmed the predictions quantitatively in the range of small values of the dimensionless lubricant source strength.

While a theory which explicitly takes into account the presence of the lubricant source had

[1] M. Muskat and F. Morgan, J. App. Phys. **9**, 393 (1938).
[2] F. Morgan and M. Muskat, J. App. Phys. **9**, 539 (1938).
[3] M. Muskat and F. Morgan, J. App. Phys. **10**, 46 (1939).
[4] F. Morgan and M. Muskat, J. App. Phys. **10**, 327 (1939).

previously been lacking, several theoretical studies of journal bearing lubrication for flooded bearings of finite length have been published. Among these[5] only Vogelpohl's work, based on an application of the Ritz variation principle to the Reynolds equation, gives any numerical results, and even there the discussion was essentially limited to the pressure distributions in the film for a single bearing length. Moreover the Ritz method, in its actual application, is exclusively numerical, although it does provide the possibility of studying systems with high eccentricities. Reissner's theory appears to be subject to question since his functions for the pressure distribution do not seem to reduce to the Sommerfeld form as the bearing lengths are made infinitely large, while Skinner's series solutions involve expansion functions which have as yet been tabulated neither with respect to analytical properties nor numerical values.

The method to be presented here is essentially nothing more than a special application of the general theory previously developed[3] for finite length journal bearings fed with lubricant sources. However, because of the absence of lubricant sources it will be possible to make the solutions for the pressure distributions satisfy the boundary conditions at the ends of the bearing rigorously for all bearing lengths. Moreover, the solutions will be developed through the fourth approximation, whereas for bearings fed with lubricant sources it was not feasible to extend them beyond the second approximation.

General Theory

We may begin at once with the dimensionless[6] form of the generalized Reynolds equation for the pressure distribution in the film, namely:

$$\frac{\partial}{\partial\theta}\left\{(1+\eta\cos\theta)^3\frac{\partial p}{\partial\theta}\right\}+(1+\eta\cos\theta)^3\frac{\partial^2 p}{\partial w^2}=-\beta\eta\sin\theta, \quad (1)$$

where the film thickness h has been expressed in terms of the radial clearance c and the journal displacement e by the equation:

$$h=c+e\cos\theta, \quad \text{(cf. Fig. 1)}, \quad (2)$$

and the dimensionless quantities η, w, and β are defined by:

$$\eta=e/c; \quad w=z/r; \quad \beta=6\mu Ur/c^2, \quad (3)$$

where z is the axial coordinate, r the journal radius, μ the lubricant viscosity,[7] and U the surface velocity of the journal. η thus represents the journal eccentricity. It will be supposed that the load is applied to the journal.

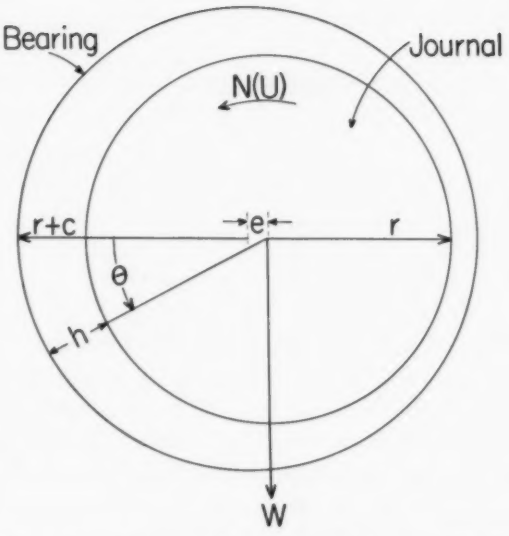

FIG. 1. Cross section of a full journal bearing system.

To solve Eq. (1) we introduce as before a successive approximation procedure in which all the physical quantities of interest are expanded in powers of the eccentricity η. That is, we assume that the pressure distribution $p(\theta, w)$ can be expanded in the form:

$$p(\theta, w)=\sum\eta^m p_m(\theta, w). \quad (4)$$

This is inserted in Eq. (1), and after the expansion of the various terms the coefficients of like powers of η are equated. We thus find a series of Poisson equations for p_m, given by:

[5] H. Reissner, Zeits. angew. Math. u. Mech. **16**, 275 (1936); G. Vogelpohl, V. D. I. Forschungsheft (1937), 386; S. M. Skinner, J. App. Phys. **9**, 409 (1938).

[6] It is supposed that both p and β are divided by a unit pressure.

[7] While the variation of the viscosity with the film temperature would be quite difficult to take into account under general conditions, the effect of the pressure can be taken care of by simply making the change of variable: $\Psi=\int(dp/\mu)$ before constructing Eq. (1). Its form will then remain invariant in the variable Ψ. (Cf. also S. Skinner, reference 5, and Bateman, *Hydrodynamics* (1932), p. 286.)

$$\left.\begin{aligned}
&\nabla^2 p_0 \equiv \partial^2 p_0/\partial\theta^2 + \partial^2 p_0/\partial w^2 = -\beta\eta \sin\theta \\
&\cdots\cdots\cdots\cdots\cdots\cdots \\
&\nabla^2 p_m = -3\left\{\cos\theta \nabla^2 p_{m-1} - \sin\theta \frac{\partial p_{m-1}}{\partial\theta}\right\} \\
&\qquad -3\cos\theta\left\{\cos\theta\nabla^2 p_{m-2} - 2\sin\theta\frac{\partial p_{m-2}}{\partial\theta}\right\} \\
&\qquad -\cos^2\theta\left\{\cos\theta\nabla^2 p_{m-3} - 3\sin\theta\frac{\partial p_{m-3}}{\partial\theta}\right\}.
\end{aligned}\right\} \quad (5)$$

The term $\beta\eta \sin\theta$ has been considered above as the zero-order term in spite of the coefficient η. This has been done in order to permit the asymptotic behavior of the system, where η approaches zero, to correspond to one where the load is nonvanishing, since in the limit of very small values of η, $\beta\eta$ becomes proportional to the load.

In constructing the solutions of Eqs. (5) we shall denote the dimensionless half-length, or ratio of length to the diameter, of the bearing by $\bar{w}$. The general conditions to be imposed upon the pressure distributions $p_m(\theta, w)$ are: (1) that p and $\partial p/\partial\theta$ reproduce themselves as θ makes the circuit of 2π around the circumference of the bearing; (2) that p reduces to the value 1 at the ends of the bearing;[8] and (3) that p shall be even in w. The second requirement will be satisfied by making p_0 equal to 1 at the ends of the bearing, and $p_m = 0$ at the ends for $m > 0$.

While, as already mentioned, Eqs. (5) are also applicable to bearings with internal lubricant point sources, we shall apply them here only to cases where the bearing is flooded, or has a circumferential groove.

Application to flooded bearings of finite length

Here we need simply to solve Eqs. (5) with no reference to a lubricant source. With this in mind we obtain for the

Zeroth approximation
$$p_0 = 1 + \beta\eta \sin\theta\left(1 - \frac{\cosh w}{\cosh \bar{w}}\right), \quad (6)$$

which clearly satisfies all the above mentioned requirements.

First approximation.—Combining Eq. (6) with the second of Eqs. (5), we have for the Poisson equation giving p_1:

$$\nabla^2 p_1 = 3\beta\eta \sin 2\theta\left(1 - \frac{\cosh w}{2\cosh \bar{w}}\right). \quad (7)$$

Its solution satisfying the required boundary conditions is:

$$p_1 = \frac{\beta\eta}{2}\sin 2\theta\left\{-\frac{3}{2} + \frac{\cosh w}{\cosh \bar{w}} + \frac{\cosh 2w}{2\cosh 2\bar{w}}\right\}. \quad (8)$$

Second approximation.—Inserting the equations for p_0 and p_1 into the second of Eqs. (5), it is readily found that p_2 must satisfy the equation:

$$\nabla^2 p_2 = \frac{3}{2}\beta\eta\left[3\sin 3\theta\left\{-1 + \frac{\cosh w}{2\cosh \bar{w}} + \frac{\cosh 2w}{6\cosh 2\bar{w}}\right\} - \frac{1}{2}\sin\theta\left\{\frac{\cosh w}{\cosh \bar{w}} + \frac{\cosh 2w}{\cosh 2\bar{w}}\right\}\right]. \quad (9)$$

Its solution may be shown to be:

$$p_2 = \frac{\beta\eta \sin 3\theta}{160}\left\{80 - 45\frac{\cosh w}{\cosh \bar{w}} - \frac{24\cosh 2w}{\cosh 2\bar{w}} - \frac{11\cosh 3w}{\cosh 3\bar{w}}\right\}$$
$$-\frac{\beta\eta}{4}\sin\theta\left\{\frac{3}{2}\frac{w\sinh w}{\cosh \bar{w}} - \frac{3}{2}\frac{\bar{w}\tanh \bar{w}\cosh w}{\cosh \bar{w}} + \frac{\cosh 2w}{\cosh 2\bar{w}} - \frac{\cosh w}{\cosh \bar{w}}\right\}. \quad (10)$$

[8] This requirement involves dropping terms of the order of h^2/r^2 in the rigorous boundary condition which refers to the normal stress in the film at the ends of the bearing.

Third approximation.—Proceeding as before, we find for the third approximation the equation for p_3:

$$\nabla^2 p_3=\beta\eta\sin 2\theta\Big[1+10\cos 2\theta+\Big(\frac{57}{64}-\frac{153}{32}\cos 2\theta\Big)\frac{\cosh w}{\cosh \bar{w}}+\frac{3(1-7\cos 2\theta)\cosh 2w}{10\cosh 2\bar{w}}$$
$$-\frac{99(2\cos 2\theta-1)\cosh 3w}{320\cosh 3\bar{w}}-\frac{9w\sinh w}{16\cosh \bar{w}}+\frac{9\bar{w}\tanh \bar{w}\cosh w}{16\cosh \bar{w}}\Big], \quad (11)$$

with the solution:

$$p_3=\frac{\beta\eta\sin 2\theta}{4}\Big[-1-\frac{5}{2}\cos 2\theta-\frac{\cosh w}{4\cosh \bar{w}}\Big(\frac{11}{4}+3\bar{w}\tanh \bar{w}-\frac{51}{10}\cos 2\theta\Big)+\frac{3w\sinh w}{4\cosh \bar{w}}+\frac{3w\sinh 2w}{10\cosh 2\bar{w}}$$
$$+\frac{7\cos 2\theta\cosh 2w}{10\cosh 2\bar{w}}+\frac{99(\frac{3}{7}\cos 2\theta+\frac{1}{5})\cosh 3w}{80\cosh 3\bar{w}}$$
$$+\frac{3}{5}\Big(\frac{12}{5}-\frac{1}{2}\bar{w}\tanh 2\bar{w}\Big)\frac{\cosh 2w}{\cosh 2\bar{w}}+\frac{6}{35}\frac{\cos 2\theta\cosh 4w}{\cosh 4\bar{w}}\Big]. \quad (12)$$

Fourth approximation.—Combining the previous solutions as indicated in Eqs. (5), we obtain as the equation determining p_4:

$$\frac{\nabla^2 p_4}{\beta\eta}=-\frac{75}{16}\sin 5\theta-\frac{45}{16}\sin 3\theta-\frac{3}{8}\sin\theta+\frac{3\cosh w}{16\cosh \bar{w}}\Big[\frac{459}{40}\sin 5\theta-\Big(\frac{77}{20}+\frac{9}{2}\bar{w}\tanh \bar{w}\Big)\sin 3\theta$$
$$+\frac{3}{2}\Big(\frac{1}{4}+\bar{w}\tanh \bar{w}\Big)\sin\theta\Big]+\frac{3\cosh 2w}{10\cosh 2\bar{w}}\Big[\frac{7}{2}\sin 5\theta+\Big(\frac{31}{10}-\frac{3}{4}\bar{w}\tanh 2\bar{w}\Big)\sin 3\theta$$
$$-\Big(\frac{41}{10}-\frac{3}{4}\bar{w}\tanh 2\bar{w}\Big)\sin\theta\Big]+\frac{99\cosh 3w}{320\cosh 3\bar{w}}\Big[\frac{19}{14}\sin 5\theta-\frac{9}{35}\sin 3\theta-\frac{11}{10}\sin\theta\Big]$$
$$+\frac{9}{70}\frac{\cosh 4w}{\cosh 4\bar{w}}(\sin 5\theta-\sin 3\theta)+\frac{9}{32}\frac{w\sinh w}{\cosh \bar{w}}(3\sin 3\theta-\sin\theta)+\frac{9w\sinh 2w}{40\cosh 2\bar{w}}(\sin 3\theta-\sin\theta). \quad (13)$$

The solution of this equation is:

$$\frac{p_4}{\beta\eta}=\frac{1}{2}\sin 5\theta\Big[\frac{3}{8}-\frac{459}{2560}\frac{\cosh w}{\cosh \bar{w}}-\frac{1}{10}\frac{\cosh 2w}{\cosh 2\bar{w}}-\frac{19\times 99}{56\times 640}\frac{\cosh 3w}{\cosh 3\bar{w}}-\frac{1}{35}\frac{\cosh 4w}{\cosh 4\bar{w}}-\frac{15}{1024}\frac{\cosh 5w}{\cosh 5\bar{w}}\Big]$$
$$+\sin 3\theta\Big[\frac{5}{16}+\frac{3}{256}\Big(\frac{109}{20}+9\bar{w}\tanh \bar{w}\Big)\frac{\cosh w}{\cosh \bar{w}}-\frac{27}{256}\frac{w\sinh w}{\cosh \bar{w}}$$
$$-\frac{3}{100}\Big(\frac{37}{5}-\frac{3}{2}\bar{w}\tanh 2\bar{w}\Big)\frac{\cosh 2w}{\cosh 2\bar{w}}-\frac{9}{200}\frac{w\sinh 2w}{\cosh 2\bar{w}}$$
$$-\frac{1}{140\times 160}\Big(\frac{852{,}991}{280}-297\bar{w}\tanh 3\bar{w}\Big)\frac{\cosh 3w}{\cosh 3\bar{w}}-\frac{297}{140\times 160}\frac{w\sinh 3w}{\cosh 3\bar{w}}-\frac{9}{490}\frac{\cosh 4w}{\cosh 4\bar{w}}\Big]$$
$$+\frac{\sin\theta}{4}\Big[\frac{3}{2}-\frac{23}{256}\frac{\cosh w}{\cosh \bar{w}}+\frac{9}{16}\Big(\frac{3}{4}+\bar{w}\tanh \bar{w}\Big)\Big(\frac{w\sinh w}{\cosh \bar{w}}-\frac{\bar{w}\tanh \bar{w}\cosh w}{\cosh \bar{w}}\Big)$$
$$+\frac{9}{32}(\bar{w}^2-w^2)\frac{\cosh w}{\cosh \bar{w}}-\frac{1}{5}\Big(\frac{31}{5}-\frac{3}{2}\bar{w}\tanh 2\bar{w}\Big)\frac{\cosh 2w}{\cosh 2\bar{w}}-\frac{3}{10}\frac{w\sinh 2w}{\cosh 2\bar{w}}-\frac{11\times 99}{6400}\frac{\cosh 3w}{\cosh 3\bar{w}}\Big]. \quad (14)$$

In a similar manner one could obtain the higher approximation solutions. However, because of their increasing complexity and the rather slow convergence of the series for high values of η we shall go no further here than the fourth. With this degree of approximation the solution should be reasonably accurate up to values of $\eta=0.6$, since actual calculations show that the higher order terms do not contribute greatly to the resultant values of pressure distribution and load components as long as η does not exceed 0.6.

To obtain the load that can be supported by the pressure distribution corresponding to

$$p=p_0+\eta p_1+\eta^2 p_2+\eta^3 p_3+\eta^4 p_4+\cdots, \quad (15)$$

one need simply integrate its components parallel and perpendicular to the polar axis. Since:

$$\int_0^{2\pi} p\cos\theta d\theta=0, \quad (16)$$

it follows that the resultant load supported by the film will be normal to the line of centers. This means, in turn, that the line of centers will always be horizontal, as the actual load on the journal, which the film must support, will be vertical. Hence, setting the integrated component of the pressure normal to the line of centers equal to the total load, and introducing the notation:

$$\left.\begin{aligned}
g_1&=2(\bar{w}-\tanh\bar{w}),\\
g_2&=-\tfrac{1}{4}\{3\bar{w}\,\mathrm{sech}^2\,\bar{w}+\tanh 2\bar{w}-5\tanh\bar{w}\},\\
g_3&=\frac{9}{32}\bar{w}^2\tanh\bar{w}\,\mathrm{sech}^2\,\bar{w}\\
&\quad+\frac{3}{4}\bar{w}\left(1+\frac{21}{32}\mathrm{sech}^2\,\bar{w}-\frac{1}{10}\mathrm{sech}^2\,2\bar{w}\right)\\
&\quad-\frac{275}{512}\tanh\bar{w}-\frac{109}{400}\tanh 2\bar{w}\\
&\quad-\frac{363}{12{,}800}\tanh 3\bar{w},
\end{aligned}\right\} \quad (17)$$

we have:

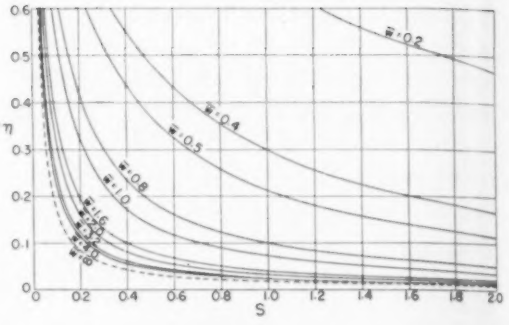

FIG. 2. The variation of the journal eccentricity, η, with the Sommerfeld variable, S, for flooded journal bearings of finite length. $\bar{w}=$(bearing length)/(bearing diameter); $S=(r^2/c^2)(\mu N/P)$, where $r=$journal radius, $c=$radial clearance; $\mu=$lubricant viscosity; $N=$journal speed (r.p.s.), and $P=$load per unit projected bearing area.

$$W=\int_{-\bar{w}}^{\bar{w}} dw\int_0^{2\pi} p\sin\theta d\theta$$
$$=\pi\beta\eta[g_1+g_2\eta^2+g_3\eta^4+\cdots], \quad (18)$$

where r^2W is the actual load. Introducing also the Sommerfeld variable defined by

$$S=(r^2/c^2)(\mu N/P),$$

where P is the load per unit projected bearing area, so that $\beta=3\pi SW/\bar{w}$, Eq. (18) may be solved for β or S, and expressed in the form

$$S=\frac{(\bar{w}/3\pi^2\eta)}{g_1+g_2\eta^2+g_3\eta^4}, \quad (19)$$

thus giving the relation between journal eccentricity η and the Sommerfeld variable S.

This relation has been plotted in Fig. 2 for various values of $\bar{w}$, and for values of η up to 0.6. The dotted curve in Fig. 2 is the variation predicted by the Sommerfeld theory, namely:

$$S_0=\frac{(2+\eta^2)(1-\eta^2)^{\frac{1}{2}}}{12\pi^2\eta}, \quad (20)$$

and gives the same expansion as Eq. (19), when $\bar{w}$ is made indefinitely large, up to terms in η^5.

It will be seen that the eccentricity assumed by the journal for a given value of S uniformly increases as the dimensionless half bearing length $\bar{w}$ decreases. This is, of course, due to the fact that the dropping off of the pressure to atmospheric at the ends of the bearing leads to smaller average pressures in the bearings of short

length, which in turn necessitate greater eccentricities and wedging effects to permit the support of loads of the same magnitude. This effect may be seen more clearly by computing the relative load carrying capacities of the finite length bearings as compared to that for the infinitely long bearing having the same journal eccentricity. Assuming equal values of r/c, μ, and N, the load carrying capacity will clearly be proportional to the reciprocal of the Sommerfeld variable. The relative load carrying capacities will therefore be given simply by S_0/S, where S_0 and S are given by Eqs. (20) and (19), respectively, or by the abscissas of the dotted and solid curves of Fig. 2. Such comparisons are shown graphically in Fig. 3 for different values of $\bar{w}$.

As Fig. 3 shows, the relative load carrying capacities for fixed eccentricities of the finite length flooded bearings are uniformly less than one. Moreover, the load-carrying capacity decreases continuously with decreasing bearing length. Thus, for a bearing length equal to the bearing diameter ($\bar{w}=1$), the load-carrying capacity for the same eccentricity will be of the order of 25–30 percent of that of the infinitely long bearing, and for a bearing length equal to one-half the diameter, the load-carrying capacities will fall to less than 10 percent of the infinitely long bearing values. These results may be contrasted with the values $\frac{2}{3}$ and $2/\pi$—for all η—obtained on the common assumptions that the axial pressure distributions fall in parabolic or trigonometric manner, respectively, from the Sommerfeld distribution along the central circumference.

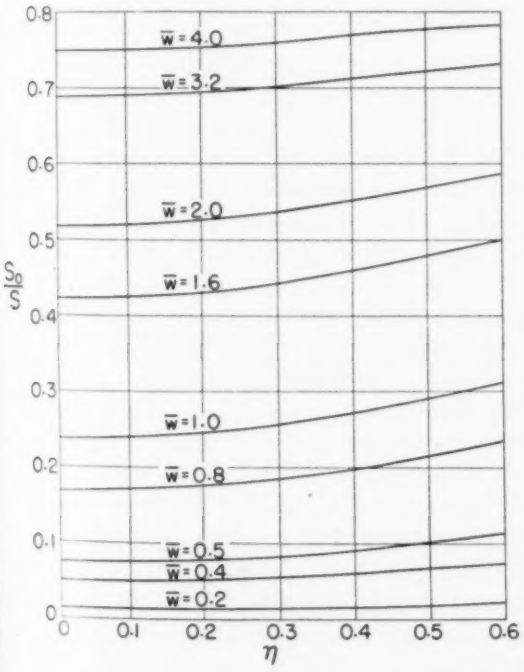

FIG. 3. Relative load carrying capacities of flooded journal bearings of finite length. S_0/S = (load carrying capacity of finite length bearing)/(capacity of infinitely long bearing of same eccentricity, η); $\bar{w}$ = (bearing length)/(bearing diameter).

These results do not, of course, necessarily imply corresponding differences in ultimate load-carrying capacities of the finite length journal bearings. Rather they give only the relative values of the load-carrying capacity of the finite length bearings as compared to those for the infinitely long bearing for the same value of η, that is, *the same geometry*. All that would be necessary to obtain in a finite length bearing any predetermined load-carrying capacity corresponding to an infinitely long bearing with fixed eccentricity would be to increase the eccentricity of the former. In principle, it will be possible to obtain arbitrarily large load-carrying capacities with the finite length bearing to the same extent that such would be possible with bearings of infinite length, although, from a practical point of view, the higher eccentricities that would be required in the case of a finite length bearing might lead to seizing or scoring of the bearing somewhat earlier than under the hypothetical case of the infinitely long bearing.

To determine the friction properties of the journal bearing systems, one must introduce the hydrodynamic expressions for the surface tractions acting on the journal bearing surfaces. The absolute magnitude of these are given by:

$$\sigma=\frac{\mu U}{h}\pm\frac{h}{2r}\frac{\partial p}{\partial\theta}, \tag{21}$$

where the + refers to the traction on the journal and the − to that on the bearing. Integrating formally the right-hand side over the complete journal or bearing surfaces, dividing the result by the load, and making use of the previously introduced notation, we find for the coefficient

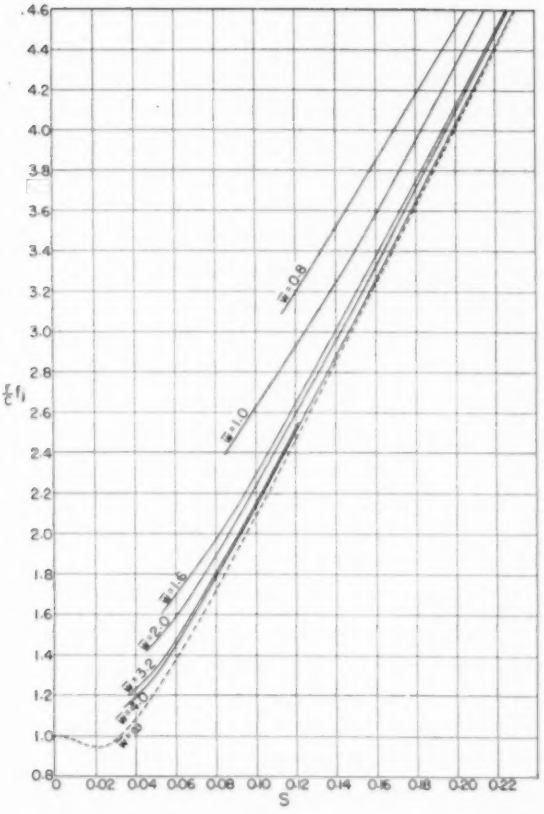

FIG. 4. Friction coefficients on the journal, f_j, *vs.* S for flooded bearings of finite length; $\bar{w}$=(bearing length)/(bearing diameter); dotted curve represents Sommerfeld curve for infinitely long bearing.

of friction, f:

$$\frac{r}{c}f=\frac{2\pi^2 S}{(1-\eta^2)^{\frac{1}{2}}}\pm\frac{\eta}{2}. \tag{22}$$

Having already determined the relation between η and S (Fig. 2), it is a simple matter to compute the friction coefficient as a function of the Sommerfeld variable S. The results of such calculations for the friction on the journal are shown in Fig. 4, the dotted curve again referring to the case of the infinitely long bearing. It will be seen that in general the friction coefficients for the finite length bearings are higher than those for the infinitely long bearing, the differences increasing as the bearing length decreases. Asymptotically, however, they all approach the Petroff line,

$$(r/c)f=2\pi^2 S, \tag{23}$$

as follows directly from Eq. (22) on letting η approach 0. The reason for the higher friction coefficients for the finite length bearings obviously lies in the higher eccentricities previously found (Fig. 2) for fixed values of S. The fact that the curves do not continue to vanishing values of S arises from the limitation of the approximation method developed here to rather small values of η. In fact, the last points on the curves correspond to $\eta=0.6$, and smaller values of S would require eccentricities that are still higher, and which cannot be quantitatively treated when one includes only fourth-order terms.

To obtain the friction coefficients on the bearing, one need only subtract from the values for the journal plotted in Fig. 4 the magnitudes of η corresponding to the abscissas S. These, in turn, may be read off the curves of Fig. 2. Although the friction coefficients on the bearing thus found will not vary so greatly among themselves nor differ so much from that for the infinitely long bearing, as in the case of the friction coefficients on the journal, the deviations will still be of appreciable magnitude, especially for the bearings of short length.

BEARINGS WITH CIRCUMFERENTIAL GROOVES

From a practical point of view, flooded bearings without any internal sources of lubricants are not of as great interest as those supplied with lubricant sources. We shall therefore consider now the case where the lubricant is supplied through a circumferential groove extended over the whole bearing perimeter. As a physical definition, we shall suppose a groove to be a channel cut into the bearing surface with dimensions which are large compared with the bearing clearance. The inflow pressure of the lubricant may, therefore, be taken as uniformly distributed over the whole length of the groove, since the pressure drop in it will be small compared to that within the lubricating film.

On the basis of this picture, putting a circumferential groove into a bearing is equivalent to cutting the bearing in two parts, and providing each part with a uniform lubricant pressure along the adjacent ends. The pressure distributions in the interior of the two parts will then become independent of each other, and each will behave as an independent bearing of length determined by the total length of the bearing and the position

of the groove. Each part, however, will correspond to a bearing with a lateral end feed, the feed pressure being that maintained at the groove. The complete bearing will therefore become equivalent to a combination of two adjacent end fed bearings with the same pressure feed.

While the pressure distribution in such end-fed bearings might offhand appear to require new types of solutions of the fundamental differential equation (1), it turns out that they may be obtained from those already derived for the flooded bearings by the simple addition of terms representing only the axial lubricant flow due to the end feed. Thus if we again denote the over-all dimensionless bearing length by $2\bar{w}$ (cf. Fig. 5) and suppose the groove to be set at the center of the bearing, the two end-fed bearings will have a dimensionless total length of $\bar{w}$, or half-length of $\bar{w}/2$. Denoting then by the subscript f the pressure distribution for a flooded bearing, it immediately follows from the linearity of the Eq. (1) that the pressure distribution in each end-fed bearing will be given by:

$$p = p_f\left(\frac{\bar{w}}{2}, \eta, \beta, \theta, w\right) + \frac{(\bar{w}-2w)}{2\bar{w}}p_g, \quad (24)$$

where the parameter $\bar{w}/2$ in p_f indicates that p_f refers to a flooded bearing of dimensionless half-length $\bar{w}/2$, η and β have their usual significance as defined in Eqs. (3), w is the dimensionless axial coordinate measured from the center of each end fed bearing with the positive axis directed toward the ends of the composite bearing, and where p_g represents the pressure maintained at the groove. It will be seen from Eq. (24) that whereas the feed pressure due to a lubricant point source adds to the resultant film pressure distribution pressures which decrease as one recedes from the point source along the perimeter of the bearing, the pressure imposed at a complete circumferential groove adds on uniformly over the whole circumference of the bearing and diminishes linearly as one recedes axially from the position of the groove.

To obtain the friction properties of a bearing with a pressure distribution given by Eq. (24) one may proceed formally without specifying in detail the exact form of the function p_f. Thus since p_f gives no resultant component parallel to the line of centers (cf. Eq. (16)), neither will the pressure distributions in the bearings with circumferential grooves. Hence denoting the total load applied to a journal in a bearing with a circumferential groove by r^2W, and that for a flooded bearing by r^2W_f, we have:

$$W = 2\int_{-\bar{w}/2}^{\bar{w}/2} dw \int_0^{2\pi} p \sin\theta d\theta$$

$$= 2\int_{-\bar{w}/2}^{\bar{w}/2} dw \int_0^{2\pi} p_f\left(\frac{\bar{w}}{2}, \eta, \beta, \theta, w\right) \sin\theta d\theta$$

$$= 2W_f\left(\frac{\bar{w}}{2}, \eta, \beta\right), \quad (25)$$

where again the parameter $\bar{w}/2$ in W_f indicates that the flooded bearing values for the load will be those corresponding to dimensionless half lengths of $\bar{w}/2$.

Recalling now (cf. Eq. (18)) that W_f is directly proportional to β or S, we obtain as a formal analog of Eq. (19) for the flooded bearing:

$$S = \frac{\bar{w}/2}{\Psi(\bar{w}/2, \eta)}; \quad \eta = \eta\left(S, \frac{\bar{w}}{2}\right), \quad (26)$$

where the functional forms of Ψ or of $\eta(S, \bar{w}/2)$ are those determined by the theory for the flooded bearing. And finally the friction coefficients for the bearing with the circumferential groove will be given by:

$$\frac{r}{c}f = \frac{2\pi^2 S}{(1-\eta^2)^{\frac{1}{2}}} \pm \frac{\eta}{2} = \frac{r}{c}f\left(\frac{\bar{w}}{2}, S\right), \quad (27)$$

where again the functional form of $f(\bar{w}/2, S)$ will be exactly that corresponding to a flooded bearing.

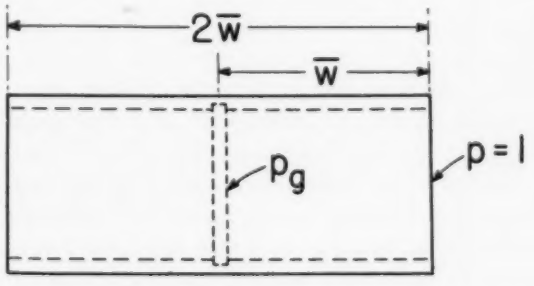

FIG. 5. Diagrammatic representation of a bearing with a circumferential groove with a feed pressure p_g.

We thus see that both the eccentricity and friction coefficients of the bearing with the circumferential groove will depend upon S in exactly the same way as do those for a flooded bearing, except that the effective bearing length must be taken to be half of that of the whole bearing. In other words, the whole behavior of the composite bearing with the circumferential groove becomes identical with that of its two halves, each acting as a flooded bearing with its own true length. While the pressure maintained at the groove does induce a uniform linear axial lubricant flow toward the two ends of the composite bearing, the behavior of the parts of the bearing separated by the groove is not affected by this axial lubricant flow nor by the magnitude of the feed pressure. The feed pressure will add on uniformly over the perimeter of the bearing and will serve to minimize or completely overcome the tendency for the development of negative pressures within the two parts of the composite bearing. In addition the actual lubricant flow through the bearing will be proportional to the groove feed pressure p_g. In fact it can easily be shown that the rate of flow, Q, will be given by:

$$Q=\pi rc^3(2+3\eta^2)p_g/3\mu L, \qquad (28)$$

where L is the true over-all length of the bearing. But the resultant effects on the load carrying and friction properties of the two parts will be nil, except insofar as one introduces the question of the maintenance of complete lubricant films by means of the pressure feed as contrasted with possible film breakdowns due to negative pressures in the ordinary flooded bearing, as will be seen below.

From the above general treatment of the bearing with circumferential grooves, we see that the detailed properties such as the variation of the journal eccentricity with S or of the friction coefficient with S will be given by exactly the same numerical results already derived for the flooded bearings, provided only that we consider the dimensionless length of the flooded bearing to be half of the true dimensionless length of the composite bearing. That is, a circumferential groove in a bearing cuts the effective bearing length in half[9] with respect to its load carrying power and friction properties. As will be seen from Figs. 2, 3, and 4, the magnitude of this effect is much larger than that which could be attributed to merely cutting the length of the composite bearing by the width of the groove, especially if the bearings are initially of relatively short length. Thus in the case of a bearing 1 inch in diameter and 1 inch long having a circumferential groove $\frac{1}{8}$-inch in width, the mere decrease in actual bearing length due to the presence of the groove would increase the journal eccentricity corresponding to $S=1$ from 0.072 to 0.0875, whereas the effective splitting of the bearing into two parts, each of $\frac{7}{16}$-inch length, would be to increase the eccentricity to 0.26. Similarly for an eccentricity of $\frac{1}{2}$, the relative load carrying capacity of the bearing with the groove would be cut from 0.29 to 0.237 if the total effect were simply that of decreasing the length by the width of the groove, whereas the actual effects as indicated above would be to cut the relative load carrying capacity to 0.081.

While it appears from these considerations that a circumferential groove would impair the lubricating effectiveness of a journal bearing from a strictly hydrodynamic point of view, there are two considerations pertinent to the practical use of journal bearings which may offset the hydrodynamic disadvantage of the circumferential groove. The first is that the rate of lubricant flow through the bearing would obviously be greater in a bearing fitted with a circumferential groove than in a flooded bearing. When the bearings are operated so that the temperature rise of the lubricant tends to become appreciable, the cooling effect of the lubricant flow and maintenance of the high viscosity of the lubricant may become a significant factor in maintaining the load supporting capacity of the lubricating film. This effect may be especially important when the bearing is operated under thin film conditions, where the fall in lubricant viscosity due to the temperature rise would tend to aggravate the tendency for metallic contact to develop and ultimately cause seizing or scoring of the bearings.[10]

[9] If the width of the groove is not negligible compared to the total bearing length, the effective lengths of the parts separated by the groove should each be diminished by half the groove width.

[10] We are indebted to Mr. R. J. S. Pigott of this Laboratory for pointing out this advantageous feature of the bearing with the circumferential groove.

An even more valuable feature of the circumferential groove may result from the possibility of overcoming the negative pressures in the lubricant film by means of the added feed pressure applied at the groove. Thus if it be admitted that the lubricant film cannot stand negative pressures, it would follow that it would be impossible to maintain a complete lubricating film in an ordinary flooded bearing except at very low loads. In actual operation, therefore, air would be sucked into the journal bearing clearance and the bearing would operate with only a partial film. Now in the theoretical hydrodynamic film the pressures over half the bearing surface are just as much below atmospheric as those in the other half are above atmospheric. Moreover the film in the half of the bearing where the pressures are below atmospheric supports just as much load as that where the pressures exceed atmospheric. It is thus clear that if the film over the pressure deficient half be broken the load supporting power of the film will be cut in half, so that a flooded bearing subjected to appreciable loads would tend to have actual load carrying powers only half of those theoretically predicted. However, since the feed pressures in the circumferential groove are uniformly distributed over the whole periphery of the bearing, these feed pressures will tend to overcome the negative pressures that would theoretically obtain in the flooded bearing. If the feed pressures are sufficiently high, the breaking of the film will be prevented, and consequently it will be able to support the full value of the load as predicted by the hydrodynamic theory. The final practical result might, therefore, well be that the bearing with the circumferential groove will actually support more load for a given eccentricity than would the flooded bearing, in spite of the fact that theoretically the effective length of the former will be only half of that of the bearing without the groove.

While the theory developed in this section has referred explicitly to bearings with circumferential grooves placed midway between the ends of the bearing, it will also clearly apply to flooded bearings with forced feeds at the ends of the bearing. In fact, Eq. (24) definitely refers just to such types of bearing, two of which constitute, from a hydrodynamic point of view, the bearing with the central circumferential groove. Likewise the same analysis will apply to bearings having two or more circumferential grooves placed symmetrically with respect to the center even though the feed pressure in the various grooves may not be the same. On the other hand, if there be one or more circumferential grooves in a bearing placed unsymmetrically with respect to the central circumference, it will in general be impossible to operate the journal and bearing and still maintain parallelism between their axes. For, in addition to the actual loads supported by each part of the bearing bounded by the circumferential grooves or the ends, there will be force moments associated with these loads. In order to maintain the axes of the journal and bearing parallel it is obviously necessary that the moments of the various parts of the bearing about the bearing center be balanced. This will clearly obtain in the case of the single central circumferential groove or when two or more such grooves are placed symmetrically with respect to the central circumference. But when the groove is not symmetrical, neither the moments nor the loads for the two parts will be equal unless the system be operated at a fixed value of the Sommerfeld variable and of the eccentricity. If the conditions of operation deviate from these, the moments from the several parts of the bearing will become unbalanced and the bearing will tilt with respect to the journal and the axes of the journal and bearing will no longer be parallel. While such a condition of lubrication does not necessarily mean immediate failure, it is certainly not the type that would be conducive to stability and satisfactory performance.

The authors are indebted to Mr. M. W. Meres for making the calculations and preparing the drawings given in this paper, and to Dr. Paul D. Foote, Executive Vice President, Gulf Research & Development Company, for permission to publish this paper.

Phosphorescence of Zinc Silicate Phosphors

GORTON R. FONDA
General Electric Company, Schenectady, New York

(Received January 9, 1939)

At low contents of the manganese activator, the decay of phosphorescence takes place in two stages. The initial stage is exponential. It is complete in less than 0.1 second and is not affected by temperature. The second stage is at a much lower intensity level. It becomes noticeable after 0.03 second and persists for more than an hour. Its speed of decay increases with temperature. At −196°C it is completely latent. A change in the intensity of the exciting light alters proportionally the luminescence caused by each stage of decay and has no effect upon the shape of the decay curves.

About fifty times as many electrons are involved in the second stage of decay as in the first. It is assumed that the second stage is caused by the retention of electrons in a metastable state, probably one associated with the presence of lattice imperfections. The exponential decay of the first stage would result from the recombination of manganese ions, relatively in excess, with those free electrons which had not been captured in the potential cups of the metastable state.

The decay of phosphors rich in manganese is always very abrupt and at a speed which rises rapidly with increase in temperature. The course of decay can be represented by the expression $p^{-2}=a+bt$ except at reduced temperatures where the two stages of decay characteristic of low manganese content are observable.

THE light emitted by a phosphor during exposure to an exciting source of radiation is known as fluorescence. In many cases the fluorescent substance continues to emit light after the exciting radiation is extinguished. Such a delayed emission of light is known as phosphorescence. It is accepted that the two are intimately related as manifestations of the same fundamental phenomenon; namely, excitation of an activator atom which is present in the phosphor at a very low concentration. When the excited electron returns directly to its normal orbit, fluorescence is observed as the result of what Lenard[1] calls an instantaneous process. When, however, the return of the electron is for any reason delayed, thus giving rise to phosphorescence, then, by way of distinction, Lenard terms the luminescence the result of a delay process.

The appearance of phosphorescence in a phosphor is proof that the delay process is contributing at least some of the luminescence, even during direct excitation. Wherever this is so, evidence of it will be seen also when the exciting radiation is first applied, for there will be a lag in the development of full luminescence. The delay process in fact is characterized by these two features—a slow rise to full luminescence when excitation is first applied, and a slow decay of luminescence when the excitation is withdrawn. This is in contrast to what is observed when all of the luminescence arises from the instantaneous process, for in that case the initial rise and final decay are limited to an instant only, of the order of 10^{-8} sec., the time involved in the jump of the excited electron. Observations on the rate of rise and rate of decay furnish, then, a means of determining whether the luminescence from a phosphor arises from the instantaneous or delay process or from a combination of both. In the last case suitable measurements would even show the relative magnitudes of the two processes.

This is illustrated in the three cases represented by the curves of Fig. 1. The exciting radiation is applied at (a) and extinguished at (c). When the instantaneous process only is active, the luminescence rises at once to the ultimate value (af), and its decay at the point (c) is equally abrupt. When the luminescence is caused altogether by the delay process, an initial rise is observable and it begins at zero luminescence. Similarly the final decay follows such a law as to demonstrate that it is proceeding downward from the value which it had at full luminescence. When both processes are present, the luminescence will rise abruptly to a point (e) and then continue at a finite rate to the full

[1] P. Lenard, F. Schmidt and R. Tomaschek, "*Handbuch der Experimental Physik*," Vol. 23, Part I (1928), p. 61.

value (af). The amount of light furnished by the instantaneous process will consequently be given by the ratio ae/af. When the excitation is extinguished at the point (c), there will be an abrupt decrease in luminescence, equal in extent to the initial abrupt rise, and thereafter a decay at a measurable rate.

An example of a simple case in the type of analysis outlined above is furnished by zinc silicate and it was therefore chosen as the phosphor used in the experiments to be described. It is activated by manganese and is notable for its high efficiency of conversion of short wave ultraviolet radiation into visible radiation lying in the green.[2] Preliminary tests

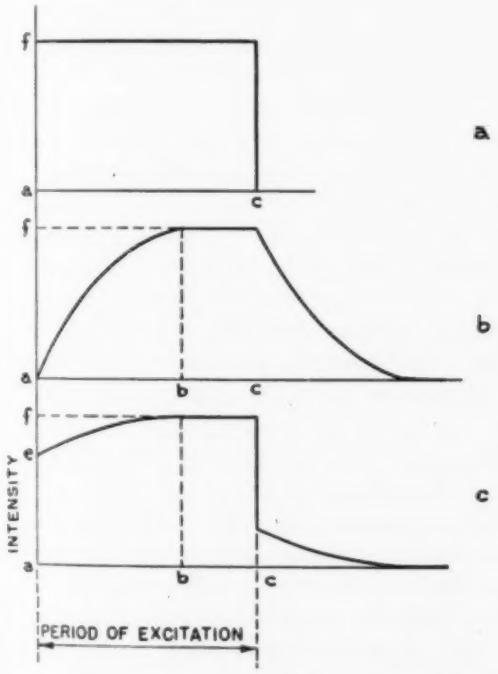

FIG. 1. Types of luminescence from phosphors. (a) Instantaneous process only. (b) Delay process only. (c) Combination of instantaneous and delay processes.

showed that its initial rate of decay is slower than that of zinc sulfide. In later periods, however, its decay becomes more rapid than that of zinc sulfide, the persistence of whose phosphorescence is very considerable. Furthermore, the phosphorescence of zinc silicate was found to vary with the composition of the phosphor and with the treatment given it, in such a way that the resulting decay curves furnish material for theoretical consideration of the factors involved in producing phosphorescence.

[2] G. R. Fonda, J. Phys. Chem., awaiting publication.

MEASUREMENTS OF PHOSPHORESCENCE

More definite information on zinc silicate was obtained by tests with a phosphoroscope which allowed variation in the time of excitation. As usual, it had two revolving disks mounted on the same shaft. There was a sector opening in each disk. On one side of the pair of disks was placed the exciting light, a low pressure mercury discharge operating at 2 amp. direct current in a quartz tube 1.8 cm in diameter. In addition to the mercury the tube contained 4 mm of argon to facilitate starting. For most of the tests, the lamp was placed 10 cm distant from the phosphor. The phosphor, mounted on a glass plate, was held between the disks. In the normal position, the side of the glass coated with the phosphor was turned toward the lamp. On the other side of the disks and directly behind the phosphor, was placed a photovoltaic cell designed by Dr. C. W. Hewlett of this laboratory. The disks were free to be set at different angular displacements between their sector openings. Consequently, the phosphorescence could be measured at various periods in its decay, depending (a) upon the speed of revolution of the disks, and (b) upon the displacement of their openings. When the two openings coincided, then at each revolution the cell was exposed to the light emitted by the phosphor during its period of direct excitation, so that the measurement was a record of the fluorescence. During this setting the cell reading included also the visible light radiated by the lamp and transmitted by the phosphor, but this could be readily measured separately. Its magnitude was given by the cell reading obtained when the plate coated with the sample was reversed, so that the light from the lamp passed first through the glass before striking the phosphor. This led to complete absorption of the far ultraviolet throughout the range of excitation of the phosphor. Accordingly, the visible light from the lamp, after some absorption and scattering in the phosphor, was the only radiation to reach the cell. The degree of this absorption and scattering was the same

in both the normal and reversed positions of the plate.

What one reads with this type of phosphoroscope is the change in intensity of luminescence during one complete revolution of the disks. In the disk between the phosphor and the cell there was an opening of 17°. Consequently the cell

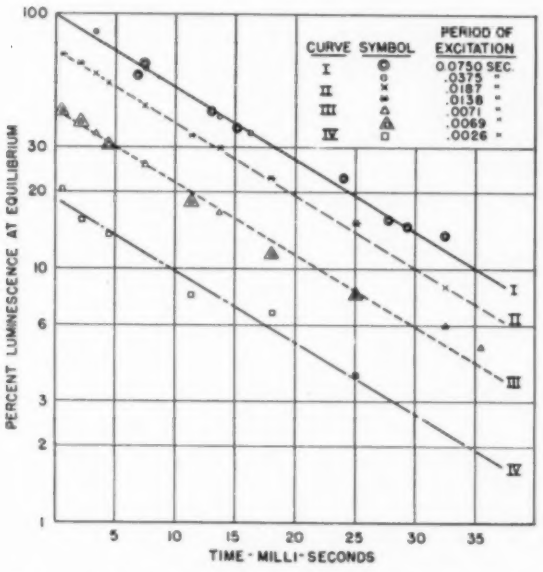

FIG. 2. Effect of duration of excitation upon rate of initial decay of phosphorescence for $Zn_2SiO_4 \cdot SiO_4$+0.4 percent Mn.

reading does not record the light intensity at an instant of time but rather the integrated value over a period that persists for 17/360 of a revolution. Any effect taking place in a shorter period of time than this would not be recorded.

The unique feature of the phosphoroscope lay in the use of several different angular openings in the disk placed between the phosphor and the lamp. This allowed corresponding variations in the time of excitation of the sample for constant speed of revolution of the disks. It made possible also a coordination of tests carried out at different speeds, and, in that way, made available a still wider range in the duration of excitation. The importance of this lies in the ability which it gave (a) to determine the duration of excitation necessary to attain a state of equilibrium between excitation of the phosphor and its emission of luminescence, and (b) to observe the characteristics of the emission before attainment of this equilibrium.

For the disk between the phosphor and the lamp, openings of 17°, 30°, 45°, 60°, and 90° were available. At a speed of 200 r.p.m. the same absolute values of phosphorescence were obtained with 45° and 90° openings, corresponding to excitation periods of 0.0375 sec. and 0.0750 sec. This demonstrated that equilibrium was attained after 0.0375 sec. In order to obtain shorter periods of excitation, faster speeds were used, so chosen that a combination of opening and speed yielded a time of excitation that overlapped with that of a combination at the next lower speed. When the sector openings were both set opposite to one another, with their outermost edges coinciding, a measurement of fluorescence was made possible. This position, however, does not represent the time from which the decay of phosphorescence starts, for up to a displacement of 17° the openings in the two disks still overlap to a decreasing extent. A slight correction therefore was necessary. It was constant at any specific speed and varied with the speed of revolution.

A set of curves for various periods of excitation is given in Fig. 2 for a zinc silicate phosphor having the composition $Zn_2SiO_4 \cdot SiO_2$+0.4 percent Mn, prepared from a gel solution of zinc nitrate in colloidal silica. All of the curves can be plotted on semi-log paper as straight lines over a decay period of about 0.04 sec. Their exponential character shows that within this range they fulfill the conditions for a monomolecular reaction as the basis of the phosphorescence emission, which can therefore be expressed as $P = P_0 e^{-kt}$. This signifies that a certain number of electrons P_0 have been liberated during the period of illumination and have been displaced into some abnormal state or states from which their return is retarded. The rate at which they return to their normal state determines the magnitude of the phosphorescence P at any instant t. The curves of Fig. 2, representing the decay rate of phosphorescence for various periods of excitation, are all parallel. This demonstrates that the decay rate k is constant regardless of the number of excited electrons formed.

In the case of the three settings which allowed an excitation period of 0.0375 sec. or greater, the decay curves intersected the Y axis at a

point corresponding to the fluorescence observed when the openings in the disks coincided. The delay process is therefore the only one involved in the emission of luminescence, and the instantaneous process is absent, for otherwise, as shown by the curves of Fig. 1, the value for fluorescence would have been above the point of intersection of the curve.

The Induction Period of Luminescence

When a silicate phosphor is exposed to an exciting light, the full luminescence does not flash on immediately but is attained only after a perceptible lapse of time. The rise is, in fact, so slow that it can be observed visually. If the phosphor is first exposed to the exciting light for a second or so, then, when a portion of its surface is skimmed off, the layer underneath is observed momentarily to be dark by contrast. It can be seen to become brighter until it attains the brightness of the rest. The existence of this induction period has already been denoted by the results of Fig. 2 which showed that fully saturated fluorescence was attained only after an excitation period of 0.0375 sec.

It was possible to measure this effect with the phosphoroscope by using disks of the various angular openings available and measuring the luminescence when the openings in the two disks coincided so that the cell would record the fluorescence emitted at the end of the excitation period. The curve of Fig. 3 illustrates the result

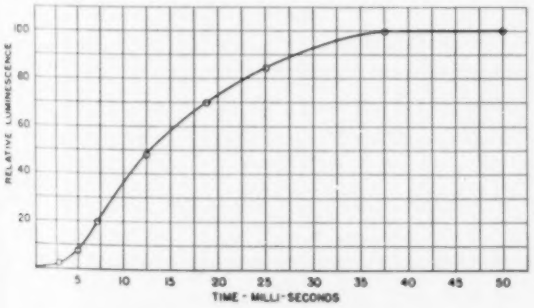

Fig. 3. Rise in luminescence during excitation of $Zn_2SiO_4 \cdot SiO_2 + 0.4$ percent Mn.

for zinc silicate containing 0.4 percent manganese. It is suspected that the initial concave portion is caused by an irregularity in recording.

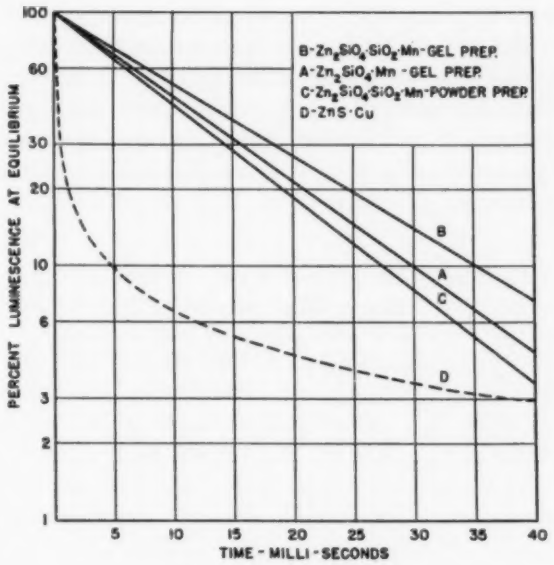

Fig. 4. Initial decay of phosphorescence of miscellaneous phosphors.

The latter convex portion can be expressed by the equation $E = E_0 e^{-kt}$, where E_0 is proportional to the total number of excited electrons formed under equilibrium conditions and E is proportional to the number that remain to be excited at any instant t. The value of E is equal to $100 - F$, where F is the percentage which the luminescence bears at the instant t to the luminescence at equilibrium F_0.

For periods of excitation below the equilibrium value, there is some evidence that the luminescence rises to a higher value immediately after extinction of the excitation than it has shown during excitation. The design of the apparatus did not permit making this observation definitive. Such overshooting effects have been observed in the phosphorescence of mercury vapor by Wood,[3] and in that of uranium glass by Wawilow and Lewschin.[4] Their experiments made possible observations at such short intervals of time that no luminescence whatever appeared until a finite time after extinction of the exciting light.

The time required for completion of excitation and attainment of the full luminescence corresponding to equilibrium conditions was only

[3] R. W. Wood, Proc. Roy. Soc. **99**, 362 (1921).
[4] S. I. Wawilow and W. L. Lewschin, Zeits. f. Physik **35**, 920 (1926).

slightly affected by the treatment or composition of the zinc silicate or by changes in temperature within the range of 77°K to 100°C. It was, however, reduced to two-thirds and less by a content of manganese lying above 2 percent. The rate of rise was in general the same as the initial rate of decay.

Factors Affecting Rate of Decay at Room Temperature

The rate of decay of phosphorescence of zinc silicate was found to vary considerably depending upon its composition and treatment. Some results are given in the curves of Fig. 4 for silicates all of which contained 0.4 percent manganese. Curve A is for the orthosilicate, Zn_2SiO_4, the only compound of zinc oxide and silica that exists. Curve B is for a silicate which contains one mole of free silica in the proportions $Zn_2SiO_4 \cdot SiO_2$. Both of these phosphors were prepared from colloidal gels of zinc and manganese nitrates in silica. The incorporation of the silica has considerably retarded the rate of decay. A similar effect, equally intense, was produced by incorporating in the orthosilicate 3 percent lithium sulfate or 1 percent powdered porcelain. When the phosphor was prepared from a mixture of powders rather than from a colloidal gel, the rate of decay was accelerated, as shown in curve C.

For the sake of comparison, the decay of zinc sulfide, activated with copper, is shown in curve D of Fig. 4. It is in an entirely different class. The initial drop is so rapid as to indicate that some of its luminescence is produced by the instantaneous process. The decay curve from 0.001 sec. on can be expressed in the manner demonstrated by Byler[5] as occurring in a succession of steps, each one of which follows the equation for a bimolecular reaction $1/\sqrt{P}=a+bt$, where P denotes the phosphorescence at an instant of time (t) and a and b are constants.

The silicates showed an initial rate of decay which for any one phosphor remained constant up to about 0.04 sec. Thereafter, the decay proceeded at a slower rate, as brought out in the curves of Fig. 5. The observed curves can be expressed as composites, as though they represented decay processes occurring in two successive monomolecular stages. The amount of phosphorescence contributed at any instant by one of these processes can be obtained by subtracting from the observed value of the phosphorescence the amount emitted by the other process, as found by extrapolation of its decay curve. A plot of the values thus obtained shows that the decay in the second stage can also be expressed as following an exponential rate over the range in which observations could be taken by this type of phosphoroscope. A comparison of the rates of decay shown by each of these stages is given in Table I, together with values

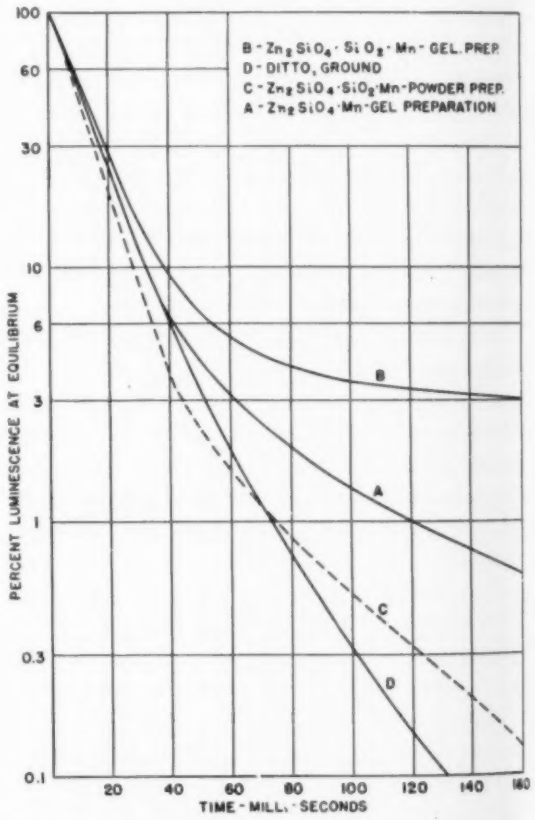

Fig. 5. Decay of phosphorescence of zinc silicate phosphors.

for the rate of rise in luminescence during initial excitation. The initial rate of decay is denoted by k_1 and the rate of the second slow stage by k_2 in the equation $P=P_0e^{-kt}$. The zinc silicate phosphors cited are of various compositions and treatment. The effect of grinding in increasing

[5] W. H. Byler, J. Am. Chem. Soc. **60**, 632 (1938).

the rate of decay is especially noteworthy. A similar effect, although not as pronounced, was brought about by prolonged heat treatment.

As shown in the curves of Fig. 6, the rate of

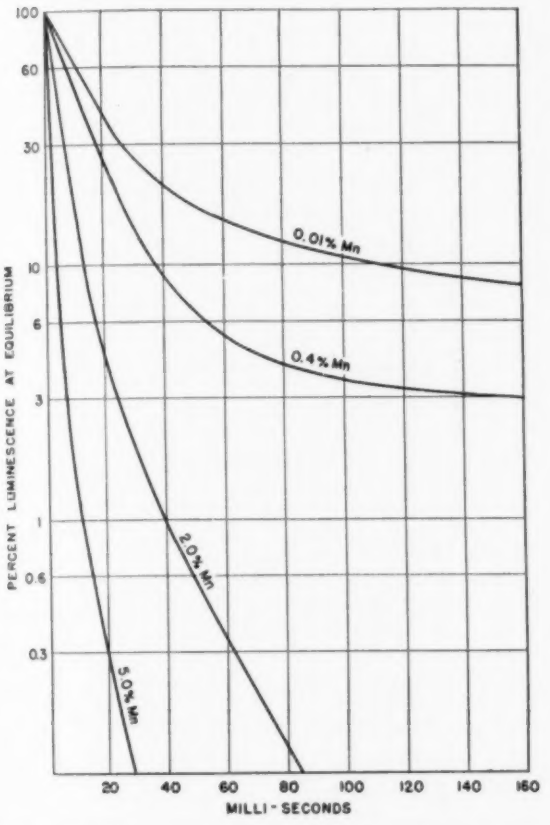

FIG. 6. Phosphorescence decay of zinc silicate phosphors for variation in manganese content.

decay was increased extremely in phosphors containing 2 percent manganese and more. For the sake of comparison, the decay as recorded in Table I is treated throughout as following an exponential equation. The results for 2 percent and 5 percent manganese, however, can be better expressed by the equation for a bimolecular reaction $1/\sqrt{P}=a+bt$. A more reasonable interpretation of their results is in fact possible by considering that the decay in presence of an excess of manganese follows a higher order reaction except at very low temperature. This will be treated more fully in the next section.

The course of the decay in later periods was determined photographically. This method was carried out on a succession of different phosphors, measured simultaneously. They were placed on small watch crystals in a row and excited by 2536A. The lamp was then extinguished. At various periods after this, a photographic film was laid for 3 seconds over all of them. The resulting exposures on the film had densities proportional to the phosphorescence from the different samples at an identical period in their decay. The decrease in phosphorescence with time was given by the relative densities recorded at the different periods. The film density was expressed in terms of phosphorescent light intensity by means of a calibrated film which had been given step exposures to establish the relation between density and light intensity.

Curves for several typical phosphors are shown in Fig. 7, where the phosphorescence of any one phosphor is expressed as the percentage which it bears to that of the normal phosphor, $Zn_2SiO_4 \cdot SiO_2$+0.4 percent Mn. The curves are composites in that they are based upon the observations made with the phosphoroscope as well as upon those made photographically, in order to bring out how the luminescence decays from its initial value up to a point two minutes after extinction of the exciting light. The initial decay is so extremely rapid that no distinctions in it are perceptible on the compressed scale of Fig. 7. The second stage of decay, on the other hand, is extended over such a long period that the characteristics of the different phosphors are emphasized to an even greater extent than in Figs. 5 and 6.

The dependence of the rate upon the presence of excess silica and upon the manganese concentration is especially notable. A unique effect due to low concentration of the activator is brought

TABLE I. *Rates of change in phosphorescence of silicate phosphors.*

Composition	Mixture	Treatment	Percent of Mn	Rate Rise K	Rates Decay k_1	Rates Decay k_2
$Zn_2SiO_4 \cdot SiO_2$	Gel	—	0.01	55	63	3
"	"	—	0.4	83	73	4
"	"	—	1.0	—	73	6
"	"	—	2.0	112	170	—
"	"	—	5.0	—	540	—
"	"	Ground	0.4	95	77	35
"	Powder	—	0.4	94	86	24
Zn_2SiO_4	Gel	—	0.4	85	77	16

out by consideration of the phosphor with 0.01 percent manganese. Although its initial luminescence, as measured under continuous excitation, is only 12 percent of that from the phosphor with 0.4 percent manganese, yet the absolute intensity of its phosphorescence 3 seconds after extinction of the exciting light is 80 percent greater, and this difference becomes still greater at later periods in the decay.

The character of the decay was not altered by varying the intensity of the exciting light. A series of measurements was made with the mercury lamp placed at variable distances from the phosphor, a zinc silicate prepared from a gel mixture and containing 1.0 percent manganese. The phosphoroscope was operated to give a period of excitation lasting 0.0375 second, sufficient to attain a state of equilibrium between excitation of the phosphor and its emission of luminescence. The luminescence of the phosphor at the end of this period of excitation was proportional to the light intensity, as brought out by the results of Table II.

The decay of phosphorescence for these three different cases is shown in the curves of Fig. 8. Its character is unaffected by variations in the intensity of the exciting light. The initial rate is uniform and has the same value as that in Table I. The slow second step of decay proceeds also at a uniform rate with no indications that the curves would ever meet, as they did in the case of the zinc sulfide phosphor described by Riehl.[6] The continued separation of the curves throughout the entire course of decay was confirmed by visual examination. Samples were exposed to 2536A at different distances and then placed side by side in the dark. The relative intensities of their phosphorescence remained proportional to the intensity of the exciting light. In the case, for instance, of a sample excited at a distance of 60 cm from the lamp, the phosphorescence was no longer visible after a period of 20 minutes in the dark, whereas a sample which had been excited at a distance of 10 cm still showed a moderate phosphorescence glow at this period and was still plainly phosphorescent after an hour in the dark.

TABLE II. *Fluorescence of zinc silicate as dependent upon intensity of exciting light.*

DISTANCE LAMP	INTENSITY OF EXCITING LIGHT	RELATIVE FLUORESCENCE
7.5 cm	100	100
15.0	25	24
22.5	11	11

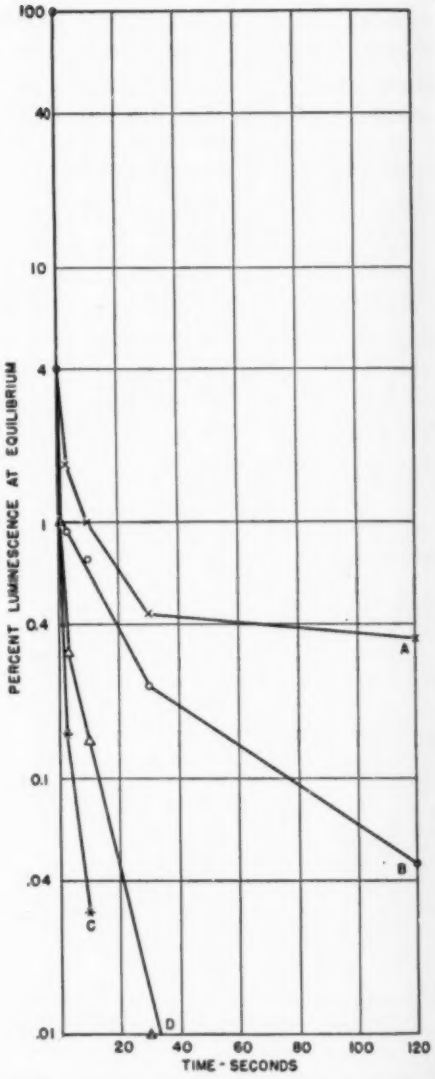

FIG. 7. Decay of phosphorescence of zinc silicate phosphors measured over extended time. A, $Zn_2SiO_4 \cdot SiO_2$ +0.01 percent Mn; B, $Zn_2SiO_4 \cdot SiO_2$+0.4 percent Mn; C, $Zn_2SiO_4 \cdot SiO_2$+2.5 percent Mn; D, $Zn_2SiO_4 \cdot SiO_2$+0.4 percent Mn—ground.

EFFECT OF TEMPERATURE UPON PHOSPHORESCENCE

Observations made with the unaided eye on the phosphorescence at other than room tem-

[6] N. Riehl, Ann. d. Physik **29**, 636 (1937).

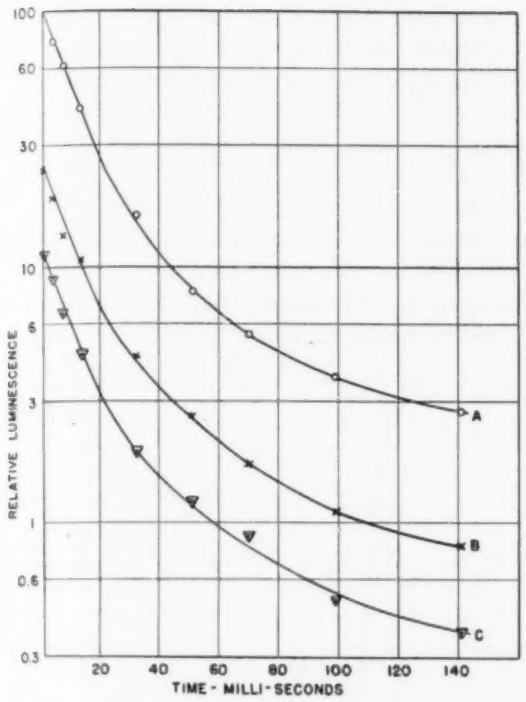

FIG. 8. Dependence of decay upon intensity of exciting light. A, Relative light intensity = 100; B, Relative light intensity = 25; C, Relative light intensity = 11.

perature brought out some significant differences. These observations necessarily pertain only to the second stage of decay because the decay in the first stage is so rapid that it is completed in less than one-tenth of a second and cannot be perceived by the eye.

On excitation at 300°C and even at 100°C the phosphorescence was seen to be low as compared to that at 25°C and the speed of its decay was more rapid, for it could be observed only for about 15 minutes instead of an hour and more. It was not intensified by cooling the sample after excitation. The effect of an increase in temperature is therefore to lower the concentration of electrons which are retained in the metastable state accountable for the second stage of decay.

The behavior below 25°C was in striking contrast. At the temperature of liquid nitrogen, −196°C, no phosphorescence whatever was perceptible. When the sample was warmed, an emission of luminescence began to appear somewhat below 0°C and at about 10°C the luminescence had become brighter than that from a sample excited simultaneously but at room temperature. When it had attained room temperature, the luminescence decayed at the same slow rate as that observed for the second stage of decay in a sample excited at 25°C. In the case of a sample which was excited at −196°C and then maintained in liquid nitrogen for five days in the dark, not only did an emission of luminescence occur when the phosphor was finally warmed, but its intensity was fully as strong.

At sufficiently low temperature then, the electrons which are effective in producing the second stage of decay are retained in a metastable state for an indefinitely long period. They remain latent and become available for the emission of luminescence when the temperature is raised sufficiently to free them.

More detailed observations were made with a modified type of phosphoroscope in which the sample was placed externally to the disks and the luminescence measured as emitted from the surface of a heavy layer upon which the exciting radiation fell. The more important tests were made at 100°C and at −196°C. The phosphor was coated upon the flat side of a metal container which was kept filled either with boiling water or with liquid nitrogen during the test. The container was held in a wooden box having a tight-fitting quartz window on the side exposed to the exciting light. In the tests at low temperature the air space between the phosphor and the window was kept dry with phosphorus pentoxide and frosting on the outside of the window was prevented by blowing over it a blast of dry air. Conditions remained so uniform during any one test that the absolute values of points on the decay curve could be checked by a succession of repeated runs. Measurements were made after 0.0350 sec. excitation, sufficient to attain equilibrium.

The initial rate of decay was the same at all

TABLE III. *Effect of temperature upon the rate of decay.*

Temp.	Initial Stage 1% Mn	Initial Stage 2.5% Mn	Second Stage 1% Mn	Second Stage 2.5% Mn
−196°C	73	87	Latent	Latent
25°C	72	221	4	Weak
54°C	72	—	14	—
100°C	70	249	Very weak	Very weak
300°C	79	—	Very weak	—

temperatures, as shown in Table III and in the curves of Fig. 9, where the results are expressed as percentages of the fluorescence observed at 25°C. It is the second stage of decay that is of particular interest. In accordance with the visual observations, it was completely absent at −196°C so that the decay continued at its initial rate at least to a reduction in luminescence of 99.9 percent. At 54°C it was still present at sufficient intensity to measure but its rate had increased to 14 from its value of 4 at 25°C. At 100°C its decay was evidently still more rapid. It was still observable to the eye but its intensity was too low to measure. A summary of all the results is given in Table III.

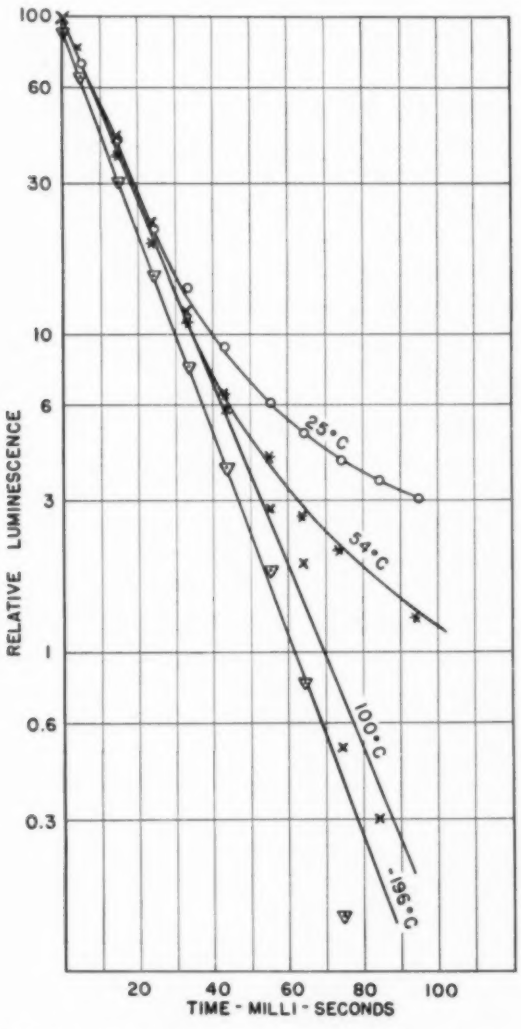

FIG. 9. Decay of phosphorescence at different temperatures of zinc silicate phosphor containing 1.0 percent Mn.

The tests at different temperatures are helpful in the interpretation of the decay in phosphors containing an excess of manganese. The curves of Fig. 10 illustrate the situation for the case of a typical one, that with 2.5 percent manganese. It is probably only at −196°C that the decay is truly that of a monomolecular reaction. At this temperature its behavior was the same as that described for the normal phosphor with 1 percent manganese. The decay was too rapid to be observed visually. When the sample which had

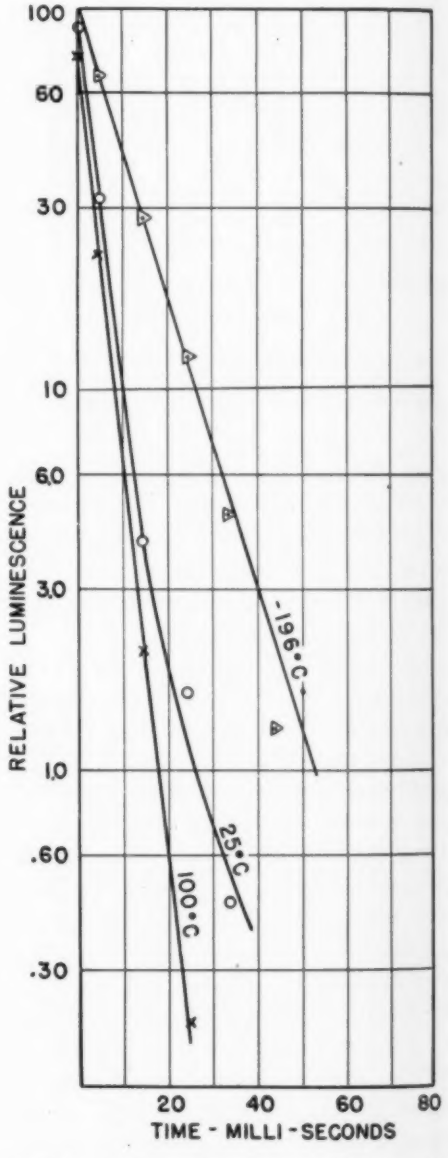

FIG. 10. Decay of phosphorescence at different temperatures of zinc silicate phosphor containing 2.5 percent Mn.

been excited at −196°C was warmed, an emission of luminescence appeared, followed by the normal rapid decay such as that noted on curve C of Fig. 7, denoting that at −196°C the process giving rise to the second stage of decay was present but latent.

The initial phosphorescence at 25°C and above can be plotted as following an exponential rate of decay. For the case of those phosphors rich in manganese, however, it seems probable that at such temperatures the decay involves a higher order reaction. The results for the greater part of the observable decay can be expressed by the equation $P^{-x}=a+bt$, where x is about 0.5 at 25°C and 0.2 at 100°C.

A basis for this is found in the behavior of their fluorescence at different temperatures.[2] At 25°C it was found to be much below normal, 20 percent below for 2.5 percent manganese and 65 percent below for 5 percent manganese. These decreases became still more marked with rise in temperature. At −196°C, on the other hand, the fluorescence had risen so far as to be only 10 percent below normal. This behavior was ascribed to the effect of thermal vibration. An increase in manganese content is accompanied by such a closer approach of manganese atoms that there is opportunity for collisions between excited and normal atoms, with a consequent loss of potential energy and of its equivalent luminescence. The decrease in luminescence observed with rise in temperature is in accord with this view in that the probability of collision is a function of the amplitude of thermal vibration.

It is significant that at −196°C this effect was reduced to a minimum and that, likewise at this temperature, the phosphorescence was observed to follow a monomolecular reaction. The behavior at higher temperatures is complicated and different from that of normal phosphors containing 1 percent or less of manganese because two factors become active in the decay, collisions of manganese ions with free electrons, giving rise to luminescence, and collisions of manganese ions and atoms, causing a loss of potential luminescence. The former factor remains constant with change in temperature but the latter is so dependent upon temperature that the rate of decay as observed rises rapidly with increase in temperature. The cause of decay is probably complicated still more by the coincidence of lattice defects at the location of manganese atoms, a feature whose possible significance will be brought out in the last section.

The Two Stages of Phosphorescence Decay

A striking feature in the decay of phosphorescence of the zinc silicates is the presence of two apparently separate stages. They are observable at room temperature in all types of silicate phosphors, regardless of treatment, composition and manganese content and regardless also of intensity and duration of excitation. The first stage, showing an exponential rate of decay, persists for 0.04 sec. at the longest, until the phosphorescence has fallen to 10 percent or less of its initial value. Then it passes by transition into a second stage, the first part of which shows also an exponential type of decay that continues, in the case of the normal phosphor, at least over the period 0.04–0.17 sec. Thereafter the rate of its decay becomes more complicated. The phosphorescence persists for a long time. For the normal phosphor, its luminescence is still readily observable to the eye in a darkened room after one hour. Despite the complex nature of the decay characterizing this second stage, it is convenient to think of it as the consequence of a mechanism which remains essentially the same throughout its long period from 0.04 sec. onward. The question arises, is this division of the decay into two stages purely an arbitrary one or does it rather represent the existence of two different processes in the decay?

The answer is given by the observations on the normal phosphor at −196°C. They show unmistakably that two different processes exist. At this low temperature the second stage is completely absent. The decay observed shows the same rate as the initial decay at 25°C and persists exponentially to as low a value of phosphorescence as could be measured, falling to 0.1 percent of its initial value within 0.09 sec. Low temperature, it is clear, has had no effect upon the mechanism involved in this first stage of decay other than to make it predominant.

Even though the process involved in the second stage is completely inactive at −196°C, it is

still present in a latent condition. This is shown by the emission of luminescence followed by a slow phosphorescence decay, which takes place when such a phosphor is warmed. It is as though the effect of low temperature were to retain electrons for an indefinitely long period in a metastable state. The first effect of excitation at such a low temperature would then be to saturate those states. The electrons liberated by additional excitation would consequently find these states unavailable and so would be free to migrate until they encountered manganese ions. The probability of this encounter would determine the character of the emission during the first stage of decay.

The number of such free electrons is relatively small compared to the number of captured electrons which are retained within the potential cup of the metastable state. The area subtended by the curve which represents the first stage of decay is only one-fiftieth that of the area subtended by the curve for the second stage of decay. As the number of manganese ions is equal to the sum of both groups of electrons, it is clear that the concentration of these ions will not be appreciably reduced by encounters with the free electrons but, at least for the case of the normal phosphor, will remain essentially constant. Their reunion will therefore have the characteristics of a monomolecular reaction and lead to the exponential rate that was observed. When the manganese content of a phosphor is increased, it is of course reasonable to find a higher rate of decay.

The first stage of decay continues until the concentration of the group of free electrons falls below the concentration of the electrons which are being emitted from the metastable state in which they have been retained. From this point on, the course of decay is that of the second stage.

Turning now to this second stage of decay, the observations denote that it arises from the retention of a portion of the excited electrons at a metastable state, and that its rate depends upon the rate at which they are emitted from this state. The state is of the nature of a potential cup, in which resistance is offered to the emission of electrons by the presence of a potential barrier. The relation between the height of the barrier and the energy content of the electrons is strongly dependent upon temperature. At -196°C it is so high as to retain the electrons indefinitely. At a temperature somewhat below 0°C it is lowered to a point where some can escape. It is lowered progressively by further increases in temperature; at 25°C it is so low that enough electrons escape to make this stage an important feature in the decay; at 54°C it is enough lower to allow the escape of so many more that the rate of decay is tripled; at 100°C it is so low that relatively few electrons are retained in the state with the result that this stage of decay does not become noticeable until the luminescence has fallen to less than 1 percent of its initial intensity.

It is interesting to inquire if there is any physical feature present in phosphors which could give rise to such a metastable state. A first approach to the question may be had by considering those other factors besides temperature which affect the second stage of decay and noting if these factors can be considered as having in common an effect upon some specific physical feature of the crystals. These factors include (a) the presence of excess silica, (b) grinding, (c) size of the oxide particles used as ingredients in the reaction and (d) manganese content. An excess of silica has the effect of bringing about, earlier in the decay, the transition from the first to the second stage and of causing the latter to proceed at a slower rate than observed for the normal orthosilicate. The other factors have an opposite effect, lowering the amount of luminescence emitted during the second stage by causing it to start at a later point in the decay and to proceed more rapidly.

These effects may be coordinated by noting that all the factors producing them have an influence upon one specific physical property of the phosphor. They determine the extent and character of lattice distortions within the silicate crystals. The grounds for this conclusion will now be taken up and at the same time the further query will be considered—how might the rate of decay in its second stage depend upon the nature and number of such lattice distortions?

Consider first the effect of an excess of silica in decreasing the rate. There is only one com-

pound of zinc oxide and silica, the orthosilicate, Zn_2SiO_4. Its rate of decay is reduced by incorporating with it a suitable foreign ingredient, such as an extra mole of silica to form the conglomerate, $Zn_2SiO_4 \cdot SiO_2$. To accomplish this it was necessary that the mixture of oxides as first fired should contain the additional silica. When the mixture was fired in the proportion for the orthosilicate and then mixed with the additional silica, further firing did not change the status from that of a mechanical mixture and had no effect upon the phosphorescence.

This signifies that the silica is intimately associated with the phosphor. Intimate association does not mean, however, incorporation in the lattice, for x-ray diagrams showed the persistence of the orthosilicate structure and the presence of free silica in addition. It must mean therefore the inclusion of small molecular groups of one ingredient within the other. This is a condition which leads to irregularities in the crystalline structure of the silicate and to the introduction of lattice defects. The same explanation would account for the similar effect shown by additions of powdered porcelain or of lithium sulfate. Rexer[7] has in fact observed that the presence of a foreign body increases the number of lattice defects.

It is therefore to be considered whether the reduction in the decay rate such as produced by these foreign additions may be due to the increase in number of lattice defects which their presence favors and to the association with these defects of those metastable states capable of capturing electrons. Such a relationship has already been assumed to account for the presence in halide crystals of color centers, whose formation has been ascribed by Pohl and Gudden[8] to the migration and retention of electrons at lattice defects. According to a recent view expressed by von Hippel,[9] these need not be present initially in the lattice. He ascribes the formation of color centers to the migration of an electron to a potential cup in the lattice. A metal ion is thereby converted into an atom and the diameter of the atom is so much larger that it leads to a distortion in the lattice, at which an electron may be trapped to become the nucleus for a color center. This view, however, represents only an additional mechanism for introducing within a crystal a localized state of disorganization of the same nature as that formed by grosser means, such as a disturbance of stoichiometric proportions, or the presence of impurities. When such a state is produced in one of the two latter ways, it should still serve as a means of retaining the excited electron whose eventual return is to give rise to phosphorescence. The impurity must of course be a neutral one, as distinguished from those injurious ones, such as certain metallic oxides, which, even at low concentration, serve as poisons to the emission of luminescence. The action of such poisons is probably due to collisions of the second kind, as the result of which the energy of an excited electron is dissipated in purely kinetic effects.

This hypothesis would explain also the increase in decay rate produced by grinding, despite the opposite conclusions drawn by Riehl and Ortmann.[10] The abnormally low tensile strength of single crystals has been ascribed to the presence of lattice defects[11] from the viewpoint that they introduce planes of mechanical weakness at which premature deformations occur. This has led Smekal to conclude that lattice defects serve as locations for phosphorescence centers and that the increase in rate of decay produced by grinding is due to a preferential splitting along the planes established by these defects. From this viewpoint the operation of grinding would bring about the conversion of relatively large, imperfect crystals into smaller and more perfect ones. This would account readily for one of its effects upon the zinc silicate phosphors; namely, that the second stage of decay does not become noticeable until the phosphorescence has fallen to a relatively lower value. The other effect, the higher rate of decay could be explained on the assumption that grinding removes preferentially those lattice defects which offer the highest potential barriers to escape of the captured electrons.

The size of the zinc oxide and silica particles,

[7] E. Rexer, Zeits. f. Physik **76**, 735 (1932).
[8] R. Pohl and B. Gudden, Zeits. f. angew. Chemie **49**, 69 (1936).
[9] A. von Hippel, J. App. Phys. **8**, 815 (1937).
[10] N. Riehl and H. Ortmann, Ann. d. Physik **29**, 556 (1937).
[11] A. Smekal, Zeits. f. tech. Physik **7**, 535 (1926).

used for the reaction is the third factor. The results of using coarse, precipitated powder rather than a colloidal gel are the same as those produced by grinding and can be laid to the same causes. A colloidal gel at best represents an aggregate of finely crystalline fragments, a condition that will augment the number of lattice imperfections in the crystalline product derived from it. By contrast, a product derived from coarse particles will allow the formation of less imperfect crystals.

High manganese phosphors are in a distinct class by themselves. A discussion has already been given of one complicating factor which is present in them at 25°C and above. At −196°C this factor was absent and the existence of a second stage of decay could be observed. At higher temperatures it seems probable that still another complicating factor enters which makes it questionable whether this second stage retains its identity. The presence of a high content of manganese atoms introduces distortions in the lattice, so that crystal imperfections appear which coincide with the location of these atoms. The presence of manganese ions at the very defects that they produce acts at normal temperatures to lower to an abnormal extent the potential barriers to which electrons retained at these defects are subjected. This would act to merge together the two stages of decay and thus to account for the shortness of the period in which phosphorescence is observable even at 25°C.

The author wishes to express his gratitude to Dr. Ralph P. Johnson for many helpful discussions.

The Reignition of Short Arcs at High Pressures

J. D. Cobine, R. B. Power* and L. P. Winsor
Harvard Graduate School of Engineering, Cambridge, Massachusetts

(Received September 21, 1938)

An investigation has been made of the reignition of short a.c. arcs in air at pressures from one to eight atmospheres, for currents less than 3.25 amperes (and with a resistance circuit). Pure graphite electrodes were used and were separated by a distance of 1 mm. The reignition voltage under these conditions increases with pressure and decreases as the current is increased. The characteristic of reignition potential *vs.* current has been found to exhibit a discontinuity at a critical current. For this current the reignition potential decreases by about 1000 volts to a new characteristic typical of the higher currents. This critical current increases with the gas pressure to a maximum of 2.25 amp. As the r.m.s. current is increased from low values to values near the critical, the number of cycles during which the reignition potential has the value given by the higher characteristic decreases. For currents equal to, or greater than the critical value, only the low reignition potentials are obtained. This transition is accompanied by an increase in the burning voltage of the arc.

Introduction

THE extensive study of electric arcs under a wide variety of conditions of electrode materials, gases and vapors has led to the division of arcs into groups, which are distinguished from one another by the nature of the processes that occur in the cathode-drop region. The oldest theory, proposed by J. J. Thomson,[1, 2] is that the electrons necessary for the arc are supplied by thermionic emission at the cathode. Thomson[3] would extend this theory even to the volatile materials by assuming a very high temperature produced in a thin surface layer by positive ion bombardment. However, for the volatile materials Langmuir[4] has proposed that the necessary electrons may be extracted from the cold metal by the high electrostatic field existing at the cathode surface due to the presence of a positive ion space-charge in the region of the cathode drop. Compton,[5]

* Kennecott Wire and Cable Company.

[1] J. J. Thomson, *Conduction of Electricity through Gases* (Cambridge University Press, second edition, 1906), p. 604; also (third edition, 1933), Vol. II, p. 589.

[2] K. T. Compton, Phys. Rev. **21**, 266 (1923).

[3] Reference 1, p. 596.

[4] I. Langmuir, Gen. Elec. Rev. **26**, 731 (1923).

[5] K. T. Compton, Trans. A. I. E. E. **46**, 868 (1927).

Langmuir,[6] Mackeown[7] and others who have considered this theory have concluded that in most cases of volatile materials the field emission theory is valid. There are, however, many special borderline cases where there is considerable uncertainty as to classification. Druyvesteyn[8] has suggested a modification of the "field" theory which is based on the glow discharge observations of Guntherschulze and Fricke.[9] In this modified form the field is presumed to be produced in an extremely thin layer of relatively high resistance material, such as an oxide, by a surface layer of positive ions. The apparent necessity[10–12] of the presence of an oxide for a stable arc indicates the possibility of this mechanism under some conditions. Naturally, the presence of low work-function impurities will increase the emission and affect the mechanism. Since the effective work-function is markedly influenced by adsorbed gas layers,[13] it is reasonable to expect that the cathode mechanism would be affected by the gas condition of the surface.[14]

Since alternating-current arcs require the reversal of anode and cathode each half-cycle, it is reasonable to expect that the reignition of the "field" arc would differ from that of the thermionic arc. The reignition voltages of fairly heavy current carbon and tungsten arcs have been found to be very low compared to the relatively high reignition voltages of the volatile metals,[15] which bears out this belief. The reignition potential of very pure carbon electrodes has been found[16–18] to be quite high for small currents and to decrease to relatively low values for high currents. These high reignition potentials of carbon are of the same order of magnitude as exist for metals, which indicates the possibility of a "field" arc for small current carbon arcs.

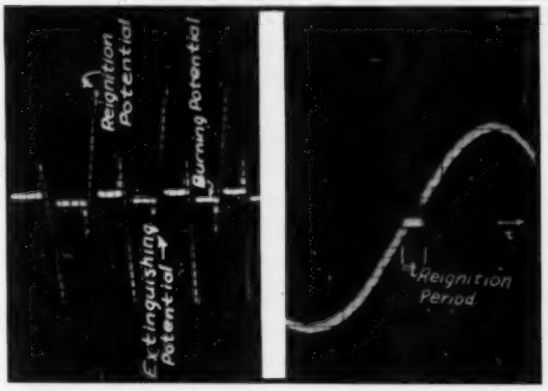

(*a*) (*b*)

FIG. 1. Cathode-ray oscillograms of arc in air at atmospheric pressure (Arc current = 0.31 ampere r.m.s.).
(*a*) Arc voltage *vs.* time. Reignition voltage = 2880 volts. (*b*) Arc current *vs.* time. Peak of current wave = 0.44 ampere. (Note—The time axis of (*b*) is different from that of (*a*).)

EXPERIMENTAL RESULTS

Power was supplied by a 15-kva 60-cycle transformer and the current was limited by a resistance in series with the arc.[18] The arc burned in air between the plane end surfaces of $\frac{1}{4}$-inch diameter spectrographic carbons. The electrodes were frequently cleaned with a file and reset to insure the accuracy of the experimental results. Spectrographic examination of the electrodes after cleaning demonstrated that no impurities were introduced by the procedure followed. Voltage measurements were made by means of a cathode-ray oscillograph connected across a portion of a high resistance shunting the arc.

Typical cathode-ray oscillograms of the discharge voltage and current are shown in Figs. 1a and 1b, respectively. These oscillograms show the relatively high voltage reached at the end of the long period of near zero current between arc extinction and reignition.

The relations between reignition potential and r.m.s. arc current for constant gas pressures are presented in Fig. 2. The 60-cycle sparking potential of the gap is indicated by the points at zero current. The effect of increased pressure

[6] I. Langmuir, Zeits. f. Physik **46**, 271 (1927).
[7] S. S. Mackeown, Phys. Rev. **34**, 611 (1929).
[8] M. J. Druyvesteyn, Nature **137**, 580 (1936).
[9] A. Guntherschulze and H. Fricke, Zeits. f. Physik **86**, 451 (1933).
[10] C. G. Suits and J. P. Hocker, Phys. Rev. **53**, 670 (1938).
[11] J. D. Cobine, Phys. Rev. **53**, 911 (1938).
[12] G. E. Doan and J. L. Myer, Elect. Eng. **51**, 624 (1932).
[13] S. Dushman, Rev. Mod. Phys. **2**, 381 (1930).
[14] O. Becken and K. Sommermeyer, Zeits. f. Physik **102**, 551 (1936).
[15] F. C. Todd and T. E. Browne, Phys. Rev. **36**, 732 (1930).
[16] S. S. Mackeown, J. D. Cobine and F. W. Bowden, Elect. Eng. **53**, 1081 (1934).
[17] J. D. Cobine, Physics **7**, 137 (1936).
[18] J. D. Cobine and R. B. Power, J. App. Phys. **8**, 287 (1937).

is to increase the reignition potential[17, 18] while an increase in arc current lowers the reignition potential. These curves exhibit three definite regions. For currents less than 0.2 ampere, the discharge is a glow for all or for most of the cycle, and the effect of the discharge current on reignition is relatively small. The burning voltage in this region is of the order of 300 volts. The other two regions are defined by a relatively abrupt decrease in reignition potential for a transition region between 1.1 amp. and 2.25 amp. The arc is quite mobile when operating on the high characteristic, but relatively fixed in position for the high current characteristic. When the r.m.s. current is increased to within about 0.25 amp. of the transition current, the reignition potential assumes at first the high value and then decreases to a low value. As the current is increased toward the indicated transition value, the number of cycles exhibiting a high reignition potential decreases until the critical value is exceeded, after which only the lower characteristic is observed. The transition current increases with pressure to a maximum of 2.25 amp. which is reached at a pressure of approximately 250 cm Hg for the gap and circuit constants of these experiments.

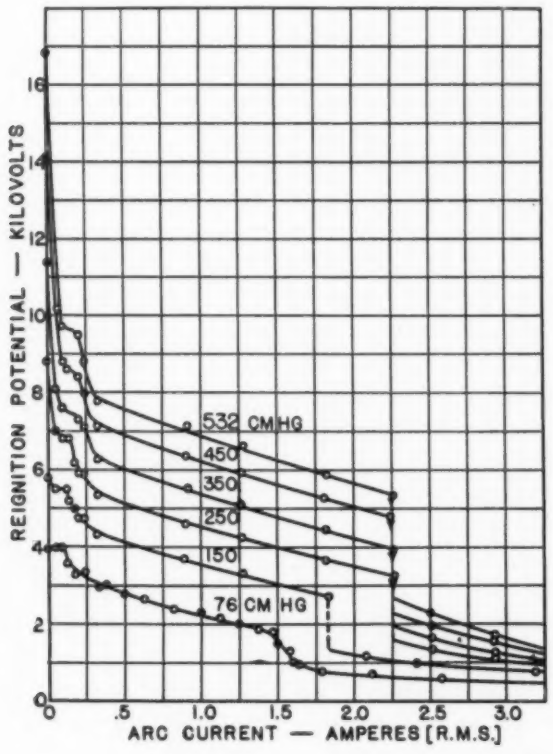

FIG. 2. Arc reignition characteristics for constant pressures. Gap = 1 mm, gas = air, parameter = pressure in cm of Hg.

It is evident that the phenomenon of different reignition characteristics might be due either to a difference in the nature of the positive columns or to some difference in the cathode-drop regions. The first possibility suggests that the discharge in the intermediate current range is not an arc but a high current high pressure glow discharge[19, 20] and the transition in reignition potential is that which would naturally accompany a change from a glow to an arc. The other possibility suggests that the arc cathode mechanism is different in the two regions, i.e., the low current region could be a "field" arc and the high current one might be a thermionic type of arc. In order to determine which of these possibilities is the more probable, a study was made of the discharge burning voltage. The high reignition potentials in these experiments made it necessary to use a potentiometer to keep the voltage at the oscillograph at a reasonable value. A two-stage amplifier facilitated the measurement of the low burning voltage of the discharge. Since the burning voltage has its minimum value at the instant of maximum current, the voltage at this instant was chosen for study. The curves marked *B* of Fig. 3 give the relation obtained between the burning voltage and the r.m.s. arc current. Each curve of burning voltage exhibits an unstable transition region at the point of reignition transition, as is shown by the curves marked *A* which are repeated for direct comparison. It is important to note that the burning voltage *increases* at this point. The transition region covers approximately 0.25 amp. in which the burning voltage varies at random from cycle to cycle between the two characteristics.

DISCUSSION

The appearance of the discharge column for currents greater than 0.2 amp. is typical of the arc in that the column consists of a very intense, highly constricted path. The glow discharge column, of low intensity and relatively large

[19] C. G. Suits, Phys. Rev. **63**, 609 (1938).
[20] J. D. Cobine, Phys. Rev. **53**, 911 (1938).

cross-sectional area, appeared only at currents less than 0.2 amp. The magnitude of the burning voltage of the discharge for currents greater than 0.2 amp. is of the same order as is usually associated with the arc[21, 22] for the current, pressure and gap used. This also indicates that the discharge under observation is an arc for all currents greater than 0.2 amp. and is a high pressure glow discharge only for currents less than this value.

It has been brought out repeatedly that a mobile cathode spot is not associated with appreciable thermionic emission.[23–27] The fact that for pure carbon this mobility of cathode spot is found in the low current region indicates that the necessary electrons may be supplied by "field" emission under these conditions. On the other hand, the higher current region is undoubtedly associated with the thermionic type of emission, since its cathode spot is relatively steady. The existence of a "field" arc for carbon is probably due to the use of electrodes free from low work-function impurities. The absence of impurities will require a much higher cathode temperature for appreciable thermionic emission, and consequently a higher arc current than is necessary for impure electrodes. The transition region, in which the reignition potential decreases and the burning voltage increases, is undoubtedly the same phenomenon as was observed by Becken and Sommermeyer[14] for both tungsten and carbon cathodes. In their experiments the burning voltage also increased when the wandering "field" cathode changed into a fixed thermionic cathode. In their experiments, as in ours, this transition was induced by permitting the cathode to heat up by continued arcing.

The gas condition of the electrode surface has an important bearing on the nature of the emission processes, for the effective work-function of the surface is influenced by adsorbed

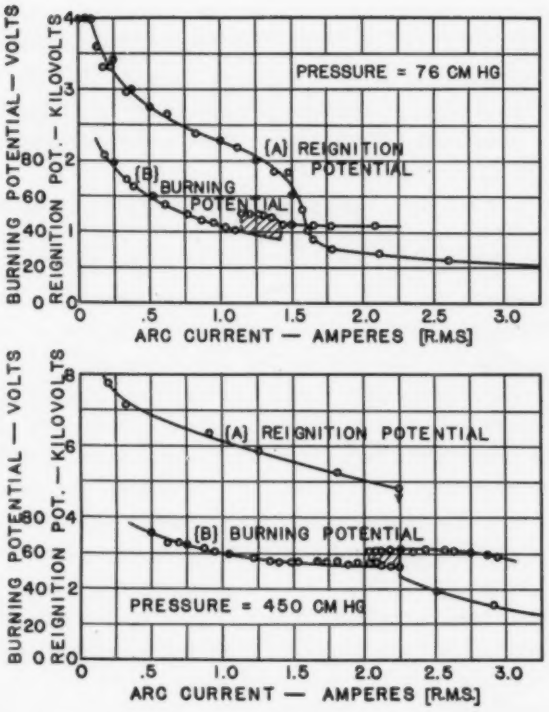
BURNING POTENTIAL — VOLTS
REIGNITION POT. — KILOVOLTS
PRESSURE = 76 CM HG
(A) REIGNITION POTENTIAL
(B) BURNING POTENTIAL
ARC CURRENT — AMPERES [R.M.S.]
BURNING POTENTIAL — VOLTS
REIGNITION POT. — KILOVOLTS
(A) REIGNITION POTENTIAL
(B) BURNING POTENTIAL
PRESSURE = 450 CM HG
ARC CURRENT — AMPERES [R.M.S.]

FIG. 3. Carbon arc characteristics in air. Gap = 1 mm.

gases. However, the most important effect to be considered in these discharges is the effect of a surface layer of positive ions drawn from the discharge column. Such a charged layer will produce a very high electrostatic field at the electrode surface.[14, 28] This will have the effect of producing an emission far in excess of that which could be obtained by the action of the average field of the cathode drop acting alone. This effect is closely related to the emission through oxide films discussed by Druyvesteyn[8] for metallic cathodes. Relatively high fields can also be produced at the points of contact between the electrode and loose particles of carbon. If the current to such a point became appreciable, local heating would result in increased emission. It is probable, as Becken and Sommermeyer point out, that the transition from "field" to thermionic emission is induced by electrode heating which drives adsorbed gases and ion layers from the active portion of the cathode. This would explain the gradual decrease in duration of the "field" phase as the critical current is approached. Since the loss of the

[21] C. G. Suits, Physics **5**, 380 (1934).
[22] A. v. Engel and M. Steenbeck, *Elektrische Gasentladungen* (Julius Springer, 1934), Vol. 2, p. 154.
[23] H. Stolt, Ann. d. Physik **74**, 80 (1924).
[24] W. Ramberg, Ann. d. Physik **12**, 319 (1932).
[25] R. Seeliger, *Physik der Gasentladungen* (Johann Ambrosius Barth, 1934), second edition, pp. 404 and 494.
[26] H. Plesse, Ann. d. Physik **22**, 475 (1935).
[27] O. Becken and R. Seeliger, Ann. d. Physik **24**, 609 (1935).
[28] L. Malter, Phys. Rev. **49**, 478 (1936).

surface charge will raise the effective work-function of the cathode, it is reasonable that the arc burning voltage should increase at the onset of thermionic emission. The arc burning voltage, as has been observed previously,[29, 30] increases with the gas pressure.

It is evident from the curves of Figs. 2 and 3 that the two types of arc cathode mechanisms are associated with different reignition phenomena. In order to interpret correctly the observed effects it is necessary to consider both the state of the gas in the discharge path, and the surface condition of the *incoming* cathode at the instant of zero current. The conductivity of the column of the high pressure arc is maintained by thermal ionization.[20, 31, 32] When the arc current becomes zero under these conditions, the gas temperature and the degree of ionization decrease at a definite rate determined by the characteristics of the gas.[33, 34] In the absence of a reapplied voltage, the gas is rapidly deionized by recombination and diffusion. Even in the presence of a reapplied voltage, deionization of the gas near the electrode surfaces is very rapid.[35] The dielectric strength thus recovered increases as the r.m.s. current is decreased. The high anode temperature of a 3-amp. carbon arc,[36] plus the relatively low heat conductivity of carbon, makes it possible for this electrode to be sufficiently active thermionically to supply all the necessary electrons when it becomes cathode. Under these conditions the low reignition potential observed is all that is required to establish the positive ion space-charge in the new cathode region and to overcome the effect of volume deionization of the column. The larger the arc current the higher the electrode temperature at any instant after extinction and the nearer the reignition potential will be to the burning voltage.

If the electronic emission in the "field" arc range of currents depends largely on a layer of positive ions on the cathode surface, the conditions at the instant of zero currents are unfavorable to reignition. A positive ion space-charge and surface layer must be established at the surface which, while acting as the anode, had just been the seat of an electron space-charge. In addition, the actual volume of ionized gas in the column is less for these lower currents so that deionization is correspondingly more rapid. It is possible that the recovery voltage first establishes a low current glow discharge. The positive ion bombardment of the new cathode during this period serves to establish the necessary surface charge. The electron emission will concentrate at surface irregularities where the electric field is high. The effects of high space-charge, surface charges, and emission by positive ion bombardment will become cumulative as the recovery voltage increases and the arc cathode spot will be established.[16] The experimental reignition voltages under these conditions are much greater than for the thermionic arc, which substantiates the foregoing reasoning. It is probable that ionization in the reignition period is largely by electronic collision. If this is true, the gradient of the column during reignition should increase with pressure, as it does, because of the shorter mean free path. It should be noted that the reignition potential will not be as high as the pressure might indicate because the pre-arc discharge takes place in a column of gas whose density, although increasing with time, is less than that of the surrounding medium, due to the heating effect of the arc. The addition of inductance to the circuit will shorten the deionization time[37] and correspondingly will reduce the reignition potential. When the main discharge is a glow, there is no thermal ionization in the column so that the deionization is very rapid and the glow reignition is high. For very small currents the reignition is essentially a spark breakdown.

The authors gratefully acknowledge the advice and assistance in connection with this research received from Dean Emeritus Harry E. Clifford and Professor C. L. Dawes of the Graduate School of Engineering, and from Professor F. A. Saunders of the Physics Department of Harvard University.

[29] D. C. Prince, Trans. A. I. E. E. **52**, 844 (1933).
[30] G. P. Luckey, Phys. Rev. **9**, 129 (1917).
[31] C. G. Suits, Physics **6**, 315 (1935).
[32] Reference 22, p. 140.
[33] C. Ramsauer, E. u. M. **51**, 189 (1933).
[34] C. G. Suits, Gen. Elec. Rev. **39**, 194 (1936).
[35] T. E. Browne, Physics **5**, 103 (1934).
[36] Reference 22, p. 136.
[37] S. S. Attwood, W. C. Dow and W. Krausnick, Trans. A. I. E. E. **50**, 854 (1931).

Wratten Light Filters

for Photography, Photomicrography, Spectroscopy, Photometry, and Astronomy

WRATTEN LIGHT FILTERS are universally used in widely separated fields of scientific research.

The Wratten list includes filters for use with all types of color-sensitive films and plates. Over one hundred different filters are available.

Complete spectrophotometric data are given in the Eastman publication, *Wratten Light Filters*; price, 50 cents. A price list of filters will be furnished free on request.

Visit the Kodak Building at the New York World's Fair

EASTMAN KODAK COMPANY

Research Laboratories **ROCHESTER, N. Y.**

NOW... *High accuracy* in ultra high frequency current measurement!

WESTON *Instruments*

WESTON

(ultra high frequency type)

THERMO-AMMETERS

Its development program constantly *in tune* with industry's needs, WESTON now is supplying all Thermo-Ammeters of a new design which furnishes a new, high order of accuracy in current measurement for transmitter and other circuits operating on ultra high frequencies. » » » Employing a new, patented principle* developed in WESTON'S laboratories, these instruments now reduce the errors to the extremely small value of 1 per cent at 50 megacycles, and 3.5 per cent at 100 megacycles; whereas, with ordinary thermo-ammeters the errors at such frequencies may rise to as high as 50% for the higher current ranges. » » » WESTON ultra high frequency Thermo-Ammeters are available in both round and rectangular shapes, in all standard panel and switchboard sizes. Complete data can be secured from the WESTON office in your vicinity; or, direct from Weston Electrical Instrument Corporation, 608 Frelinghuysen Avenue, Newark, New Jersey.

*WESTON *Thermo-Ammeters employ a heated member of tubular structure to maintain the effective resistance, and consequent temperature rise, nearly constant up to very high frequencies.*

Innovations in Instruments

General Electric Receives Television License

A television transmitter, designed to broadcast pictures with improved picture definition, will be put into operation within the next three months by General Electric at Indian Ladder in the Helderberg Hills, twelve miles from Schenectady, New York. Built on top of a 1500-foot hill with an antenna strung on 100-foot towers, this station will be at least 250 feet higher than the one atop the Empire State building in New York. To the south are higher hills which, with a directional antenna, will tend to prevent the signal from causing any possible interference with stations in New York City. With a power output of 10 kilowatts, its coverage will be the area comprising Schenectady, Albany, Troy, Amsterdam and Saratoga, known as the Capital District, with a combined population of more than 500,000.

The television studio will be located in Schenectady, in quarters occupied by WGY until this station moved into its new broadcast home last summer. Its equipment will incorporate many new features developed by General Electric engineers who not only pioneered but have spent years in television research. These developments assure a more perfect pick-up and broadcast of pictures. As such times as studio programs are not available, motion picture film will be used much the same as electrical transcriptions now fill in on broadcast programs.

From an ultra-short wave transmitter on top of the studio building, the images will be relayed over the 12-mile gap on a 1.4-meter band to the main transmitter in the Helderbergs, where they will be broadcast for public reception on a wave-length in the 66–72 megacycle band or on about 4½ meters. The voice accompanying the picture will also be broadcast on the same band, on a frequency immediately adjoining the picture, assuring reception with less interference from static than experienced on the regular broadcast channels.

More than 250 vacuum tubes will be utilized in the complete television transmission equipment, which is five times as many as now used for voice broadcasting. Many of these tubes are of new design. The antenna will also be different, resembling a cube of wires as strung from the three 100-foot poles. The station is being built so that changes may be made from time to time as new developments in television occur.

Cut-Away Triode Shows Electrode Operation

To show plainly what goes on inside a three-electrode vacuum tube and the effect of a magnetic field on a stream of electrons flowing through a vacuum, Westinghouse engineers have built a triode 27 inches high and seven inches in diameter, to be exhibited at the New York World's Fair. It is similar to a standard radio tube except that it has two filaments and two grids on opposite sides of the plate, so that the action is visible from both directions.

The surface of the plate is coated with fluorescent material, so that wherever electrons impinge on the plate, a green color shows. By changing the negative biasing voltage supplied to the grid, the stream of electrons to the plate can be varied from zero to the maximum of which the tube is capable. A pattern on the face of the plate shows the area normally bombarded by electrons.

By placing a permanent magnet near the tube, the electron stream can be deflected by the magnetic field. The effect of the field on the electron stream can be seen plainly. This effect varies according to the way the magnet is applied to the tube.

The circuit used is similar to that in audioamplifiers. A 60-cycle frequency is applied to the grid and the tube output is connected to a loudspeaker. The loudness of the audiosignal corresponds to the area of the green glow on the plate of the tube.

Reflector Photoflood Lamp

A new photoflood lamp which includes within its bulb both light source and reflector has been added to the line of Mazda photographic lamps manufactured by the Westinghouse Lamp Division of the Westinghouse Electric & Manufacturing Company, Bloomfield, New Jersey. It will be called Mazda reflector photoflood lamp No. R2. The new lamp produces a cone of light covering about 60 degrees. The color of its light is about the same as that of conventional photoflood lamps, insuring good color radiation in black and white films. The lamp also is recommended for color photography. Because the distribution and quantity of light is similar to that of a regular No. 2 photoflood in a good reflector, the same exposure data are applicable to both lamps.

The new lamp closely resembles in appearance the R-40 reflector spot lamp; however, the photoflood lamp has a special filament shape, size and position and the inside frosting is somewhat heavier, providing a wider light distribution well adapted to photographic service. The lamp contains also a reflecting disk mounted on the stem just behind the focal point of the reflecting surface to utilize that part of the light which is projected toward the unsilvered neck of the bulb and which would otherwise be lost. Its heavily metalized reflector stays efficiently bright during its life of 6 hours. Its medium screw base fits the usual socket. It is made for 105- to 120-volt circuits.

Four-Foot Fluorescent Lamps

A new larger fluorescent Mazda lamp, available April 1, was announced by the Westinghouse Lamp Division, Westinghouse Electric & Manufacturing Company, Bloomfield, New Jersey. The significance of this new lamp

"JAGABI" RHEOSTATS

A Jagabi *Screw-Drive* Rheostat
10-inch size

For Fine Adjustment and Control of Electric Current

"We have always found these rheostats satisfactory . . . Attempts to purchase cheaper ones have been disappointing . . . Every rheostat purchased from you during the past 10 years is still in use."

——————————University

Do you have on file our Jagabi Rheostat Bulletin 1515-R. Write.

JAMES G. BIDDLE CO.

ELECTRICAL AND SCIENTIFIC INSTRUMENTS

1211-13 ARCH STREET. PHILADELPHIA, PA.

highest purity...
for all purposes

Linde Rare Gases and Linde Rare Gas Mixtures are available for the study of electrical discharges, for use in rectifying and stroboscopic devices, and in inert atmospheres where heat conduction must be reduced. Additionally, the facilities of Linde laboratories are available for the preparation of special mixtures for experimental uses. Write any Linde office for folder and full information about Linde Rare Gases.

The word "Linde" used herein is a registered trade-mark.

THE LINDE AIR PRODUCTS COMPANY
Unit of Union Carbide and Carbon Corporation
NEW YORK AND UCC PRINCIPAL CITIES

THE WORLD'S LARGEST PRODUCER OF OXYGEN AND OTHER GASES OBTAINABLE FROM AIR

EPPLEY STANDARD CELLS

for students' use

A CADMIUM STANDARD CELL FOR POTENTIOMETRIC DETERMINATIONS

The new style molded bakelite case presents definite advantages in both protection and appearance over the old style support.

For students' use, where protection from accidental current drains is desired, we offer this cell with a 10,000 ohm protective series resistance. This unit is of particular value when setting up experimental circuits.

Cat. No. 102R Standard Cell, Eppley, Students' Type. Voltage approximately 1.018 volt at average room temperatures. Guaranteed accurate to ± 0.1%. With 10,000 ohms protective series resistance $14.00

Cat. No. 102 Standard Cell, Eppley, Students' Type. Same as above but without protective series resistance $12.00

Write for descriptive folder.

EPLAB

THE EPPLEY LABORATORY, INC.
SCIENTIFIC INSTRUMENTS
NEWPORT, R.I.
U. S. A.

TYPE S POTENTIOMETER

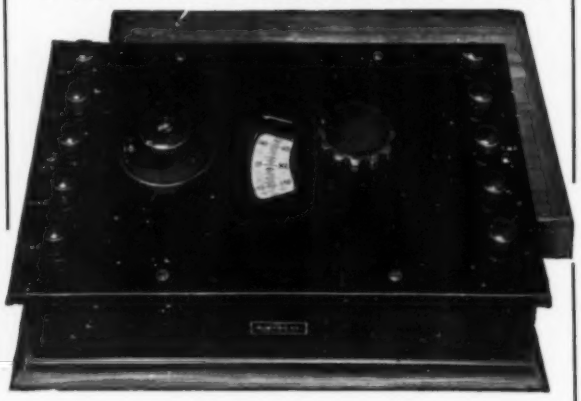

An accurate and inexpensive laboratory potentiometer suitable for all measurements of potential difference and for student instruction in the potentiometer method. Two ranges—1.6 volts and 16 M.V. Coils are accurate to within 1/20 per cent. Price seventy-five dollars.

ASK FOR BULLETIN 270.

RUBICON COMPANY

Electrical Instrument Makers

29 N. SIXTH STREET PHILADELPHIA, PA.

FINE WIRES

TAYLOR PROCESS

THE TAYLOR PROCESS is a method for making wires from substances which lack ductility. The elements or alloys, because the drawing is done in glass or quartz, are in a very pure state. Lengths of more than a few feet cannot be obtained. The wires may be had with or without the glass insulation. We make Taylor Process wire of Pt, Rh, Au, Ag, Cu, Fe, Zn, Cd, Pb, Sb, Bi, Sn, Se, Te, Tl, Ga, and In, Constantan, Bi-Sn, Cd-Sb (used where large E.M.F. is desired) and many other alloys. Our wires are packed in containers holding one foot and, with few exceptions, the sizes are from one *mm* to one micron. We manufacture, too, fine wire by the Wollaston Method, by extrusion and by bare drawing.

WE ARE SPECIALISTS IN PLATINUM AND CAN SUPPLY IT IN WHATEVER FORM YOU REQUIRE

BAKER & CO., INC.

113 Astor Street, Newark, New Jersey

Innovations in Instruments (*continued*)

lies in its extension of fluorescent lamp usage, because of the increased light output now obtainable from a single lamp. The new size, being of the same diameter and having the same brightness as two of the four existing sizes, can be used with these sizes in designing lines of lamps placed end to end.

The complete list of sizes now is:

Length	Diameter	Watts
18 inches	1 inch	15
18 "	1½ "	15
24 "	1½ "	20
36 "	1 "	30
48 "	1½ "	40

The light output of the 48-inch lamp is 1400 lumens, compared with 1050 lumens for the 36-inch size. The new lamp will be available in daylight and warm white.

Electric Carillons

Two new electric carillon systems, one an instrument which rivals the music of a carillon of 26 giant bells and the other a five-note Westminster chime have been announced by the RCA Manufacturing Company. Designed to take the place of costly, space-consuming bell carillons used in churches, schools, banks, public buildings, and other similar institutions, the new electric carillons are compact and easily operated. They may be installed by connection with any public address system or electric organ amplifying unit.

The 26-note system, encompasses all the musical range of a huge bell carillon in its two-octave piano keyboard. The chime system may, if desired, be operated from a time clock to give the Westminster peal at fifteen-minute intervals. Its hour-note is one octave lower than normal to assure good quality response. These simplified electric carillons produce clear, ringing bell-notes from slender metal reeds. Vibrating at the tap of little striking hammers actuated from the keyboard, the reeds, which are connected to magnetic coils, induce in the coils a current which varies exactly with the vibrations. This current is amplified in radio tubes and conducted to high quality loudspeakers which reproduce the bell-notes.

Excello Drafting Machine

The Eugene Dietzgen Company, Chicago, announces a new drafting machine which is "free floating." It uses lightweight alloys and roller bearings and is made in a precision manner. It has a so-called gravity control which eliminates friction brakes and overhanging weights. It may be used for drawings up to 36″×60″.

STABILIZED A-C VOLTAGE

INPUT 95-130 volts
Instantaneous action
A magnetic unit

OUTPUT
115 volts ±1%
Stabilizes at any load within rating

No moving parts. Nothing to wear out.

RAYTHEON Voltage Regulator

APPLICATIONS Broadly it insures stable operation of all precision apparatus obtaining its power from an A.C. source, for example:—

- Insures constant brilliancy from all types of lamps.
- Improves the operation of X-ray equipment.
- Stabilizes all electronic apparatus.

Write for Bulletin 48-71G6P.

RAYTHEON MFG. CO. WALTHAM, MASS.

PHOTRIX UNIVERSAL PHOTOMETER

MODEL A:
4 measuring ranges
With single cell:
0-2.5, 0-10, 0-50, 0-250 ft. cdl.
$57.00

With double cell:
0-0.25, 0-1, 0-5, 0-25 ft. cdl.
$100.00

MODEL B:
3 measuring ranges
0-12, 0-60, 0-1000 ft. cdl.
$37.50

UNEQUALLED SENSITIVITY
PERMANENT STABILITY

ALSO INDIVIDUAL PHOTOCELLS:

ELECTROCELL
SELF-GENERATING PHOTO-ELECTRIC ELEMENTS
(Barrier Layer Cells)
Great variety of sizes and shapes.
Round cells from ½" to 2½" diam.
Unmounted or mounted.

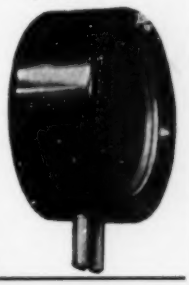

DR. F. LOEWENBERG
10 East 40th St. New York City

Now... at Low Cost!

QUICK-TEST YOUR TUBES WITH NEW RCA TUBE TESTER!

COSTS ONLY **$37.95**
Stock No. 156-A

Model illustrated is counter type. Also available in carrying case for portable use as Stock No. 156, $39.95—All prices net.

This splendid new instrument enables you to tell in a jiffy if your tubes are in proper working order. And not only is the RCA Tube Tester amazingly simple to operate . . . not only does it test all tubes including the new "LOKTAL" types—but it's exceptionally inexpensive, too!

Be sure you're using good tubes! Quick-test them with the RCA Tube Tester—at low cost!

For finer radio performance—RCA Radio Tubes

RCA Test Equipment

RCA MANUFACTURING COMPANY, INC., CAMDEN, NEW JERSEY
A SERVICE OF THE RADIO CORPORATION OF AMERICA

MOLDED
S·S·White HIGH VALUE RESISTORS

Actual Size— All Values

.... 15 Megohms to 1,000,000 Megohms

Developed for use in scientific and industrial control and measurement equipment, and in laboratory and experimental units. Carried in stock in a large assortment of values. Prices from $.40 ea. to $3.50 ea. Quantity prices on request.

Full details in RESISTOR BULLETIN 37
Free copy with Price List on request. Write

S. S. WHITE

The S. S. White Dental Mfg. Co.
INDUSTRIAL DIVISION
Department B, 10 East 40th St., New York, N. Y.

INDEX TO ADVERTISERS

Name	Page
AJAX ELECTROTHERMIC CORP. — Ajax-Northrup high frequency electric furnaces from laboratory to plant sizes.	viii
BAKER & CO., INC. — Platinum crucibles, dishes, triangles, filter cones, anodes, cathodes, electrodes, platinum tipped crucible tongs, fine wires and bismuth foil.	xii
JAMES G. BIDDLE COMPANY — "Jagabi" Rheostats; Adam Hilger and Kipp & Zonen Optical Instruments; "Pointolite" Lamps; Electrical Testing and Speed-measuring Instruments.	xi
P. BLAKISTON'S SON & CO., INC.	vi
CENTRAL SCIENTIFIC COMPANY — Manufacturers of Cenco Physical Apparatus and Instruments to meet all requirements of University, College and High School Physics Laboratories. Specializing in high vacuum pumps and development of instruments and apparatus for various sciences.	Cover 4
CLIFFORD MFG. CO. — Hydron metallic bellows for temperature and pressure control devices. Data for engineers.	xiv
EASTMAN KODAK COMPANY — Purified Organic Chemicals for research purposes; Plates for Photography, Photomicrography, Spectroscopy, Photometry, Astronomy; Wratten Light Filters; Cameras and Films.	ix
THE EPPLEY LABORATORY, INC. — Standards of e.m.f. (standard cells). Precision electrical instruments; potentiometers, bridges, temperature bridges, volt boxes. Thermopiles and pyrheliometers.	xi
GAERTNER SCIENTIFIC CORP. — Spectroscopes, Spectrometers, Spectrographs, Spectrophotometers, Heliostats, Measuring Microscopes, Comparators, Cathetometers, Reading Telescopes, Interferometers, Chronographs, Dividing Machines, etc.	iv
GENERAL ELECTRIC VAPOR LAMP. CO. — Uviarc lamp for ultraviolet radiation. Sodium Lab-Arc Lamp.	v
GENERAL RADIO COMPANY — Manufacturers of electronic measuring instruments; vacuum-tube voltmeters, amplifiers and oscillators; wave analyzers, noise meters and analyzers, stroboscopes; laboratory standards of capacitance, inductance and frequency; impedance bridges, decade resistors and condensers; air condensers and variable inductors; rheostats, Variacs, transformers; other laboratory accessories.	Cover 3
G-M LABORATORIES, INC. — Photoelectric Cells; Photoelectric Relays; Slide Wire Rheostats; Galvanometers; Galvanometer Suspensions; Laboratory Stands and Clamps.	ii
INTERNATIONAL RESISTANCE COMPANY — Manufacturers of metallized and wirewound fixed and variable Resistors including high voltage and high frequency types.	iv
LEEDS & NORTHRUP COMPANY — Manufacturers of Galvanometers, Resistors, Bridges, Condensers, Inductances, Potentiometers, Testing Sets; Temperature Measuring, Recording and Controlling Apparatus; Instruments for Measuring and Controlling Conductivity of Electrolytes and Hydrogen Ion Concentrations.	i
THE LINDE AIR PRODUCTS CO. — Oxygen, Argon, Helium, Krypton, Neon, Xenon, Rare Gas Mixtures, Nitrogen, Hydrogen, Calcium Carbide, Acetylene, equipment for Oxy-Acetylene welding and cutting.	xi
LOEWENBERG, DR. F. — Light measuring instruments, single and double cell types. Self-generating photo-electric elements, wide variety of electrocells.	xiii
MCGRAW-HILL BOOK CO., INC.	iii
RAYTHEON MFG. CO. — Voltage stabilizers and regulators. Electrical measurement and control instruments.	xiii

INDEX—*Continued*

Name	Page
RCA MANUFACTURING CO., INC. — RCA Oscillators and Oscillographs, RCA Test Equipment, RCA Ultra-Sensitive DC Meter.	xiii
RUBICON COMPANY — Galvanometers, electrometers, potentiometers, Wheatstone and Kelvin bridges, resistance boxes, hydrogen ion and conductivity apparatus.	xii
W. M. WELCH SCIENTIFIC CO. — Scientific instruments—laboratory apparatus. Catalog lists 10,000 items.	vi
WESTON ELECTRICAL INSTRUMENT CO. — Industrial temperature gauges, photographic exposure meters, electrical measurement instruments.	ix
S. S. WHITE DENTAL MFG. CO. — Resistors, 1000 ohms to 1,000,000 megohms.	xiii
JOHN WILEY & SONS, INC.	vii

POSITION WANTED

Instrument maker with complete shop equipment. College connection anywhere desired. 20 years experience in design, building, engineering, physical, chemical instruments, including balances, etc. Address Box K3-7. Rm. 1502, 175 Fifth Ave., New York, N. Y.

Classified advertisements are accepted under these three headings: Employment, Want to Purchase and Educational Institutions. The rate is 75c per line (six words average) and minimum is three lines.

HYDRON
Metallic Bellows

HYDRON Metallic Bellows are used as control elements in temperature-and-pressure-control devices, and for liquid or gas seals of compressors and pumps. We are specialists in the design and production of complete thermostatic and pressure units for temperature and pressure controls. We are, therefore, prepared to extend the fullest co-operation to engineering departments of control manufacturers in the solution of design and engineering problems.

Write for 44 PAGE ENGINEERS' DATA BOOK

CLIFFORD MANUFACTURING CO.
564 E. FIRST STREET, BOSTON
BOSTON CHICAGO DETROIT LOS ANGELES
PRODUCERS OF BELLOWS EXCLUSIVELY
SERVING AUTOMATIC CONTROL MANUFACTURERS